Tyre noise over impedance surfaces - Efficient application of the Equivalent Sources method

François-Xavier Bécot

CHALMERS

Tyre noise over impedance surfaces
- Efficient application of the Equivalent Sources method

FRANÇOIS-XAVIER BÉCOT

Department of Applied Acoustics
CHALMERS UNIVERSITY OF TECHNOLOGY
Göteborg, Sweden 2003

Vibration - Acoustics Laboratory (LVA)
INSA - SCIENTIFIC AND TECHNICAL UNIVERSITY
Lyon, France 2003

INSA
LYON

CHALMERS UNIVERSITY OF TECHNOLOGY
SE-412 96 Göteborg, Sweden
Telephone: +46-(0)31 772 10 00
www.chalmers.se

The noise due to the contact between the tyre and the road represents now the major contribution to road traffic noise. Acoustical absorption from the road surface can help to reduce its contribution. Parametrical studies are needed to design and to optimise the acoustical properties of the road surface. In this respect, the work presented in this thesis provides modelling tools which aim at predicting and understanding the mechanisms of tyre / road noise above an absorbing surface.

Le bruit dû au contact entre le pneumatique et la chaussée représente aujourd'hui la contribution majeure au bruit de trafic routier. L'absorption acoustique de la chaussée peut aider à réduire cette contribution. Des études paramétriques sont nécéssaires afin de concevoir et d'optimiser les propriétés acoustiques de la chaussée. Dans ce contexte, le travail présenté dans cette thèse fournit des outils de modélisation destinés à prédire et à comprendre les mécanismes du bruit pneumatique / chaussée au-dessus d'une surface absorbante.

N° d'ordre 03ISALXXXX Year / *Année* 2003

PhD thesis / *Thèse*

Tyre noise over impedance surfaces – Efficient application of the Equivalent Sources method

Presented to / *Présentée devant*
L'Institut National des Sciences Appliquées de Lyon, France
&
Chalmers university of technology, Göteborg, Sweden

For / *Pour obtenir*
The grade of doctor of philosophy / *le grade de docteur*

Doctoral school / *Ecole doctorale* : M.E. G. A.
(Mécanique, Energétique, Génie civil, Acoustique)
Spécialité : Acoustique

By / *Par*
François-Xavier BÉCOT

Defended the 8th september 2003 in front of the examination committee
Soutenue le 8 septembre 2003 devant la Commission d'examen

Jury

KROPP	Wolfgang	Professor at Chalmers (Göteborg, Sweden), *Directeur de thèse*
GUYADER	Jean-Louis	Professor at INSA (Lyon, France), *Directeur de thèse*
DUHAMEL	Denis	Professor at ENPC (Paris, France), *rapporteur*
OCHMANN	Martin	Professor at T.F. (Berlin, Germany), *rapporteur*
KRISTIANSEN	Ulf	Professor at Norwegian Institute of Technology (Trondheim, Norway)
HAMET	Jean-François	Research director at INRETS – LTE (Bron, France)

Research laboratories / *Laboratoires de recherche* :

Vibrations – Acoustics Laboratory (*LVA*), INSA of Lyon, France
&
Department of Applied Acoustics, Chalmers university of technology, Göteborg, Sweden

Thesis for the degree of Doctor of Philosophy

Tyre noise over impedance surfaces

Efficient application of the Equivalent Sources method

François-Xavier Bécot

Department of Applied Acoustics
Chalmers University of Technology
Göteborg, Sweden

&

Vibrations - Acoustics Laboratory (LVA)
Insa – Scientific and Technical University
Lyon, France

May 2003
Report F03-03

Tyre noise over impedance surfaces – Efficient application of the Equivalent Sources method

François-Xavier Bécot

ISBN 91-7291-313-4

Doktorsavhandlingar vid Chalmers tekniska högskola
Ny serie Nr 1994
ISSN 0346-718X

Department of Applied Acoustics
Chalmers University of Technology
SE 412 96 Göteborg, Sweden
Telephone + 46 (0) 31-772 2200
Fax + 46 (0) 31-772 2212

Printed in Sweden by Chalmers Repro Service
Göteborg, Sweden

Abstract

Tyre noise over impedance surfaces – Efficient application of the Equivalent Sources method. François-Xavier Bécot. Report F03-03 – ISBN 91-7291-313-4

Reduction of the transportation noise nuisance has become an important challenge in today's societies. As a consequence of engine noise reduction, tyre / road contact noise is now the main source of traffic noise under normal driving conditions. In this respect, the aim of the present work is to understand and to control the mechanisms of tyre radiation by designing accurate tools to predict the tyre noise radiation over arbitrary impedance surfaces.

Tyre radiation is modelled using the Equivalent Sources method. Besides low frequency limitations because of two–dimensional simplifications, this model is proved to be an accurate tool for predicting tyre noise over acoustically rigid surfaces. Ground effects induced by absorbing surfaces are only approximated. Therefore, a model for the propagation of sound due to an arbitrary order source over an arbitrary impedance plane is developed. It is mainly an alternative to integral equation methods. In addition, the exact solution to this problem is presented.

Based on the two previous models, an iterative model of the tyre radiation over arbitrary impedance surfaces is implemented. Comparison with horn effect sound amplification indicate that this model is accurate for homogeneous as well as inhomogeneous absorbing surfaces. Using this model, trends for the tyre radiation over absorbing surfaces are discussed in a parametrical study.

The work presented in this thesis gives further insights into the mechanisms of tyre / road noise radiation; furthermore, it allows to study the possibilities of reducing traffic noise by the use of so–called "low–noise" road surfaces.

Keywords : tyre / road noise, tyre radiation, horn effect, equivalent sources method, method of auxiliary sources (MAS), ground impedance, cylindrical wave reflection coefficient, integral equations.

Résumé

Bruit de pneumatique au–dessus d'une surface d'impédance donnée – Application efficiente de la méthode des Sources Equivalentes. François-Xavier Bécot.
Report F03-03 – ISBN 91-7291-313-4

La réduction du bruit des tansports est devenue un enjeu majeur dans nos sociétés. En raison de la réduction du bruit de moteur, le bruit de contact pneumatique / chaussée est aujourd'hui la principale source du bruit de trafic en conditions normales de conduite. Dans ce contexte, le but du présent travail est de comprendre et de contrôler les mécanismes de rayonnement du pneumatique, ceci en concevant des outils de prédiction efficients pour la propagation du bruit pneumatique / chaussée au dessus de surfaces d'impédances arbitraires.

Le rayonnement du pneumatique est modélisé à l'aide de la méthode des Sources Equivalentes. Malgré des limitations en basses fréquences dues au caractère bi–dimensionel du modèle, calculs et mesures indiquent que cet outil convient bien au rayonnement au–dessus de surface totalement réfléchissantes. Les effets de sol induits par des surfaces absorbantes n'est réalisée que de manière approchée. Un modèle d'effets de sol dus à un plan d'impédance donnée est donc dévelopé pour des sources de directivité arbitraire. Cette technique est essentiellement une alternative aux méthodes dites des équations intégrales. Par ailleurs, la solution exacte du problème est présentée.

Basé sur les deux outils de prédiction précédents, un modèle iteratif est dévelopé pour le rayonnement d'un pneumatique au–dessus de surfaces dont l'impédance est arbitraire. Des comparaisons avec des mesures d'amplification sonore due à l'effet dièdre montrent que ce modèle est efficient pour des surfaces absorbantes homogènes et inhomogènes. A l'aide de ce nouvel outil, une étude paramétrique examine les tendances du rayonnement du pneumatique au–dessus de chaussées absorbantes.

Le présent travail apporte de nouveaux éléments en matière de rayonnement de pneumatique / chaussée; il contribue en outre à l'étude des possibilités de réduction du bruit de trafic, notamment en utilisant des chaussées dites "silencieuses".

Mots clés : Bruit pneumatique / chaussée, rayonnement pneumatique, effet dièdre, méthode des sources équivalentes, impédance de sol, coefficient de réflection pour ondes cylindriques, équations intégrales.

Acknowledgements

During my doctoral studies, I had the unvaluable chance to take the most of the supervision of Prof. Wolfgang Kropp and Dr. Jean-François Hamet. This work results from the numerous fruitful and thorough discussions we have had. Therefore, I would like to extend my warmest regards to them for their wise guidance and support along this time.

I am also very grateful to Prof. Tor Kihlman from the Chalmers University of Technology and Prof. Jean-Louis Guyader from Insa of Lyon for giving me the opportunity to do this work. I also would like to thank Jacques Beaumont for welcoming me at Inrets.

I would like to thank all the staff of the department of Applied Acoustics for the studious and warm atmosphere they all contribute to. I especially thank Gunilla Skog and Börje Wilk for their precious and friendly help with the administrative and the computer things during this time.
Cordial thanks to the members of the tyre noise group and the members of the outdoor sound propagation group for their skillful advice, comments and support.

I send my sincere regards to the members of the Transport and Environment Laboratory of Inrets, with a special mention to the members of the "Acoustique physique" group. Thanks to all of you!

This work would not have been possible without the love and the patience of Sylvaine. Sylvaine, this work is yours too.

Context of the doctoral studies

The PhD work of François-Xavier Bécot had the frame work of a collaboration between
Department of Applied Acoustics of Chalmers University of Technology
and
Vibrations – Acoustics Laboratory (LVA) of Insa of Lyon.
The research activities took place
in Sweden at the Department of Applied Acoustics of Chalmers University of Technology
and in France at the Transport and Environment Laboratory (LTE) of Inrets.

The work was also financially supported by Région Rhône-Alpes (France).

Table of Contents

Notations used in the text

The following text is organised in a number of
CHAPTER's, numbered as 1, 2, ... They are subdivided in a number of
Section's, numbered as 1.1, 1.2, ..., 2.1, 2.2, ..., which themselves contain a series of
Paragraph's, which are not numbered. All these are followed by
APPENDIX number I, II, ...

Below, a number of abbreviations used in the following text are explained.

dB	:	decibels $= 10 \log_{10} \mid pressure(N.m^{-2}) \mid^2$
2D	:	two-dimensional
3D	:	three-dimensional
FE	:	finite element (method)
BE	:	boundary element (method)
ES	:	equivalent sources method
SPL	:	sound pressure level, in decibels
SVD	:	singular value decomposition
resp.	:	respectively
$Eq.3-5$	:	Equation 5 in Chapter 3
Fig. 2-6	:	Figure 6 in Chapter 2
Fig. III-1	:	Figure 1 in Appendix III

The following notations correspond to

j	:	imaginary number ($= \sqrt{-1}$),
$i, j, m, n, \ldots$	:	integer indices.
$\mathbf{A}$	:	matrix which contains the element denoted A_m
$\mathrm{H}_m^{(2)}$	:	Hankel functions, second kind, of order m
$\times$	:	scalar product or matrix product,
$\cdot$	:	vector product.
∇	:	vector gradient (sometimes denoted *grad* in the literature).
$\vec{u}_r$ and $\vec{u}_\varphi$	:	unit vectors in the radial and tangential direction,
u, v	:	(dummy) variable of integration.

Introduction : Transportation Noise Nuisance

In the last century, car has turned from a "cult object" to the undesired host of our cities. Today's tendency in town planning is to make vehicles disappear from the city centres, this by developing public transports, by encouraging individual but non–polluting transportation means (bicycle, rollers, skate–board, trottinette, ...) or by encouraging alternate use (and vision) of our vehicles (car–pooling, car–sharing, ...). The objective of these efforts is to restore a more pleasant and, above all, a more healthy atmosphere in our towns.

The pollution, to which we are exposed, is composed of the atmospheric pollution and the noise pollution. Whereas, the first one has engaged a large concern from politics, the effort for fighting the second one has been quite moderate during the last thirty years. For instance in France, almost 40 % of the population declare to be annoyed by noise, a large part of which originates from the transportation network [Dufour 1990]. The study in [Stanners 1995] values to 45 % the part of the population in Europe exposed to noise levels between 55 and 65 dB(A) and to 20 % the population exposed to levels higher than 65 dB(A). To get the measure of these values, a noise level of 60 dB is characterised as "annoying"; it corresponds for instance to a conversation taking place in the listener's room. In addition, dB(A) is an average value over 24 hours, which means that measured noise levels may occasionally be higher, most likely, during day hours.

Besides auditory effects such as hearing loss or communication disturbance, a noisy environment may also impact people's physiology [Stansfeld 2002]. For the exposed population, noise may be the cause of hypertension, cardio–vascular diseases or psychological disorder. Especially among children, noise may be incriminated as altering the memory and the cognitive ability.

Finally, noise is often involved in sleep disturbance for a large part of the exposed population. The reduction of the noise nuisance is even more crucial as most of the effects mentioned above are not reversible, which means that they cannot be repaired by stopping the noise disturbance [Miedema 2001].

In Europe, to reduce this nuisance, the norms restricting the vehicle noise emission have been constantly thightened during the last decades. However, the decrease of roadside noise levels during this period has not been significant [Kragh 1991; Sandberg 1993]. In fact, the reduction of engine noise has been partially masked by an increasing tyre noise. As a result, tyre noise is dominant at driving speeds as low as 40 km/h for cars and 70 km/h for trucks [Sandberg 2001]. Therefore, in reply to the work in [Sandberg 1982], one may argue that tyre noise is very likely to become the limiting factor of vehicle noise reduction.

In this context, experts are needed to propose technical solutions to reduce traffic noise, and in particular tyre noise. Several solutions are available, which migh be combined to offer the optimal and most durable noise reduction [Watts 1999]. One drastic solution is to decrease the traffic volume; this is however a fairly unrealistic solution, at least in a nearby future. Another solution is to attenuate the propagation of vehicle noise, e.g. by placing noise barriers between the source and the receiver. This alternative, which is the subject of a large research effort, has been put in practice, for instance, on the borders of motorways. However, the noise reduction offered by this type of solution might be very local and might also lead to a deterioration of the visual environment. A last solution is to control the source itself, i.e. the interaction between the tyre and the road, either by controlling the tyre parameters or by controlling the road parameters [Ballie 2000; Ejsmont 1998].

As a part of a larger numerical tool for tyre noise prediction, the work presented in this thesis participates to the effort of controlling the noise source. This tool is based on the study in [Kropp 1992], and is under current development at the department of Applied Acoustics of the Chalmers University of Technology. It chiefly comprises a model for the tyre dynamics, a model for the contact between the tyre and the road, and a model for the tyre noise radiation. In this respect, the present work aims at improving the radiation module by introducing the influence of the acoustical properties of the road surface.

To achieve this goal, a number of techniques are available, the applications of which cover the field of the noise radiation from vibrating structures to outdoor sound propagation; these methods are reviewed in the next chapter.

Chapter 1

Tyre / Road Contact Noise and Ground Effects

Traffic noise is a term, which may take on different meanings. It may stand for a nuisance as explained in the previous introduction, and thus it may refer to the subjective aspects of sound. In contrast, this chapter will look at tyre / road noise as regards to its physical aspects. The objective is to define a strategy to design a model for the tyre radiation, which could account for the ground effects due to the acoustical properties of the road.

First, the major characteristics of the involved sources of noise are presented. The modelling effort is then reviewed concerning the tyre / road noise prediction. The possibilities of introducing the road absorption into a tyre radiation model are then discussed and the approach adopted in this thesis is presented.

1.1 Tyre road noise generation and radiation

General description

Traffic noise usually results from a few main contributions. According to [Sandberg 2002], power train noise dominates at low driving speeds, namely up to around 40 to 50 km/h for light vehicles and up to around 50 to 60 km/h for heavy vehicles. At higher driving speeds, tyre / road contact noise dominates vehicle noise. At very high speeds (over 150 km/h), which might be considered, as non usual driving conditions, the aerodynamic noise due to the air flow around the vehicle body produces the major part of the total vehicle noise.

To appraise the tyre / road noise, a number of measurements techniques have been developed. For instance, one can roll the tyre on a test–drum, as described in [Hayden 1971]. This equipment can be used for measuring both the radiated noise and the tyre dynamics, as shown for instance in [Hamet 1991; Périsse 2002]. However, real road surfaces cannot be laid on the drum surface. Therefore, special trailers which avoid the contribution of power train noise, have been designed to measure tyre noise *in–situ* [Ronneberger 1990]. With this equipment, measurements can be performed using for instance the Near Acoustical Holography [Burroughs 2001], in order to identify the regions of high sound pressure levels. This technique consists in placing the sensors on a plane in order to re-build the pressure field on a distant surface, which

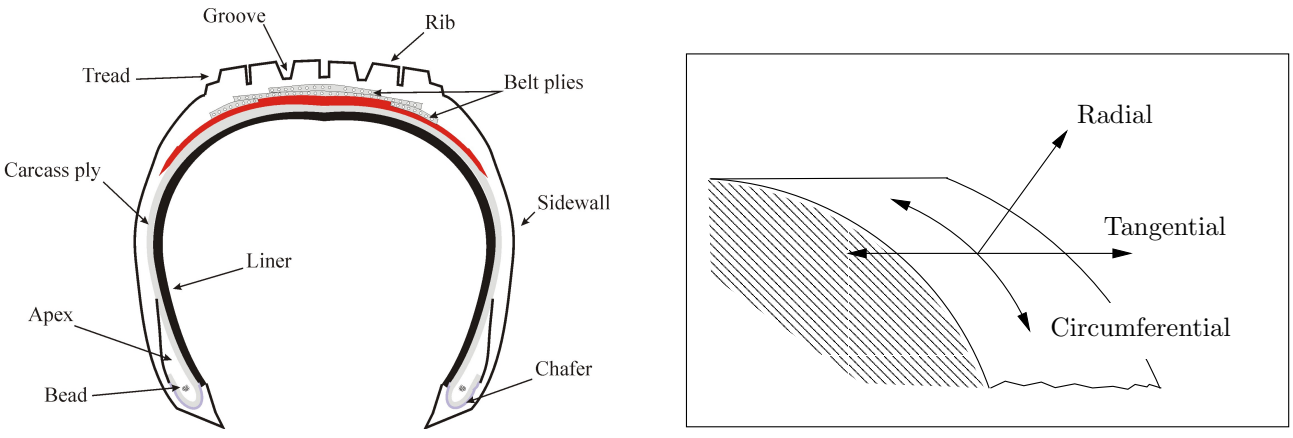

(a) Tyre structure cross section

(b) Directions of motions

Figure 1-1: *Structure and geometry of the tyre.*

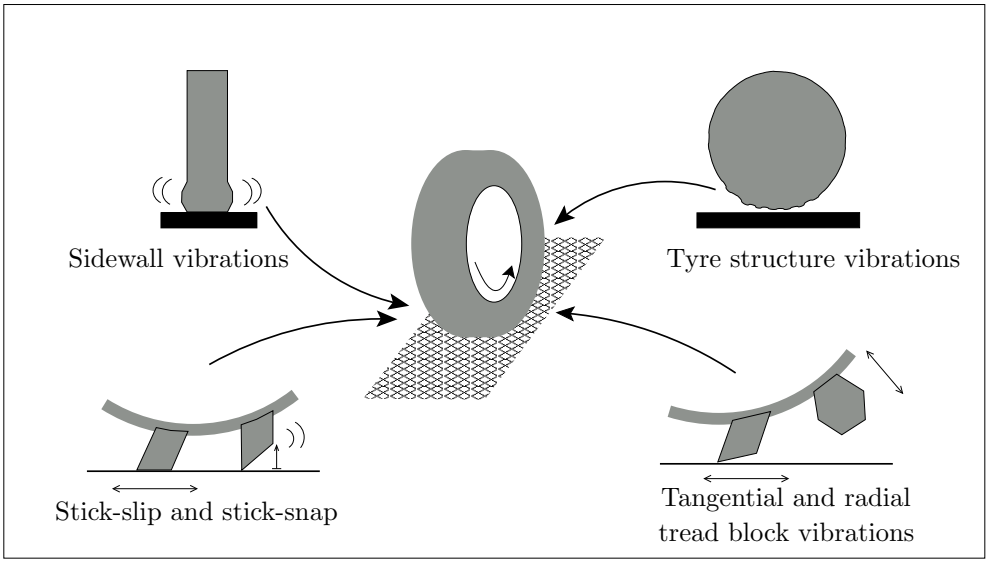

Figure 1-2: *Illustration of the mechanical sources of tyre noise.*

is flat or not as suggested in [Maynard 2001][1]. Measurements presented in [Ruhala 1999] locate the main sources of noise at the sidewall in the low and medium frequency range, up to around 600 Hz, and at the tyre / road interface at higher frequencies.

Many of these measurements show that the noise sources can be divided into two groups : the structure-borne sound sources, to which the sidewall vibrations belong, and the air-borne sound sources. Their description, a good review of which can be found in [Heckl 1986], is the subject of the two following paragraphs. The reader may refer to Fig. 1-1 for the different elements of the tyre structure.

Mechanical sources

The mechanical sources of noise are induced by time varying contact forces leading to the structural vibrations of the tyre structure. These vibrations are the main sources of noise at low frequencies. Illustrated in Fig. 1-2, they are identified as follows.

Under the rolling process, the roughness peaks excite the tyre structure to radial and tangential vibrations. As a consequence of the belt deformation, the sidewalls are bent like a membrane. This is expected to contribute to the radiation of sound, especially out of the plane of the tyre, even though this contribution has never been clearly quantified. Moreover, inside the contact

[1]The *ES* method can be used for the reconstruction of the field (see *Appendix I*).

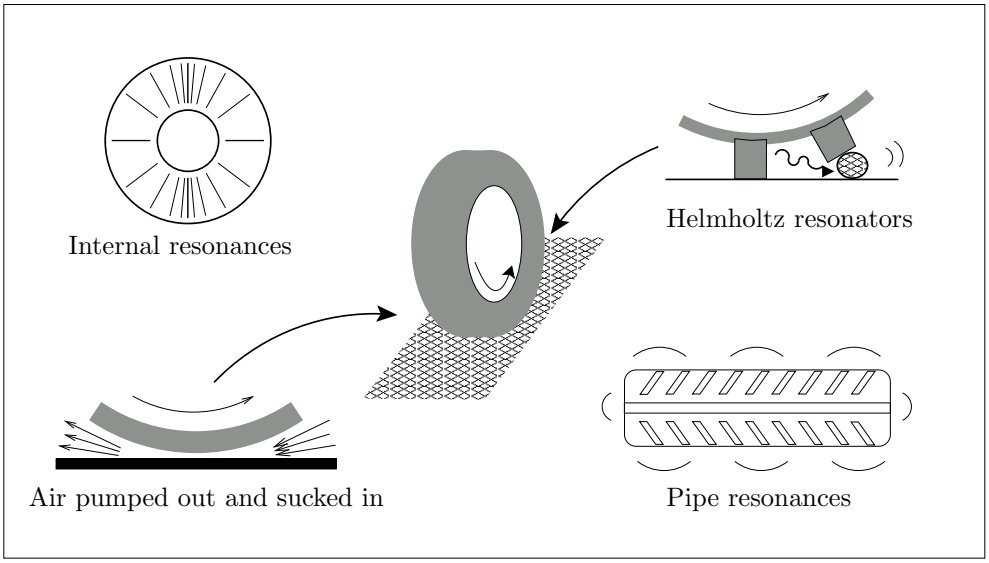

Figure 1-3: *Illustration of the air-borne sound sources of tyre noise.*

patch, friction and adhesive forces, force the motion of the tread blocks in the tangential and in the radial directions. The contribution of this phenomenon, usually referred to as stick-slip and stick-snap motion, is significant for rather smooth road surfaces. Finally, for a patterned tyre, the tread blocks hit the road surface in the leading edge and they are released when leaving the contact patch at the trailing edge. The tread block motions contribute generally at higher frequencies than the belt and the sidewall vibrations.

Air-borne sound sources

The air-borne sound sources include all displacements of air inside or near the tyre / road interface, which are not induced by the tyre vibrations. The following mechanisms have been identified (see Fig. 1-3). They are dominating the tyre / road noise in the high frequency range, namely above 1000 Hz.

Resonances of the air cavity contained inside the tyre contribute to the radiation of sound in narrow frequency bands, as suggested in [Nilsson 1979]. Therefore, their contribution may not be visible in terms of radiated sound power. At the leading and the trailing edge, the air cavities contained between the tread blocks and the outer road surface act as Helmholtz resonators. Very similar to these sources, resonances inside the tyre grooves are known as pipe resonances. Finally, air is pumped out or sucked in when the tread enters or leaves the contact area.

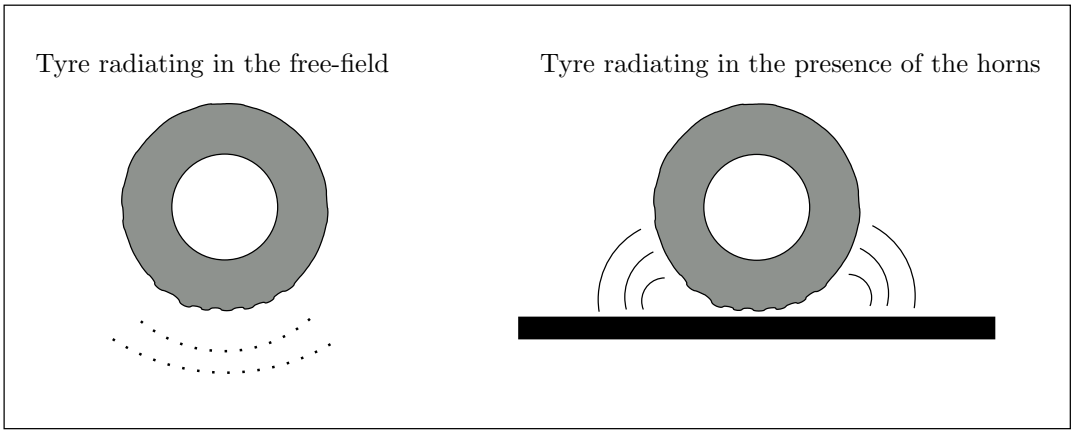

Figure 1-4: *Principle of the horn effect sound amplification*

A last noise source, which cannot be classified in either of the two previous categories, is the noise induced by the local deformation of the tyre. Sharp roughness peaks penetrate the tread cap leading to the deformation of the rubber locally around the rouhgness peak. The resulting displacement of air, which is often referred to as air–pumping, contributes mainly at high frequencies.

Horn effect

In addition, the conditions of the tyre radiation modify significantly the aspect of the noise generation. In the contact region, the tyre surface and the road form together a horn like geometry (see Fig. 1-4). As a consequence, the radiation efficiency of the sound sources located in this region is substantially enhanced compared to the case where the same sound sources are radiating in the free-field [Kropp 1992, 2000b; Ronneberger 1989]. The corresponding amplification coefficients are obtained by the ratio of the pressure radiated by the tyre in the presence of the horn, relative to the pressure radiated by the same tyre in the free-field.

It has been shown by measurements, in [Ronneberger 1989; Schaaf 1982] among many others, that the level and the frequency at which the maximum amplification occurs depend on the geometry of the horn. In certain situations, the sound amplification could reach around 20 to 25 decibels in the middle frequency range around 1000 Hz. This means that the region of maximum amplification corresponds to the frequencies having the dominant contribution in A–weighted sound levels.

Another parameter which affects both the noise generation and the noise radiation, is the

possible acoustical absorption due to the road surface. This effect is discussed more thorougly in *Section 1.3*.

1.2 Tyre road noise prediction models

According to the previous section, many levels of modelling could be considered, which include more or less noise generation mechanisms. A good review of the exisisting models for the prediction of the tyre / road contact noise can be found in [Heckl 1979, 1986], and more recently in [Kuijpers 2001] and [Hamet 2001b]. These are classified as statistical models, deterministic models and hybrid models.

Statistical models

The principle of these models is to find the correlation between measured noise levels and few parameters which are assumed to characterize the tyre / road interaction. These models are mainly used to assess traffic noise.

In [Huschek 1996; Sandberg 1980], A–weighted noise levels are given as a function of selected bands of the road texture spectrum. These models correlate the low frequency noise to the macro–texture on one hand, and the high frequency noise to micro–texture of the road on the other hand. This approach clearly follows the traditional classification of noise generation mechanisms as presented above, i.e. vibrational sources and aero–dynamical sources. However, in the case where the road texture is not the more relevant parameter of the tyre / road interaction, e.g. for porous road surfaces, these models fail to predict correct noise levels [Klein 2000].

Deterministic models : principle

In order to optimise the properties of the tyre road interface, deterministic models are needed. These models embrace successive sub–models, which simulate the tyre dynamics, the contact between the tyre and the road, and the tyre radiation.

The first sub–model predicts of the so-called Green functions of the tyre, that is, the response of the tyre to an elementary excitation (an impulse force). It requires the knowledge of the rubber mechanical properties, such as stiffness and Young's modulus, and the tyre dimensions.

In a second model, the contact forces are computed. Since the contact between the tyre and the road irregularities is non–linear, the calculation is performed in the time domain. As a

result, the convolution between the tyre Green functions and the contact forces gives the time history of the belt deformation as the tyre rolls.
Finally, the third sub–model comcerns the simulation of the radiated noise due to the previously predicted tyre vibrations. The input is the belt deformation in the radial direction[2], and the output is the sound pressure field at a given receiving position of space, including the sound amplification due to the horn effect.
The models which proceed in this way are reviewed in the next paragraph.

Deterministic models : review

Concerning the simulation of the tyre dynamics, one of the first attempt represents the tyre as a ring under the tension caused by the inflating pressure [Böhm 1966]. This so–called ring model, mainly valid at low frequencies, includes motion in the radial, tangential and circumferential directions. An approach based on the same description of the tyre was also proposed in [Huang 1987, 1992]. In [Saigal 1986; Soedel 1975] the tyre is considered as a toroidal membrane. The problem is then derived and solved according to a finite element scheme. This approach was proved to give a good approximation of the free response of a tyre at low frequencies.
At frequencies above the ring frequency, namely above 300 Hz to 400 Hz, the wave propagation is not influenced by the tyre curvature. Given this, works in [Kropp 1989, 1992] proposes to represent the tyre as an orthotropic plate[3], the vibrations of which can be described accurately by the standard bending wave equation. In [Hamet 2001c], the Green functions of this model are calculated analytically. This model has been extended to take the multi–layered structure of the tyre [Larsson 2002a] and the tread blocks [Andersson 2002; Larsson 2002b] into account. Studies in [Pinnington 2000, 2002] propose to model the tyre as a beam, along which impedances are introduced to include the presence of the sidewalls.
As the computational power increases, a increasing number of tyre models are based on the finite element method. For instance, work in [Richards 1991] describes the structural vibrations of the tyre belt under the loading of the surrounding medium. The work in [Fadavi 2001, 2002] uses a finite element method to predict the tyre dynamics with a view to the tyre radiation prediction.

The contact between the tyre and the road can be modelled by a Winkler bedding as suggested

[2]The motions in the two other directions are of less importance for the sound radiation.
[3]An orthotropic plate has different bending stiffnesses in the circumferential and in the tangential direction.

in [Johnson 1985]. This consists in considering a series of independent springs attached to the tyre belt. This model has been adopted in [Kropp 1992] which solves the problem in the time domain according to the scheme proposed in [Mc Intyre 1979] for musical instruments. It has been extended to model a *3D* contact in [Kropp 2001]. Hertz theory can also be applied to contact the contact forces between the tyre and the road [Fujikawa 1999]. In [Clapp 1985], the tyre tread is modelled as an elastic half space having the rubber stiffness.

One of the first modelling studies of the tyre radiation mechanisms was presented in [Ronneberger 1989]; this was however only dedicated to the simulation of the horn effect sound amplification. Concerning the tyre radiation modelling, the study in [Kropp 1992] uses a multipole expansion to reproduce the field radiated by the vibrating tyre. The horn effect is included by introducing a mirror image source. This *2D* model is proved in [Kropp 2000b] to be accurate from around 600 Hz to higher frequencies for rigid surfaces. This approach has been adopted in [Klein 1998], which further extends it to *3D* geometries [Klein 1998] and includes the road absorption [Klein 2002].

Radiation models are presented in [Kuo 2002], which make use of the expected behaviour of the tyre at low and high frequencies. For the medium frequency range, a *3D* model based on the boundary element method is proposed [Graf 1999, 2002]. The boundary element method is also used in [Anfosso 1996; Fadavi 2001, 2002] to reproduce the tyre radiation in *2D* or *3D* geometries. So far, these models do not include the road absorption.

In conclusion, deterministic models for the tyre / road noise prediction can be built using the aforementioned works. Works in [Kropp 1992] uses the orthotropic plate model for the tyre dynamics, together with the Winkler bedding model for the contact and the multipole model for the tyre radiation. In addition, this work includes a model based Hayden's approach [Hayden 1971] for the air–pumping. Although the radiation model is limited at low frequencies due to its *2D* character, it is shown in [Wullens 2002] that it could be an efficient tool for studying the possibilities of a reduction of tyre / road noise.

The TRIAS[4] model [Gerretsen 1996; de Roo 2001] is developed on the basis of the orthotropic plate model presented by Kropp. This model includes the noise contribution from the power–

[4]Tyre Road Interaction Acoustic Simulation

train, the tyre / road interaction and the so–called air–pumping. This model still needs to be validated [Gerretsen 2001].

Hybrid models

As previously mentioned, statistical models do not account for the whole variety of tyre / road combinations. Therefore, hybrid models have been developed that could give noise levels as a function of a parameter which desribes better the tyre / road interaction than the road texture. For instance in [Clapp 1985], it is proposed to relate contact forces to noise levels. For this, the tyre deformation is estimated by modelling the penetration of the roughness peaks into an elastic half space.

A similar approach is proposed in [Hamet 2001a; Klein 2000], which uses the othotropic plate model and a dynamic contact model to predict the contact forces. The model proposed in [Beckenbauer 2001] adopts the same approach and builds the statistical part of the model on more than 800 tyre / road combinations. Finally, the hybrid model presented in [Fong 1998] relates the sound intensity to contact pressure spectra.

1.3 Acoustical characterisation of road surfaces

Since the generation and the radiation of tyre road noise is strongly influenced by the acoustical properties of the road surface, an accurate model for the tyre radiation must include these properties. Therefore, the next paragraph reviews the impedance models available from literature. Then, the possible strategies for introducing the road absorption into a tyre model are discussed.

Impedance models

To model a possible sound absorption by the ground, the sound propagation must be described within this medium. In acoustics, the propagation in a given medium is characterized by two parameters [Zwikker 1949] : its propagation constant, which provides with the attenuation information, and the wave impedance, which relates the pressure and the velocity in this medium. From these two values, the specific impedance of the material is determined at the interface between the ground and the air above it. In this way, the sound propagation within the ground is fully represented by a single variable defined at the interface, i.e. the acoustical impedance

usually given in the normal direction to the surface.

A large number of impedance models can be found in the literature; a good review of the research works can be found for instance in [Attenborough 2001]. These techniques are classified in two major groups, depending on the scale of observation : the microstructural approach and the phenomenological approach.

On one hand, the microstructural approach, as indicated by its name, investigates the sound propagation within a pore of ground and extends this observation to a macroscopic scale. Depending on the number of parameters considered to describe the wave propagation, several impedance models are then derived. A widely used model, presented in [Delany 1970], gives the impedance as a function of the effective flow resistivity only. Many studies have proved that this so–called one–parameter model, originally derived for fibrous materials, describe accurately a large range of ground surfaces. More parameters such as the tortuosity, also called twistiness, or the porosity of the ground can be included, which results in other impedance models [Attenborough 1985; Rasmussen 1981; Thomasson 1977]. Sophisticated impedance models have been developed recently to include the effects of the surface roughness [Attenborough 2000].

On the other hand, in a phenomenological approach, the ground medium is considered as a dissipative, compressible fluid. This thorough representation, proposed in [Hamet 1992], includes effects of the viscosity and thermoconductivity. The resulting impedance model is a function of the flow resistivity, the tortuosity and the porosity. This model was found to be particularly suited to the determination of the acoustical properties of porous road surfaces [Bérengier 1997].

Lastly, it should be mentioned that the application of these impedance models, as accurate as they may be, is limited by the difficulty in measuring the parameters they depend on (the flow resistivity, the tortuosity, etc.). Therefore, in parallel to the research efforts towards more elaborated impedance models, a number of measurement techniques are being developed to determine the acoustic absorption of road surfaces. A good summary of these techniques can be found in [Bérengier 2001]. These experimental methods are particularly interesting because they allow access to the material data without directly measuring them. For instance, one can match some measured absorption values with those obtained with a given impedance model.

In this way, the impedance model is optimised for this particular ground surface[5].

Modelling strategies for outdoor sound propagation

Once the acoustical properties of the road are known, by measurements or by prediction, sound propagation including the ground effects can be tackled. This problem is very complex, both analytically and numerically, and is still the subject of numerous research works, as suggests the discussion in [Kragh 2001]. Therefore, the purpose here is not to review this large research effort. Instead, it aims at identifying general trends in the modelling in order to draw out the possible strategies of introducing absorption into a tyre radiation model.

To deal with outdoor sound propagation, one can distinguish two main strategies. Firstly, one chooses to proceed with the mathematical derivations, hoping that, besides the number of approximations leading to obvious simplifications of the situation, one obtains an expression that is better suited to a numerical evaluation. Or one treats the problem numerically straight from the beginning; this results in a computationally heavy method. However, this method is able to solve almost any kind of situations.

Belonging to the first group of methods, the following works must be mentioned. Considering *2D* geometries, works in [Chandler-Wilde 1995] proposed to write the pressure field due to an omnidirectional sound source above a homogeneous impedance plane as

$$p_{total} = p_{direct} + p_{image} + p_{ground}$$

In this expression, p_{direct} and p_{image} fulfill together a rigid boundary condition on the ground. Thus, p_{ground} compensates for the difference between an infinite impedance value and the actual impedance value of the ground[6]. This last term was then evaluated using the steepest descent method, which had as a consequence to limit the accuracy of the solution to the far field of the source. Besides its limitations, this solution is widely used nowadays, especially in *2D BE* models, to include the effects of a homogeneous impedance plane without having to discretise the ground surface. The study in [Mechel 2000] proposed to expand the well known reflection

[5] One of these methods, the level difference technique, is presented in *Appendix IV*.

[6] A similar approach has been adopted in *Chapter 3* and in *Chapter 4* of the present thesis, where p_{ground} is calculated using the *ES* method.

factor for plane waves into cylindrical harmonics. The resulting solution, again restricted to the far field of the source, is valid for *2D* monopoles only.
To be complete, one should also mention that for *3D* situations, a reflection factor for spherical waves was first proposed in [Ingard 1951], and then corrected in [Thomasson 1976]. Finally, works in [Chien 1975, 1980] proposed the numerical implementation of Q_s defined as

$$p_{total} \;=\; p_{direct} \;+\; Q_s \times p_{image} \quad \text{with} \quad Q_s \;=\; R_p \;+\; (1 - R_p) \times F(w)$$

where R_p is the reflection factor for plane waves and $F(w)$ is an error function, which can be seen as compensating for the error made when considering that spherical waves are reflected as if they were plane. This solution is valid only for omnidirectional point sources radiating over homogeneous impedance grounds. Furthermore, all of the above solutions are valid only for flat grounds, as they make use of an image source.

Alternatively, one may choose to work directly with the general solution to the wave equation, which is expressed as an integral equation. The numerical implementation of such an approach often results in *BE* related methods. It is well known that these approaches demand a large computational effort. However, they have the great advantage of handling the most general situation : a source of arbitrary type radiating over an impedance surface, flat or not, which has a point-wise impedance distribution.
The derivation of such a fundamental approach can be found for instance in [Chandler-Wilde 1985; Habault 1984, 1985]. From this basis, modified methods are designed to optimise the calculation time. In [Jean 1998], a variational approach of the basic integral equation is proposed, a method which was also adopted in [Fadavi 2002]. Also with a view to lowering the calculation time, works in [Defrance 1999] assumed that only objects inside the first Fresnel zone contribute significantly to the radiated sound. One can also mention the work in [Coyette 2000], which proposes an approach especially dedicated to low frequency predictions.

1.4 Summary

In this chapter, the general characteristics of the tyre / road noise are presented. An important fact is that tyre / road contact noise dominates the overall traffic noise at driving speeds as low as around 50 to 60 km/h. At low frequencies, tyre noise is mainly due to the tyre vibrations, whereas at higher frequencies, aero–dynamical sources contribute mostly to tyre noise. The "cross–over" frequency depends on the tyre and the road properties, but it is generally situated between 800 Hw to 1000 Hz.
The problem is further complicated by the radiation condition of the tyre. The horn formed by the tyre and the road in the contact region enhances the radiation efficiency of the sources located in this area. Another factor that influences not only the radiation but also the noise generation is the acoustical absorption from the road surface.
From the modelling point of view, due to the large research effort during the last decades, a number of tools are available for the prediction of tyre noise. They can be classified into statistical models, deterministic models and hybrid models, which use approaches of the two previous categories.

However, none of these models take the road absorption into account neither is adapted to perform the necessary parametrical studies to optimise the tyre / road interface properties. Therefore, a model for the tyre / road noise above arbitrary impedance planes, which is both accurate and numerically efficient, may combine a simple model for the tyre radiation with an integral equation based method to include the ground effects.

In this respect, works in the present thesis are organised as follows.
In *Chapter 2*, a multipole model for the tyre radiation, which is based on works presented in [Kropp 1992], is presented. In *Chapter 3*, an *ES* based model for the ground effects is derived as an alternative method to pure *BE* methods. Resulting from the combination of the two previous models, a model for the tyre radiation over arbitrary impedance planes is derived in *Chapter 4*. Finally, *Chapter 5* presents a short parameter study where the general trends of the tyre noise over impedance surfaces are discussed.

Chapter 2

A Multipole Model of the Tyre Radiation

As seen in the previous chapter, a crucial point of the noise radiation simulation is the reproduction of the sound amplification known as the horn effect. This chapter presents a model based on earlier studies that includes this effect. Special attention is addressed to the understanding of the noise radiation and to the numerical efficiency of the resulting model.
In the first section, the sound amplification is characterized and explained. The multipole model of the tyre radiation is then presented together with the theoretical basis of the approach. In the third section, the model implementation is precised and a number of numerical examples as well as comparisons to measurements are presented to appraise the robustness and the validity of the present model.

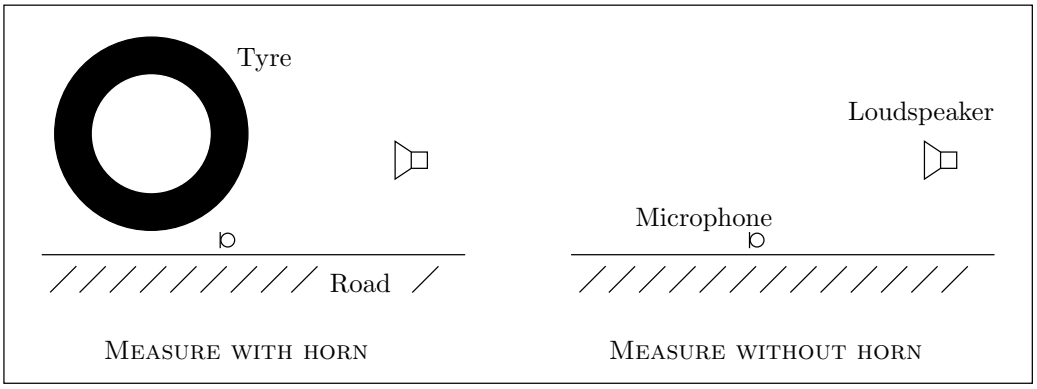

Figure 2-1: *The reciprocity principle applied to measurements of horn effect amplification factors.*

2.1 The tyre as an acoustical source : definitions

Experimental results

The noise emitted by a rolling tyre would have little importance for roadside inhabitants if the noise sources were not placed in a sensitive area. As mentioned in Chapter 1, sound sources are located close to the contact patch, on the leading edge as well as on the rear edge of the tyre / road interface. The horn-like geometry formed by the tyre and the road surface in the contact region significantly amplifies the generated noise and modifies its radiation pattern directivity. This phenomenon known as *horn effect* can be illustrated by measuring the sound pressure level of a given sound source in the presence of the horn and without the horn, for instance by removing the tyre. By taking the ratio of these two measurements, one obtains an amplification factor corresponding to the source and the receiver positions, at a given frequency.

Practically, the characterisation of horn effect is usually performed using the reciprocity principle. Also found in optics, it was first applied in acoustics in [Rayleigh 1945][1]. This principle states that, in a homogeneous media, the source and the receiver positions can be exchanged without changing the properties of the sound propagation between them. A measurement setup making use of this principle is schematised in Fig. 2-1. In such a setup, the noise source is positioned in front of the tyre, in place of a standard microphone position, whereas this latter is set in the contact patch, between the tyre and the road surface. Such measurements of horn

[1]The reader may also refer to [ten Wolde 1973] for a general view on the principle and to [Cremer 1973] for practical applications.

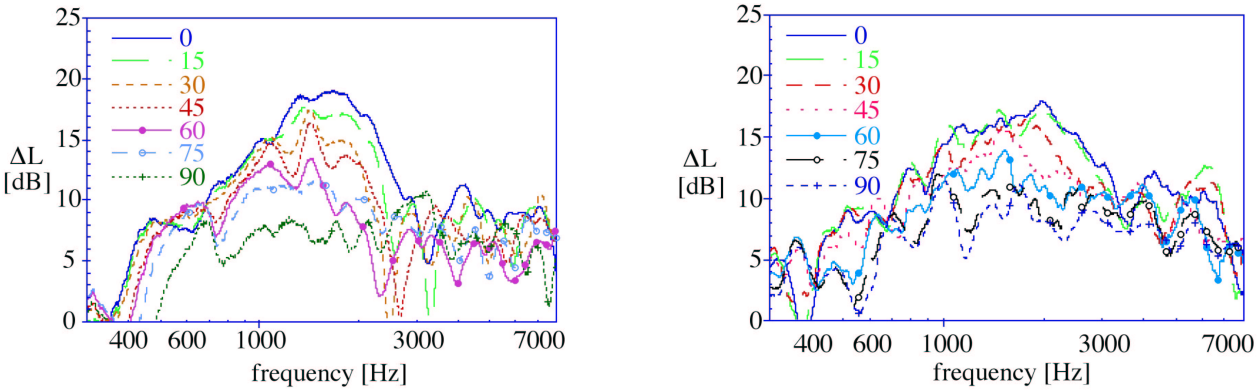

(a) Tyre alone

(b) Tyre mounted on a vehicle

Figure 2-2: *Amplification coefficient for different receiving angles directly over ground 7.5 m distance from the centre of the contact (distance of the source d=10 mm). (Also in [Kropp 2000b])*

effect amplification factors are shown in Fig. 2-2 (similar measurements can be found in earlier studies, e.g. [Schaaf 1982]). Transfer functions are recorded for a series of source positions in the horizontal plane around the tyre. The surface of the road, a rigid asphalt, is considered as acoustically totally rigid.

First, in Fig. 2-2(a), the tyre is standing alone, that is without the influence of the car body. For all incidences, the amplification increases with frequency. Below 400 Hz the amplification is negligible, because the sound wavelength is not influenced by the presence of the tyre. At these frequencies, the sound wavelength is at least about 5 times larger than the tyre width. Around 1–2 kHz, the amplification reaches a maximum. For frequencies above this maximum, the amplification varies because of interferences between different transmission paths. In this frequency range, the amplification rarely exceeds 10 dB. Not surprinsigly, the overall maximum value is found for measurements in the plane of the tyre, i.e. for 0° of incidence; it reaches almost 20 dB at approximately 1.5 kHz. When moving out of the plane of the tyre, the maximum amplifications are lower and the frequencies at which they occur are shifted downwards. However, for 90° of incidence, the amplification still reaches 10 dB, which is quite substantial. For angles close to the perpendicular, the inference pattern is less significant. Amplification factors vary within a few decibels around 10 dB in the measured frequency range.

Fig. 2-2(b) shows the influence of the car body on the horn effect. For this, transfer functions are measured when the tyre is mounted on a light passenger vehicle. Maximum values of

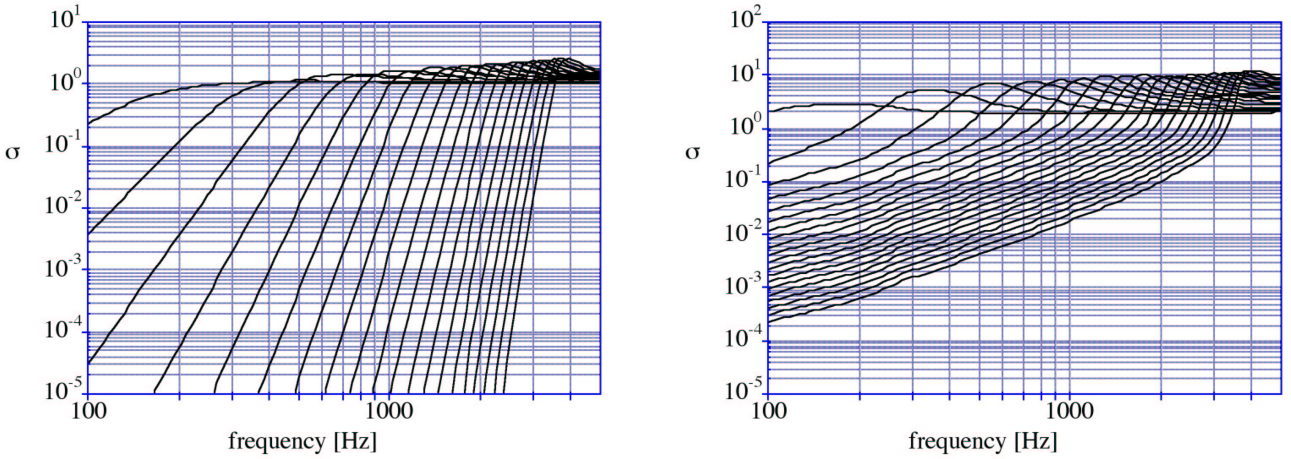

(a) In the free-field

(b) In presence of the road

Figure 2-3: *Compared radiation efficiencies of cylinders. 20 first modes modes in circumferential direction (from left to right). The tyre radius is 0.3 m. (From [Kropp 2000b])*

amplification are somewhat lower than if the tyre is standing alone. However, measured levels in this case are less different for different angles compared to Fig. 2-2(a). This is due to the fact that many more reflections contribute to the sound pressure level when the vehicle body is present, which has the consequence of "equalising" the frequency spectra. The overall maximum is still measured in the plane of the tyre and reaches here around 17 dB. From this set of measured data, the contribution of the horn effect to pass-by noise levels can be estimated. Calculations of Figure 13 and 14 in [Kropp 2000b] prove the horn effect to have a significant influence on pass-by measurements.

Therefore, it seems crucial that an accurate tool for the tyre / road noise prediction includes the correct estimation of the horn effect. Besides a clear simplification of the true geometry, two-dimensional models could give deeper insights into the physics of the sound amplification, as shown in the next paragraph.

Radiation efficiency of vibrating cylinders

In *2D* models, the tyre is represented as an infinitely long cylinder. The radiation efficiency of such a structure can easily be calculated as shown in [Cremer 1973]. The full details of the calculation can also be found in [Kropp 1992]. The cylinder surface is assumed to vibrate with

a normal velocity given as

$$v_n(\varphi) = A_n \cos(n\varphi + \varphi_0)$$

where φ is the angular position of a point on the tyre surface and φ_0 determines the orientation of the mode with respect to the vertical direction. A_n is the amplitude of the n-th mode. Fig. 2-3(a) shows the radiation efficiency of such a cylinder vibrating in a free-field for the first 20 modes. All curves exhibit the same behaviour : the efficiency increases with frequency up to a maximum when the wavelength on the cylinder corresponds to the wavelength in the ambient medium. In the frequency range shown here, that is up to 5 kHz, the low order modes seem responsible for most radiation of sound. This observation has to be related to the results presented in [Kropp 1989] that prove the high order modes to be dominant for the determination of the vibration pattern in the same frequency range. Furthermore, the efficiencies have fairly low levels. All these observations would concur to conclude that the free-field tyre is a rather ineffective radiator.

If the road surface is taken into account, the picture significantly changes. To correspond to a "real" vibration pattern in presence of the road, the contact point always coincide with a node in the vibrational mode. Radiation efficiencies obtained in this case are shown in Fig. 2-3(b). They always have higher values than in the case of a free-field tyre, both below and beyond the coincidence frequency. This result proves that the radiation efficiency is well enhanced by the presence of the road surface. However, special care must be taken to calculate the pressure field when the road is included. Due to the presence of the surface, the vibrational modes do not constitute an orthogonal basis any longer. Therefore, one must include all possible interactions between the modes to obtain the radiated field.

Furthemore, computations presented in [Kropp 1992] show that correct predictions are obtained by including a low number of increasing modes. This confirms the fact that the low order modes are responsible to a major extent for the sound radiated by the tyre whereas higher order modes determine the vibration velocity. This result is of great interest on the numerical point of view because it proves that *2D* models are suited for the prediction of the sound radiation from tyres.

In this respect, a two-dimensional multipole model based on the Equivalent Sources method is presented in the next section.

2.2 The multipole model

The Equivalent Sources method basis

The *ES* method has been successfully applied to deal with the sound radiation from vibrating structures as well as to model the scattering of sound by objects of arbitrary shapes. *Appendix I* presents a thorough review of the method and its applications, in the field of acoustics and electromagnetics. The basic idea of this approach is to reproduce the sound field scattered or radiated by an object by a series of sources, i.e. *equivalent sources*, located inside the body envelop. The unknown source amplitudes are determined so that a given boundary condition on the object surface is best reproduced. Once this is done, the field from the equivalent sources can be calculated at any point outside the body envelop. The accuracy of the prediction depends on how well the boundary condition is fulfilled.

On this basis, a two-dimensional model for the radiation of sound by a tyre rolling on a road surface could be designed [Kropp 1992]. The tyre is set to be an infinite cylinder, the points of which vibrate in phase along its axis. Taking this geometry is an obvious shortcoming to the real shape of a tyre. However, it has the major advantage to allow *2D* cylindrical harmonics to be used as equivalent sources. So that the resulting wave front matches the shape of the object if such a multipole source is located at the tyre centre. This mutlipole is called the original multipole because it is placed above the road surface. Its pressure field can be written as the superposition each elementary harmonics of order m

$$p(r,\varphi,\omega) = \sum_{m=-\infty}^{m=+\infty} A_m \mathrm{H}_m^{(2)}(kr)\mathrm{e}^{\mathrm{j}m\varphi} \tag{2-1}$$

where $k = \omega/c$ is the wave number considered. $\mathrm{H}_m^{(2)}$ is the Hankel function, second kind of order m. A time dependence in $\mathrm{e}^{+\mathrm{j}\omega t}$ is understood and will be omitted in the following. r and φ are the distance and the angle from the multipole position to the observation point. Finally A_m is the amplitude of the m-th harmonic. It has the dimension of a pressure, that is a force per unit are $N \cdot m^{-2}$ or $kg \cdot m^{-1} \cdot s^{-2}$.

The influence of the road surface is accounted for using the image source technique. By placing the mirror image of the multipole symmetrically aside the road surface, an impedance boundary condition can be fulfilled on the infinite plane between them. The strength of the image multipole is set equal to that of the original multipole so that zero normal velocity is achieved on the road surface. The total pressure field at a point above the road surface and outside the

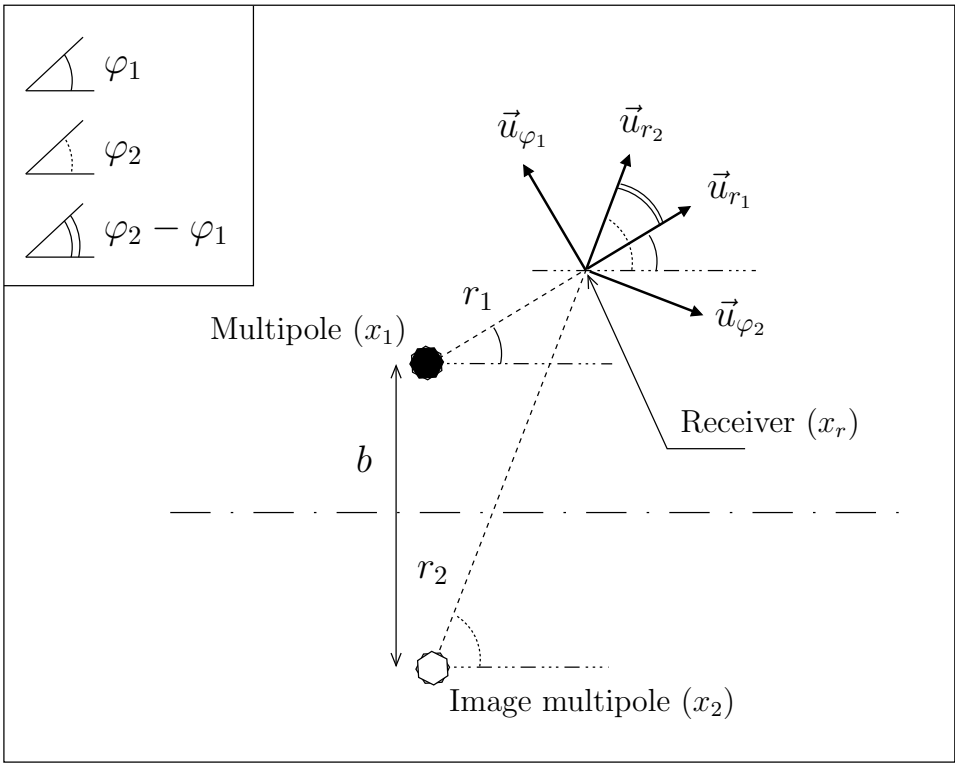

Figure 2-4: *Radial and tangential directions of the contribution from the multipole source and its image.*

tyre body is then expressed as

$$\begin{aligned} p(r,\varphi,\omega) &= p_1(r_1,\varphi_1,\omega) + p_2(r_2,\varphi_2,\omega) \\ p(r,\varphi,\omega) &= \sum_{m=-\infty}^{m=+\infty} A_m \left[\mathrm{H}_m^{(2)}(kr_1)\mathrm{e}^{\mathrm{j}m\varphi_1} + \mathrm{H}_m^{(2)}(kr_2)\mathrm{e}^{\mathrm{j}m\varphi_2} \right] \end{aligned} \tag{2-2}$$

where the subscript 1, respectively (resp.) 2, relates to the co-ordinates of the original multipole, resp. the image multipole. The conventions used for the model geometry are shown in Fig. 2-4.

Theoretically, any kind of velocity distribution can be reproduced by using an infinite number of harmonics. However numerically, one can only include a limited number of these. Therefore, the summation is truncated beyond the order N_{max} which corresponds to the highest harmonic to be included. The determination of N_{max} is discussed in section 2.3.

From the value of N_{max} strongly depends the ability of the resulting multipoles to reproduce the given boundary condition. As far as the modelling is concerned, the sound radiation is determined by the rate of change of the belt deformation, in other words, by the normal par-

ticle velocity of the belt points. This is the boundary condition of the present model. Thus the velocity field due to the present sources is needed on the tyre surface in order to form the boundary condition equation. The calculation of the multipole velocities on the tyre surface is presented in the next paragraph.

Multipole velocity field

With the given time convention, the total velocity due to the original multipole at a point $x_r(r, \varphi)$ in the direction $\vec{n}$ is written

$$v_{total,n}(x_r) = v_{n_1}(x_r) + v_{n_2}(x_r) = -\frac{1}{\mathrm{j}\omega\rho}\nabla p_1 \cdot \vec{n} \; - \; \frac{1}{\mathrm{j}\omega\rho}\nabla p_2 \cdot \vec{n} \tag{2-3}$$

In cylindrical coordinates, the gradient is

$$\nabla p_i = \frac{\partial p_i}{\partial r_i} \cdot \vec{u}_{r_i} \; + \; \frac{1}{r_i}\frac{\partial p_i}{\partial \varphi_i} \cdot \vec{u}_{\varphi_i} \tag{2-4}$$

where $\vec{u_{r_i}}$ and $\vec{u_{\varphi_i}}$ are the unit vectors determining the direction of the field due to the multipole i $(i = 1, 2)$ at the observation point (see Fig. 2-4).

To simplify the calculations, at least for one multipole, the origin of the coordinate system is set to coincide with the location of, for instance the original multipole. In this case, at any point of the tyre surface, $\vec{u_{r_1}}$ is parallel to $\vec{n}$ and $\vec{u_{\varphi_1}}$ is perpendicular to $\vec{n}$. Thus at every point x_{tyre} of the tyre surface, ∇p_1 is parallel to $\vec{n}$ and we obtain

$$v_{n_1}(x_{tyre}) \; = \; -\frac{1}{\mathrm{j}\omega\rho}\,\frac{\partial p_1}{\partial r_1} \; = \; -\frac{1}{\mathrm{j}\omega\rho}\sum_{m=-N_{max}}^{m=+N_{max}} A_m \; k \; \mathrm{H}_m^{(2)'}(kr_1)\mathrm{e}^{\mathrm{j}m\varphi_1} \tag{2-5}$$

The " ' " symbol stands for the derivative of the Hankel function with respect to its argument, here kr_1, which can be written according to [Abramowitz 1972]

$$\forall z \neq 0, \quad \mathrm{H}_m^{(2)'}(z) \; = \; \mathrm{H}_{m-1}^{(2)}(z) \; - \; \frac{m}{z}\,\mathrm{H}_m^{(2)}(z) \tag{2-6}$$

Thus, at a given frequency, the velocity field due to the first multipole is constant over the tyre surface; it does not depend on the angle of incidence. This property will be used in the next paragraph for the determination of the unknown multipole amplitudes.

For the image multipole, the picture is a bit more complicated because the field has a component in both the radial and the tangential directions. The velocity due to the image multipole,

indicated by the subscript 2 can be expressed as

$$v_{n_2}(x_{tyre}) = -\frac{1}{\mathrm{j}\omega\rho}\,\nabla p_2 \cdot \vec{n} \;=\; -\frac{1}{\mathrm{j}\omega\rho}\left[\frac{\partial p_2}{\partial r_2}\;\vec{u_{r_2}}\cdot\vec{n} \;+\; \frac{1}{r_2}\frac{\partial p_2}{\partial \varphi_2}\;\vec{u_{\varphi_2}}\cdot\vec{n}\right]$$

Since φ_1 also gives the direction of the normal to the tyre surface, one can write

$$v_{n_2}(x_{tyre}) = -\frac{1}{\mathrm{j}\omega\rho}\left[\frac{\partial p_2}{\partial r_2}\;\cos(\varphi_2-\varphi_1) \;+\; \frac{1}{r_2}\frac{\partial p_2}{\partial \varphi_2}\;\sin(\varphi_2-\varphi_1)\right]$$

The cosine and the sine function can be expressed as depending only on φ_1 by using the following relationships :

$$r_2\cos\varphi_2 = r_1\cos\varphi_1 \quad \text{and} \quad r_2\sin\varphi_2 = r_1\sin\varphi_1 + b$$

where b is the distance between the two multipoles (see Fig. 2-4). One obtains then

$$\cos(\varphi_2-\varphi_1) = \frac{r_1 + b\sin\varphi_1}{r_2} \quad \text{and} \quad \sin(\varphi_2-\varphi_1) = \frac{b\cos\varphi_1}{r_2}$$

At this point one can show that these results are in concordance with those presented in [Klein 1998], who uses the angle with the vertical such that $\Phi_1 = \varphi_1 + \pi/2$. With such a convention,

$$\begin{aligned}\cos(\varphi_2-\varphi_1) &= \frac{r_1 + b\sin(\Phi_1-\pi/2)}{r_2} = \frac{r_1 - b\cos\Phi_1}{r_2}\\ \sin(\varphi_2-\varphi_1) &= \frac{b\cos(\Phi_1-\pi/2)}{r_2} = \frac{b\sin\Phi_1}{r_2}\end{aligned}$$

which are the expressions presented in [Klein 1998]. Finally the velocity on the tyre surface due to the image multipole is written as

$$\begin{aligned}v_{n_2}(x_{tyre}) \;=\; -\frac{1}{\mathrm{j}\omega\rho}\sum_{m=-N_{max}}^{m=+N_{max}} A_m\Bigg[\, k\;\frac{r_1 + b\sin\varphi_1}{r_2}\;\mathrm{H}_m^{(2)'}(kr_2)\\ + \mathrm{j}m\frac{b\cos\varphi_1}{{r_2}^2}\;\mathrm{H}_m^{(2)}(kr_2)\Bigg]\,\mathrm{e}^{\mathrm{j}m\varphi_2}\end{aligned} \tag{2-7}$$

Thus, the total velocity at a point of the tyre surface is the superposition of the fields given by Eq. 2-5 and Eq. 2-7. It has to fulfill the velocity boundary condition on the tyre surface (see section 2.3).

Calculation of the modal amplitudes

The crucial step in the *ES* method is the calculation of the equivalent source strengths. The present unknowns, the multipole amplitudes A_m, are determined so that both multipoles fulfill

together the velocity boundary condition on the tyre surface, which is written ${v_{given}}^2$. Given the sources in presence, the condition that the tyre belt is acoustically rigid can be written as

$$v_{n_1}(x_{tyre}) + v_{n_2}(x_{tyre}) = v_{given}(x_{tyre})$$

More explicitely the boundary equation writes

$$\begin{aligned} v_{given}(x_{tyre}) \;=\; -\frac{1}{\mathrm{j}\omega\rho} \sum_{m=-N_{max}}^{m=+N_{max}} A_m \Big[& k\ \mathrm{H}_m^{(2)'}(kr_1)\mathrm{e}^{\mathrm{j}m\varphi_1} \\ & + k\ \frac{r_1 + b\sin\varphi_1}{r_2}\ \mathrm{H}_m^{(2)'}(kr_2)\ \mathrm{e}^{\mathrm{j}m\varphi_2} \\ & + \mathrm{j}m\frac{b\cos\varphi_1}{{r_2}^2}\ \mathrm{H}_m^{(2)}(kr_2)\ \mathrm{e}^{\mathrm{j}m\varphi_2} \Big] \end{aligned}$$

where (r_1, φ_1) and (r_2, φ_2) are defined on Fig. 2-4 for x_{tyre} being the receiver. At this point, one may notice that the problem may be ill–posed if x_{tyre} happens to be also a point of the road surface. This occurs if the boundary is directly in contact with the road. In this case, a single point would be given two different velocity values : 0 due to the fact that the multipole amplitudes are such that the road surface is rigid, and the value of the given velocity on the tyre surface, which might be different from zero. The difficulty is removed by introducing a small gap between the tyre and the road. A possible interpretation of the presence of such a gap is discussed in section 2.4.

If one write the above equation for all points of the boundary, an equation system is formed. The left hand side contains the velocity distribution on the tyre surface. The matrix on the right hand side is composed of all the transfer functions from the original multipole and from the image multipole to the boundary points. The vector of unknowns comprises the source amplitudes A_m and has $(2N_{max} + 1)$ elements.

Because of the large values of the Hankel function for large orders, the resulting equation system may be badly scaled and approach a singular system. A simple solution to overcome this consists of scaling the multipole amplitudes by the first constant term $\mathrm{H}_m^{(2)'}(kr_1)$ [Klein 1998]. The above equation is then solved for the new unknowns A_m^* defined as

$$A_m^* \;=\; A_m\ \mathrm{H}_m^{(2)'}(kr_1) \tag{2-8}$$

[2]The consequences of the choice of v_{given} are examined in section 2.3.

Therefore, the boundary condition on the tyre surface becomes

$$\begin{aligned} v_{given}(x_{tyre}) &= -\frac{1}{\mathrm{j}\omega\rho} \sum_{m=-N_{max}}^{m=+N_{max}} A_m^* \Big[k\, \mathrm{e}^{\mathrm{j}m\varphi_1} \\ &\quad + k\, \frac{r_1 + b\sin\varphi_1}{r_2}\, \frac{\mathrm{H}_m^{(2)'}(kr_2)}{\mathrm{H}_m^{(2)'}(kr_1)}\, \mathrm{e}^{\mathrm{j}m\varphi_2} \\ &\quad + \mathrm{j}m \frac{b\cos\varphi_1}{{r_2}^2}\, \frac{\mathrm{H}_m^{(2)}(kr_2)}{\mathrm{H}_m^{(2)'}(kr_1)}\, \mathrm{e}^{\mathrm{j}m\varphi_2} \Big] \end{aligned} \tag{2-9}$$

The next step is to invert this equation system and compute the unknowns A_m^*. The multipole source strengths A_m can then be computed using Eq. 2-8. Thereupon, the pressure field at any points above the road surface and outside the tyre envelop can be calculated from Eq. 2-2 and Eq. 2-13. And thereby the modelling of the tyre radiation due to a given vibration pattern is completed.

2.3 Implementation and amplification factors

In the following section, the numerical implementation of the model is presented. First, the computation of the multipole source strength is explained. The choice of the boundary condition, which is addressed to the calculation efficiency, is also justified. Finally the possible amplification factors due to the horn effect are presented.

Numerical solution

Using matrix notations, Eq. 2-9 can be written as

$$\mathbf{V}_{given} = \mathbf{M}\, \mathbf{A}^* \tag{2-10}$$

where

$$\begin{aligned} \mathbf{V}_{given} &= [\, \ldots, v_{given}(x_{tyre}), \ldots \,]^T \\ \mathbf{A}^* &= [\, \ldots, A_m^*, \ldots \,]^T \qquad \text{for} \quad m = -N_{max}, \ldots, +N_{max} \end{aligned}$$

Depending on the size of the transfer function matrix $\mathbf{M}$, a number of inversion techniques are available. If N_{tyre} denotes the number of points set to discretize the tyre surface, the size of the matrix $\mathbf{M}$ is $(N_{tyre} \times (2N_{max} + 1))$.

The simplest case, which also gives the most accurate solution, occurs if the matrix is square, that is if $N_{tyre} = (2N_{max} + 1)$. It corresponds to taking as many equivalent sources as points on the boundary. This yields a classical collocation technique, and the matrix inversion can be performed using standard Gaussian elimination, also called method of pivots. In this case, the system has a unique solution and the prediction error on the boundary is zero at each point. The major drawback of this technique is that it becomes cumbersome when dealing with large meshes because the size of the system increases with the square of the number of boundary points. In the worst case, the *ES* becomes comparable to boundary integral equation based methods, which also use collocated systems.

The most common case, but not the simplest one, is $\mathbf{M}$ being non-symmetric and having dimensions such that $N_{tyre} > (2N_{max} + 1)$. This is encountered when the situation requires a fine mesh while one wants to optimize the computational effort by keeping a reduced set of sources. The resulting equation system is then over-determined and a minimisation technique must be employed.

From a mathematical point of view, the inversion of a non-square matrix needs to be performed. This can be done by using, for instance, the Singular Value Decomposition (*SVD*). The basic idea of this technique is to isolate the eigen-values with the following scheme by introducing a column orthogonal matrix $\mathbf{V}(N_{tyre} \times (2N_{max}+1))$ and a square orthogonal matrix $\mathbf{W}((2N_{max}+1) \times (2N_{max}+1))$.

$$\mathbf{M} \;=\; \mathbf{V} \begin{bmatrix} \Psi_{-N_{max}} & \dots & 0 \\ \dots & \ddots & \dots \\ 0 & \dots & \Psi_{+N_{max}} \end{bmatrix} \mathbf{W}^T$$

The determination of $\mathbf{V}$ and $\mathbf{W}$ can be found for instance in [Press et al. 1986]. The central matrix, say $\mathbf{L}$ contains all the eigen values of $\mathbf{M}$ on the main diagonal.

The inverse of $\mathbf{M}$ is

$$\mathbf{M}^+ \;=\; \mathbf{W}\; \mathbf{N}^+\; \mathbf{V}^T$$

$\mathbf{M}^+$ and $\mathbf{N}^+$ are called pseudo-inverse because they are not square matrices.

The elements of $\mathbf{N}^+$ are the form $1/\Psi_i$ $(i = -N_{max}, \dots, +N_{max})$, all located on the main diagonal. Clearly, if the matrix is nearly singular, few eigen-values are close to zero. To avoid the obvious numerical problems in the computation of $\mathbf{N}^+$, $1/\Psi_i$ is replaced by 0 if Ψ_i is smaller than the computer round-off error. Therefore $\mathbf{M}^+$ can be computed with good acuracy and the optimisation process can be performed.

It is important to note that, by using such a technique, the set of solutions

$$\mathbf{A}^* \;=\; \mathbf{M}^+ \, \mathbf{V}_{given} \quad \text{do not satisfy} \quad \mathbf{V}_{given} \;=\; \mathbf{M} \, \mathbf{A}^*$$

but provide the minimum mean square error ε defined as

$$\varepsilon = \frac{1}{\sqrt{N_{tyre}}} \mid \mathbf{M} \, \mathbf{A}^* \;-\; \mathbf{V}_{given} \mid$$

The solutions A_m^* of the equation system are said to be solutions in the least square sense.
The same procedure can be applied when $N_{tyre} < (2N_{max} + 1)$. This situation is however not recommended because it corresponds to consider very few points on the boundary. This would lead to a useful frequency range limited to low frequencies where the multipole model is expected to be inaccurate due to its two-dimensional character.
The calculation of the multipole source strengths A_m is then straightforward using Eq. 2-8.

Boundary condition

The values of the multipole amplitudes depends strongly on the prescribed velocity. Different distributions yield undoubtedly to different amplifications. The amplification factors can be defined in several ways depending on the type of boundary condition : either the tyre is considered as a radiator or it is viewed as a scatterer. Actually, the scattering case can be also seen as a radiation case where the multipole inside the tyre has to radiate in such a way that a presecribed velocity on the tyre surface is fulfilled. Mathematically, the two approaches yield different derivations, which are emphasised in the following.
On one hand, the tyre belt is assumed to be vibrating. This is referred to as the *radiation* case because the tyre is effectively the noise source. The input to the model of the horn effect prediction is the tyre belt velocity. As only radial motions of the tyre belt contribute to the radiation of sound, the velocity is given only in the direction normal to the tyre surface. Examples of velocity distributions are shown in Fig. 2-5. In this figure, the broken line indicates the position of the tyre belt at rest. The velocity pattern can take the form of a Hanning-like distribution or a less smooth distribution such as a piston inserted in the tyre belt. More generally for the calculation of sound amplification, it can be the superposition of one single mode or the superposition of an infinite number of modes. However, the Hanning-like distribution is the more realistic pattern as it is most similar to the tyre belt deformations due to the contact with the road. In this case, the prescribed velocity is directly given and the boundary condition

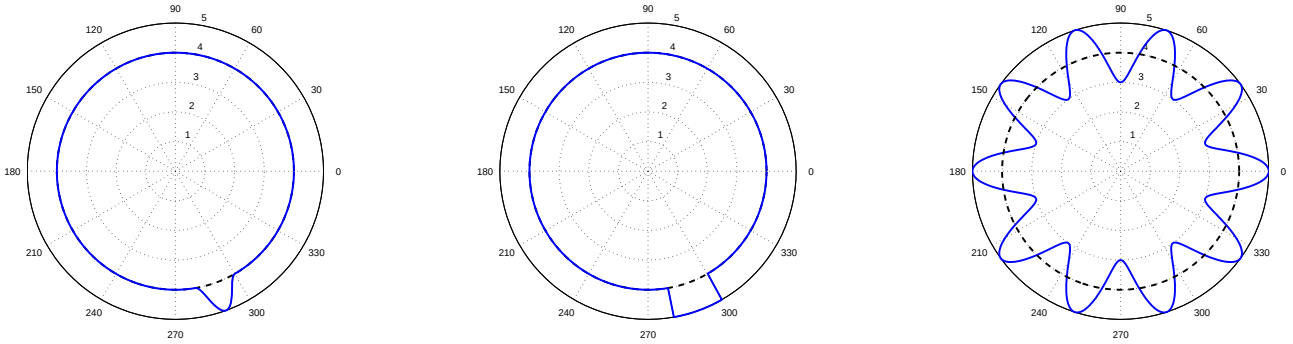

(a) Hanning-like (b) Piston-like (c) 10-th mode

Figure 2-5: *Examples of velocity distributions in the "radiation" case.*

writes

$$v_{given} = v_{rad,n} \qquad \text{and} \qquad v_{n_1} + v_{n_2} = v_{rad,n}$$

On the other hand, the acoustical source responsible for the noise radiation can be considered to be located somewhere inside the horn-like region. This assumption may be based on measurements to localise the noise sources of a rolling tyre (see section 1.1 and for instance [Ruhala 1999]). In this case, the noise source is a simple source placed outside the tyre envelop and the tyre belt is assumed to be rigid, i.e. it is not vibrating. This situation is referred to as the *scattering* case because the tyre surface scatters the field produced by an external sound source. The boundary condition in this case writes

$$v_{given} = 0 \qquad \text{and} \qquad v_{n_1} + v_{n_2} + v_{scat,n} = 0$$

Unlike the radiation case, the normal velocity distribution on the tyre belt must be deduced from the field due to the source inside the horn. In most studies, this latter source is assumed to be omnidirectional even though it can take any form from a dipole to more complicated sound sources.

Between these two cases, the problem will be expressed as the *scattering* one throughout this work. This choice is justified by the fact that most work found in litterature use this assumption (see for instance [Graf 2002; Klein 1998]) and it may be useful to compare the results of these studies with calculations from the present model. Moreover, this type of boundary condition allows the use of the reciprocity principle, which presents several advantages. First, it permits

one to best reproduce the experimental setup and thus to compare more closely measured amplification factors with calculated ones. Secondly, it will be shown in the next section that it is numerically of advantage in terms of accuracy and computational time to use the reciprocity principle also for modelling.
For the sake of completeness however, horn effect predictions obtained considering a *radiation* problem are shown in *Appendix II*.

Horn effect amplification factors

The above paragraph showed that in the *scattering* problem, an acoustical source exterior to the tyre body is introduced. In this case, the pressure field from the source is given and the resulting velocity field on the tyre surface must be deduced. This paragraph first derives the corresponding field expressions. According to the expression of the pressure field, the amplification factors due to the horn effect are presented.
In this study, a *2D* monopole is chosen to represent the noise source. Its pressure field may be written as

$$p_{scat}(x_0 \mid x_r) = q_{scat} \cdot G_0(x_0 \mid x_r) \quad \text{with} \quad G_0(x_0 \mid x_r) = -\frac{\mathrm{j}}{4}\mathrm{H}_0^{(2)}(k \mid x_r - x_0 \mid) \tag{2-11}$$

$G_0(x_0 \mid x_r)$ is the free space Green function calculated at a point x_r due to a source placed in x_0. q_{scat} is the strength of such a source; it is homogeneous to a pressure.
The velocity on the tyre surface is derived from the previous equation. If $\vec{n}$ is the normal vector at a point x_{tyre} of the boundary, it writes

$$v_{scat,n}(x_0 \mid x_{tyre}) = -\frac{1}{\mathrm{j}\omega\rho}\nabla p_{scat} \cdot \vec{n}$$

Because the Green function shows only a radial dependency, the resulting velocity is

$$v_{scat,n}(x_0 \mid x_{tyre}) = -\frac{1}{4\rho c}\, q_{scat}\, \mathrm{H}_1^{(2)}(k \mid x_{tyre} - x_0 \mid)\, \vec{u}_{r_0} \cdot \vec{n} \tag{2-12}$$

where $\vec{u}_{r_0}$ is the unit vector that indicates the direction of the field due to the source located at x_0. Eq. 2-11, resp. Eq. 2-12, define the pressure field, resp. the velocity field, of this monopole source placed in the free-field. In order to take into account the presence of the road surface, a mirror image source is included. The total pressure is then

$$p_{scat}(x_0 \mid x_r) + p_{scat}(\overline{x_0} \mid x_r) = q_{scat} \cdot \left[\, G_0(x_0 \mid x_r) + G_0(\overline{x_0} \mid x_r) \,\right] \tag{2-13}$$

where $\overline{x_0}$ is the position of the monopole mirror source.

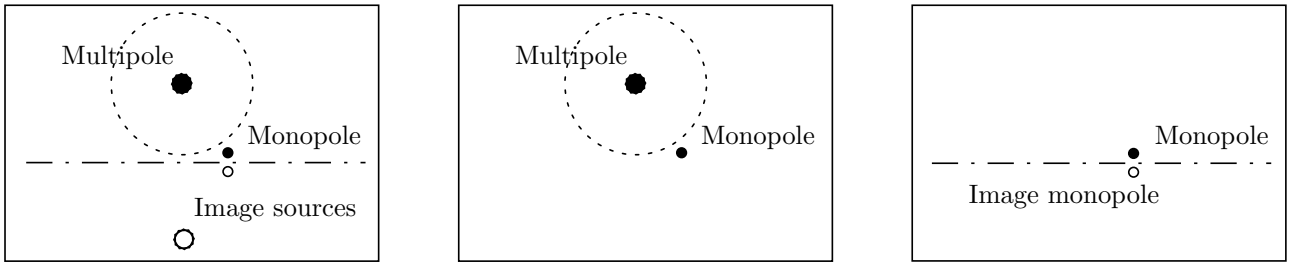

(a) With the horn : p_{tot} (b) Tyre in free-field : p_{ref_1} (c) Road in free-field : p_{ref_2}

Figure 2-6: *Sources in presence for the different horn effect amplification factors.*

Given this type of boundary condition, the total pressure field due to the tyre in the presence of the horn can be computed. It results from the superposition of the fields from the mutlipole located at the tyre centre, the monopole placed close to the contact, and their associated mirror image sources (see Fig. 2-6(a)).

To calculate the amplification factors, two different reference pressures can be considered, which results in two different sound amplifications.

One reference pressure corresponds to the case when the road is removed, that is when the tyre is in free-field. The image sources are removed and the remaining sources are the multipole and the monopole (see Fig. 2-6(b)). In this case the velocity boundary condition on the tyre has changed from the situation where the horn was formed. Indeed, the monopole source, the field of which determines the velocity distribution on the tyre surface, is no longer baffled by the road surface. Therefore, new multipole amplitudes should be computed according to the new boundary condition. The resulting multipole pressure field is denoted $\widetilde{p}_1$ in Eq. 2-14(b). This new pressure field is added to that of the monopole to obtain the reference pressure p_{ref_1}.

The second reference pressure is defined when the tyre is removed, that is when the road is in "free-field" (see Fig. 2-6(c)). In this case, the multipole source and its image are removed. Thus the reference pressure is the superposition of the field form the monopole and its mirror image. It is denoted p_{ref_2} in Eq. 2-14(c). It can be noticed that this reference pressure is usually the one used in the experimental determination of amplification factors, mainly because measurements are easier to perform in this case than in the case of a free radiating tyre.

The expressions of the pressure field corresponding to the Fig. 2-6 are summarised below :

$$\begin{aligned} &\text{(a)} \quad p_{tot}(x_r) &&= p_1(r_1,\varphi_1) + p_2(r_2,\varphi_2) + p_{scat}(x_0 \mid x_r) + p_{scat}(\overline{x_0} \mid x_r) \\ &\text{(b)} \quad p_{ref_1}(x_r) &&= \widetilde{p}_1(r_1,\varphi_1) + p_{scat}(x_0 \mid x_r) \\ &\text{(c)} \quad p_{ref_2}(x_r) &&= p_{scat}(x_0 \mid x_r) + p_{scat}(\overline{x_0} \mid x_r) \end{aligned} \tag{2-14}$$

The amplification factors in decibels are then expressed as

$$\begin{aligned} AF_1 &= 10\log\left|\frac{p_{tot}(x_r)}{p_{ref_1}(x_r)}\right|^2 \\ AF_2 &= 10\log\left|\frac{p_{tot}(x_r)}{p_{ref_2}(x_r)}\right|^2 \end{aligned} \tag{2-15}$$

2.4 Model validation

From the basis of the *ES* method [Machens 1999; Ochmann 1980, 1995], the correct prediction of the boundary is necessary for the good functionning of the method (see also *Appendix I*). However, this condition is not sufficient : a very good prediction of the boundary condition may yield to poor field predictions. For instance, in the case of a vibrating tyre, the modes which are important for the fulfillment of the boundary condition may not be those that are relevant for the correct sound prediction.
In this regards, the fulfillment of the boundary condition is first examined. The computation of the radiated field is then discussed focusing especially on the stability of the predictions. Finally, horn effect amplification factors are compared to measurements to complete the model validation.

Boundary condition prediction

As previously mentioned, the maximum order of the multipole determines to a large extent its ability to reproduce the prescribed velocity on the tyre belt. In this paragraph, the achieved boundary condition is examined as a function of both N_{max} and the size of the equation system. The geometry used in this study is shown in Fig. 2-7. A tyre of 0.3 m radius is placed at 1 mm above a rigid road surface and a monopolar line source is placed at a distance d of the horn centre. The receiver is located on the same side of the tyre as the monopole, 1 m ahead of the multipole, at the same height. Mirror image sources are placed symmetrically aside the

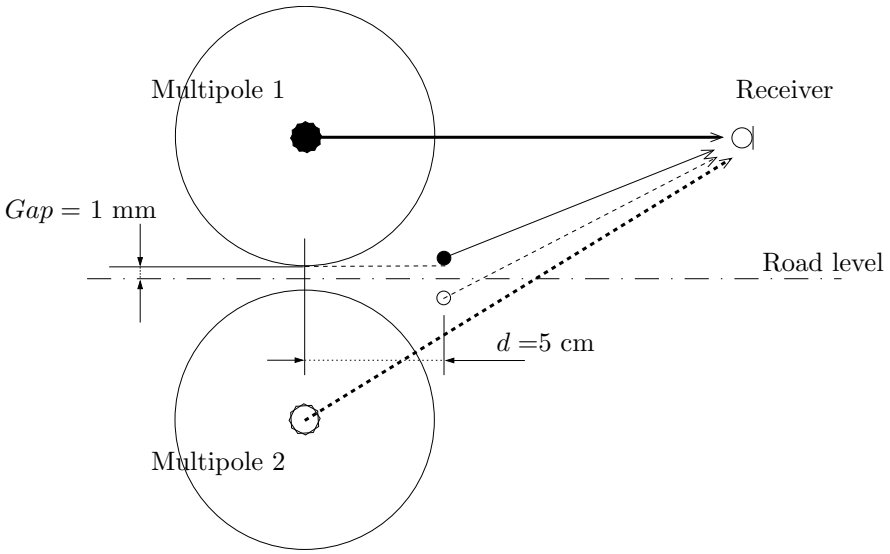

Figure 2-7: *Scheme of the model used for the numerical examples.*

road level so that the road surface is rigid. In Fig. 2-7, the fields from the image sources are indicated by broken lines to distinguish them from the fields of the original sources. All calculations are run at a frequency of 500 Hz. At this frequency, using a 32 order multipole corresponds to take 20 boundary points per wavelength in a collocation situation and even more using over-determined systems. Doing so, possible numerical difficulties due to a too poor discretisation are removed.

Fig. 2-8(a) shows the achieved velocity on the boundary for different multipole orders using collocated equation systems. In this case, the number of boundary points is the same as the number of equivalent sources. Due to the collocation technique, the error at the boundary points is always zero. Therefore the velocity shown on this figure has been computed for a larger set of control points on the tyre surface and the boundary error at these points is shown in Fig. 2-8(c). In this latter figure, the smaller the value, the better the achievement of the boundary condition. It is observed that the prescribed velocity may be well reproduced provided that sufficiently high orders are included. It should be noted here that the results using a multipole of order 32 may not be reliable. This is due to a too low boundary discretisation (65 boundary points using collocated systems), which is not adapted to the rapid variations of the given distribution.

When using over-determined equation systems, the situation changes substantially (see Fig. 2-8(b)). The amount of boundary points is chosen to be twice the number of multipole harmonics

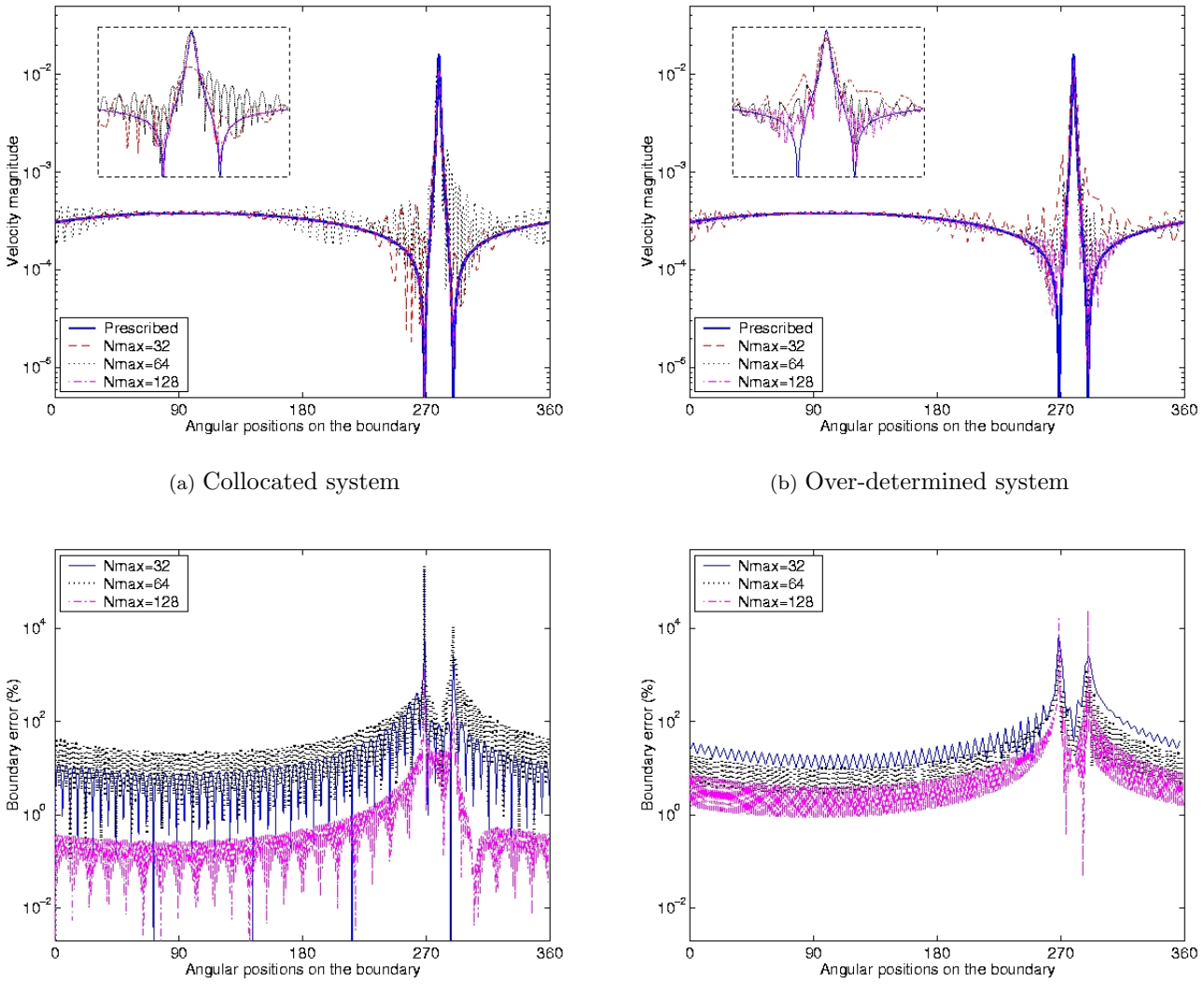

(a) Collocated system

(b) Over-determined system

(c) Collocated system

(d) Over-determined system

Figure 2-8: *Comparison of obtained boundary velocities for different sizes of the equation system using the "direct" geometry. The region of maximum velocity is focused on in the broken-line box.*

($N_{tyre} = 2 \times (2N_{max} + 1)$). Unlike the previous picture, Fig. 2-8(b), resp. Fig. 2-8(d), shows the velocity, resp. the boundary error, computed at the boundary points directly. Because in this case, the error made at these points is the least but not compulsorily zero; larger deviations are expected at points between the boundary points. In fact, even a 128 order multipole cannot provide a satisfactory correspondence with the boundary condition. Using higher order sources would lead to numerical instabilities in the computation of the Hankel functions and

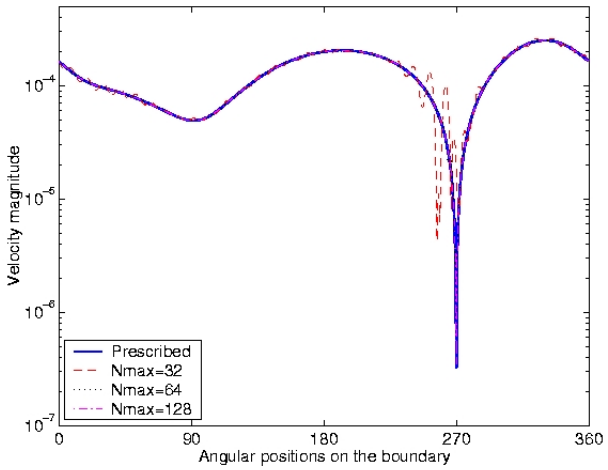

(a) Collocated system

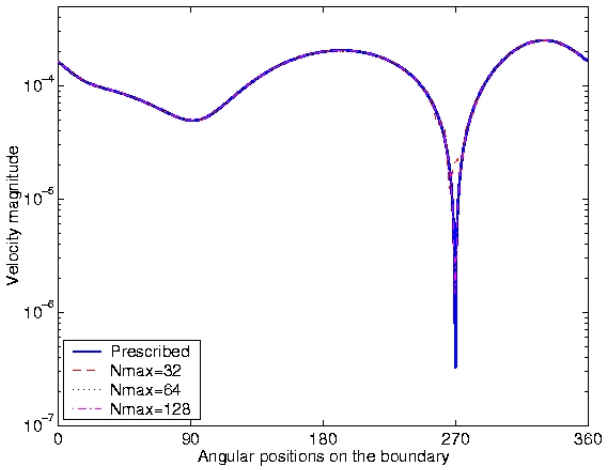

(b) Over-determined system

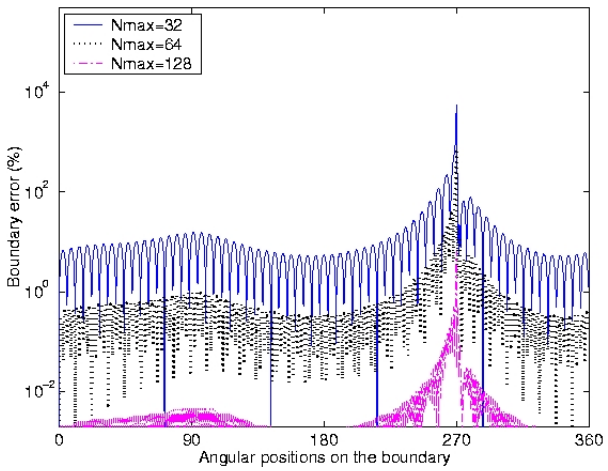

(c) Collocated system

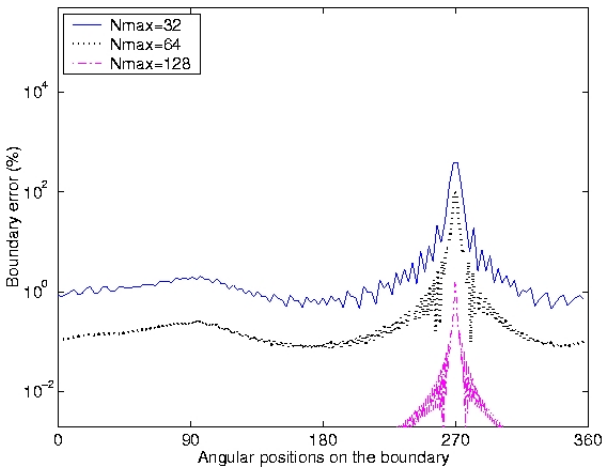

(d) Over-determined system

Figure 2-9: *Same as Fig. 2-8 but using the "reciprocal" geometry.*

the solution would not be accurate anymore. The failure of the *SVD* technique in this case is due to the rapid changes in the velocity distribution, the pattern of which cannot be well reproduced using least square methods. Increasing the number of boundary points reduces the boundary error at the expense however of the computational time.

Thus, the collocation method seems more suitable to yield an accurate solution in the case of a "direct" geometry. The direct term is employed here to distinguish with a geometry that

applies the reciprocity principle. In such a "reciprocal" geometry, the positions of the noise source and the receiver are exchanged. It is interesting to examine this situation as it best approaches the configuration used to measure the horn effect amplification factors.

The model is run for the same parameters as in Fig. 2-8, but setting the monopole sound source in place of the receiver, and the receiver in place of the monopole. As in the "direct" configuration, a mirror image monopole is used to account for the presence of an infinite rigid surface. As before, results are shown for both collocated equation systems in Fig. 2-9(a) and (c), and over-determined equation systems in Fig. 2-9(b) and (d).
The main consequence of the new position of the monopole is that the prescribed boundary velocity has a "smoother" pattern even though it presents a sharp and sizable minimum. With this type of geometry, the predictions for both approaches are significantly better than using the direct geometry. Achieved velocities using a 64 order multipole cannot be distinguished from the given velocity distribution. Particularly, the *SVD* technique seems very accurate using such a geometry as yet a 32 order multipole yields a good prediction of the boundary condition.

Therefore, the "reciprocal" geometry appears to be an interesting configuration to study the horn effect from a modelling point of view too. With this type of geometry, both the collocation method and the least square technique show a true convergence towards the prescribed distribution as the multipole order increases. Nevertheless, the use of collocated systems seems preferable for it gives more stable solutions and higher calculation speeds.
If a very fine boundary discretisation is required, over-determined systems combined with a reciprocal geometry could be thought of as an interesting alternative because it allows to use an average number of sources together with a large set of boundary points. This property is used for the comparison with measurements presented in the last paragraph of this section.

Pressure field prediction

After the boundary condition prediction is discussed, this paragraph examines the calculation of the multipole amplitudes and the consequences on the calculation of the radiated field.
For the horn effect predictions, pressures corresponding to the tyre in free-field and in presence of the road must be computed. An example of multipole amplitudes computed in these two situations is shown in Fig. 2-10 for different frequencies. When the tyre is in free-field (Fig.

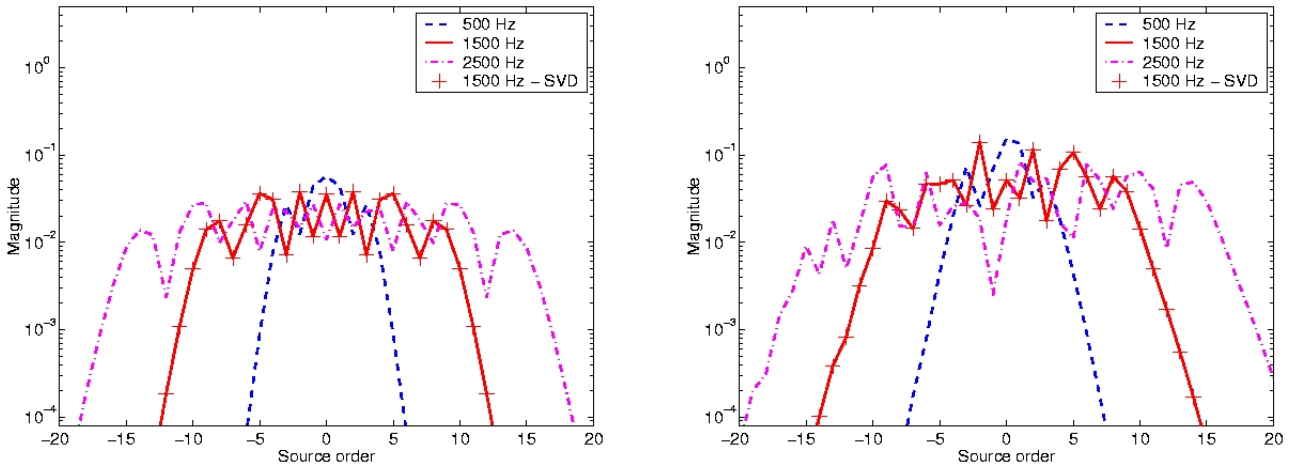

(a) Tyre free-field

(b) Tyre with road

Figure 2-10: *Set of multipole source strengths computed using collocated systems and a reciprocal geometry. $N_{max} = 128$, only the 20 first positive and negative orders are shown.*

2-10(a)), sources of equal order in absolute value have equal amplitudes, as expected. When the road surface is included (Fig. 2-10(b)), the set of source strengths is clearly not symmetrical. This means that all possible interactions between the modes should be accounted for in the calculation of the radiated power. It is also observed that a larger number of modes contribute significantly to the pressure field when the road surface is considered.

In the same figure, the amplitudes of a 64 order multipole obtained using an over-determined equation system at 1500 Hz have been plotted (indicated by crosses). The number of boundary points is set to be the same as for a 128 order multipole using a collocated system, that is $2N_{max} + 1 = 257$. Therefore, the boundary velocity "seen" by the multipoles is the same in both cases. The two sets of amplitudes are almost identical[3], which proves the reliability of the least square minimisation proposed above. This two sets of sources would yield the same field calculation, and thus the same horn effect prediction.

It is worth noting here that the solution using over-determined equation systems leads to higher calculation times compared to the solution using collocated systems. Even though, in this example, the number of elements of the matrix $\mathbf{K}$ to be inverted, is reduced when using the *SVD* technique ((257×129) elements) compared to when using the collocation method ((257×257)

[3]Significant deviations are observed for higher orders, which can not be noted in the set of amplitudes shown in these figures.

elements). Therefore, the difference in calculation times is only due to the type of resolution. Negligible at low frequencies, it increases in the medium and high frequency range to reach around 15 % increase at 5000 Hz, a value which becomes significant, e.g. when carrying parameter studies.

The question is still left open how the stability in the fulfillment of the boundary condition relates to the computation of the amplification factors. For this, horn effect predictions are computed for the geometries corresponding to Fig. 2-8 and Fig. 2-9. Results are shown in Table 2-1 and Table 2-2. It can be observed that using the direct geometry yields more fluctuating amplification factors than using the reciprocal geometry. This latter shows indeed a true convergence of the results.

N_{max}	AF_1 (in db)		AF_2 (in db)	
	Pivot technique	*SVD technique*	*Pivot technique*	*SVD technique*
32	15.5340	18.6206	8.5590	15.9110
64	18.9572	18.5585	15.7395	14.4892
128	18.4799	18.5288	14.2167	14.5267

Table 2-1: Compared horn effect predictions using a **direct** geometry (see Fig. 2-8).

N_{max}	AF_1 (in db)		AF_2 (in db)	
	Pivot technique	*SVD technique*	*Pivot technique*	*SVD technique*
32	18.5171	18.3602	14.5075	14.3506
64	18.5283	18.5264	14.5187	14.5167
128	18.5284	18.5284	14.5188	14.5188

Table 2-2: Compared horn effect predictions using a **reciprocal** geometry (see Fig. 2-9).

Given these considerations, it seems reliable to use the present model to investigate some properties of the horn effect, for instance, the re-direction of sound in space. For this, the *ES* model has been run using a reciprocal geometry for several monopole positions in the space

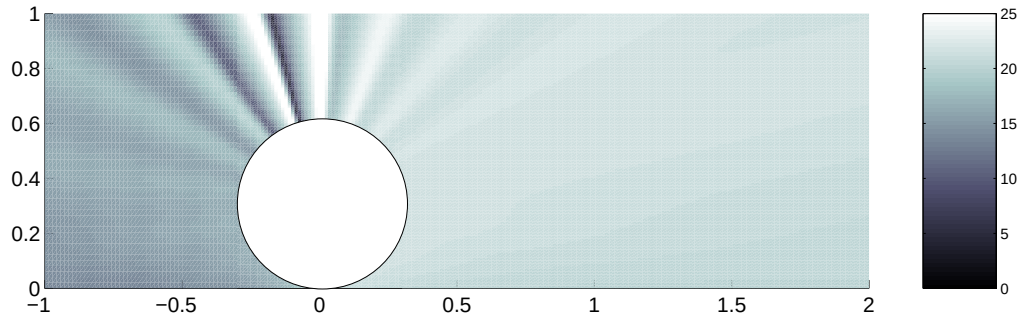

Figure 2-11: *Re-direction of sound due to the horn effect at 1.5 kHz. Reference pressure is* p_{ref_1} *in Eq. 2-14, distances are in meter. The right scale is in dB.*

above the road and outside the tyre envelop. In a direct geometry, this corresponds to moving the receiver while the monopole position is fixed. Again, the two possible reference pressures as defined in Eq. 2-14 have been used to calculate the amplification factors. Results are shown in Fig. 2-11 and Fig. 2-12 where the circular white part represents the tyre body.

Comparing these two figures clearly proves that the different reference pressures yield different amplification factors, both in terms of the spatial distribution as well as the levels of amplification. In fact, taking the freely radiating tyre as reference pressure gives globally higher amplification factors, as also shown in [Klein 1998]. As previously explained, the reason is that the road plane has a stronger baffle effect than the cylinder. Moreover, in both cases, the sound amplification is lessen on the rear side of the tyre compared to the front of the tyre, as expected. Above the tyre, that is opposite to the monopole position, the sound is either amplified or decreased depending on the chosen reference pressure. Interferences in this region of space are important because they may be enhanced by the presence of the wheelhouse. Finally, the re-distribution of sound illustrated in these figures may substantiallly decrease the efficiency of roadside noise protections such as noise barriers.

Comparison to measurements

In order to complete the validation of the multipole model, measurements of horn effect amplification factors are compared to calculations obtained using the present *ES* model and a *BE* model, used as a reference approach.

Measurements have been carried out outdoors over a rigid asphalt, which was assumed to be acoustically rigid. Surrounding objects were far enough so that possible reflections could

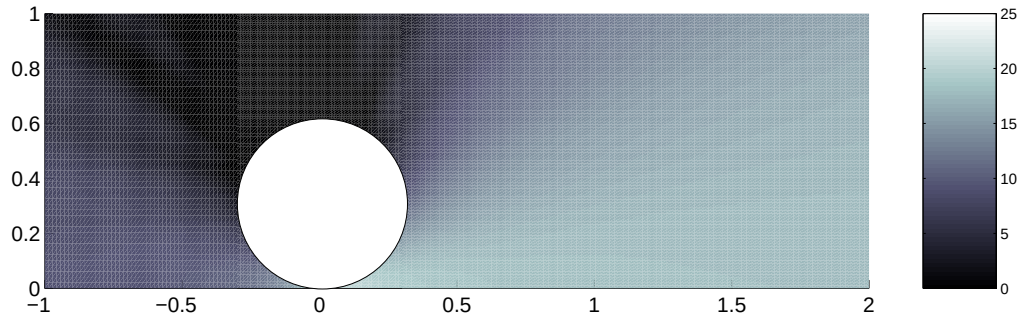

Figure 2-12: *Re-direction of sound due to the horn effect at 1.5 kHz. Reference pressure is p_{ref_2} in Eq. 2-14, distances are in meter. The right scale is in dB.*

be removed by windowing the time signals. As already mentioned, the reciprocity principle was used. This means that the noise source was placed in front of the tyre, 1 m ahead at the ground level. The noise source was a loudspeaker driven with sequences of white noise organised according to the MLS[4] procedure. Transfer functions were recorded by an electret microphone mounted flush with the ground, in presence of the horn and without the horn by removing the tyre. Measurements have been repeated for several values of the distance d from the contact point to the microphone (see Fig. 2-1). The tyre, unloaded, was treadless; its diameter was 62 cm and its width 22 cm.

The multipole model is run using these parameters. Concerning the boundary discretisation, 6 points per wavelength are usually chosen to obtain a correct convergence. This means that a set of 200 boundary points would have been enough up to a frequency of 6 kHz. However, in order to insure a sufficient sensitivity of the model regarding the source displacements inside the horn, the inter-nodal distance is set to be at least three times smaller than the smallest source displacement. This gives a set of 700 boundary points. This implies the use of at least a 350 order multipole in a collocated method, which would undoubtedly would give rise to numerical difficulties. Therefore, it is decided to keep a 87 order multipole and to make use of the least square minimisation presented in section 2.2 to determine the multipole amplitudes.

In parallel, calculations using the boundary element method are performed to remove experimental uncertainties that could false the model validation, e.g. concerning the placement of the noise source inside the horn, and the model limitations, namely it two-dimensional character. Thus, a *BE* model is implemented using the SYSNOISE© software. Elements of type LINE2

[4]Maximum Length Sequence (see for instance [Borish 1983; Schroeder 1979] for more details).

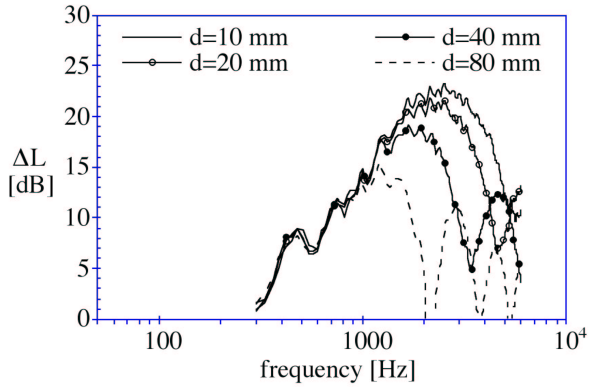

Figure 2-13: *Measured horn effect amplification factors for several distances d (cf. Fig. 2-1). (Also in [Kropp 2000b])*

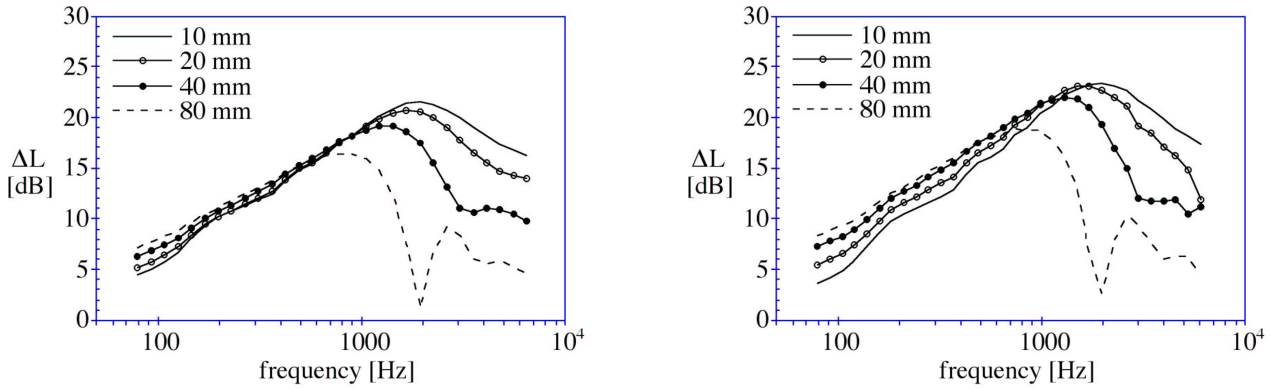

(a) *ES* model (b) *BEM* model

Figure 2-14: *Predicted amplification factors related to measured values in Fig. 2-13. (Also in [Kropp 2000b])*

are used to model an infinite rigid cylinder. The noise source is a cylindrical monopole of unit source strength placed at the ground level. A space of 1 mm is set between the tyre and the ground plane to remove possible singularities.

These two numerical models were run for each distance d. The reference pressure corresponding to the ground in free-field is used for the calculation of the amplification factors (p_{ref_2} in Eq. 2-14). It is worth mentioning here that the required *CPU* time using the *BE* code is approximately five times longer than using the multipole model. Both models were run on the same computer for similar mesh size. Moreover, the *ES* model implemented in MATLAB© was not compiled. Larger differences are therefore expected for a compiled version.

Measured amplification factors are shown in Fig. 2-13. The amplification increases with frequency up to a maximum which position depends on the distance d. As d decreases, that is, as the noise source gets closer to the contact point, the maximum of amplification increases. It reaches 22 dB at 2 kHz for a source 10 mm away from the centre of the horn.

The predictions are shown in Fig. 2-14(a) for the *ES* model and in Fig. 2-14(b) for the *BE* model. Calculated amplification factors are clearly over estimated at low frequencies, due to the two-dimensional character of the models. Besides this discrepancy, the maximum levels as well as the frequencies at which they occur are correctly predicted. The interference pattern is also well reproduced at high frequencies. The very good correspondence between the *ES* model and the *BE* model validate the present approach[5].

Besides the position of the source inside the horn, a key parameter for the horn effect is the position of the reflecting plane. Indeed, lifting up the tyre over the road surface has the same influence as moving the source out of the horn. For instance, the peaks of a very rough road may induce a shift between the position of the outer road surface on which the tyre lays, and the position of the acoustical reflecting plane. This parameter essentially determines the strength of the amplification.

This effect is investigated experimentally by measuring amplification factors for different heights of the tyre above the road. The tyre height is successively set to 0 mm (contact), 1.5 mm, 3 mm, 5.5 mm. The road surface is compact enough to liken the outer surface with its reflecting plane. Measurements are shown in Fig. 2-15. A behaviour similar to that of Fig. 2-13 is observed. Whereas the amplification is identical at low frequency, there exists a frequency, different for each tyre height, from which the amplification is decreased in comparison to the case when the tyre is in contact with the road. This frequency is lower for increasing heights. Calculations from the *ES* model displayed on the same figure follow well this behaviour. These results may explain the somewhat suprising observation that rolling on very rough roads leads to lower radiation at high frequencies compared to rolling on roads having a smaller roughness amplitude. This effect is also investigated numerically in *Appendix II* for the "radiation" problem.

[5]These results have been presented in [Kropp 2000b]

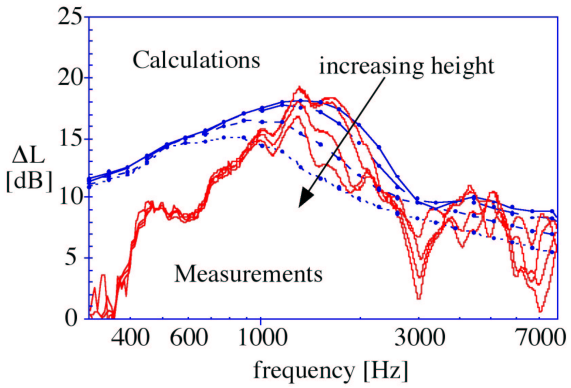

Figure 2-15: *Measured horn effect amplification for different height of the tyre above the road. (Also in [Kropp 2000b])*

2.5 Summary

In this chapter, a mathematical model for the tyre noise radiation has been derived on the basis of the *ES* method. This choice is addressed to the numerical efficiency of this technique compared to other approaches such as *BIE* based methods.

The horn effect amplification factors calculated using the present model are in excellent correspondence with those obtained using *BE* codes. Furthermore, comparisons with measurements prove the *ES* model limitations to be only due to its two-dimensional character. Namely above 500 Hz, the *ES* model gives correct levels of amplification and reproduces well the interference pattern due to the multiple reflections occuring inside the horn.

Because it is as accurate as to be sensitive to key parameters such as the source position inside the horn or the position of the reflecting plane, the present model allows to give further insights into the physics of the tyre / road noise emission. In particular, the vibrational modes responsible for the noise emission were identified and distinguished from those determining the vibrational velocity. Due to its numerical efficiency compared to *BE* codes, this model could be used to perform the parametrical studies needed for the optimisation of the properties of the tyre / road interface.

But some improvements are still needed. For instance, a *3D* model would be required for the correct prediction of tyre noise at low frequencies. This drawback is partially masked by the use of $L_{eq}(A)$ levels to assess the roadside noise levels because this spectral filter reduces the contribution of the low frequency components and strengthens the spectrum around 1 kHz, frequencies at which the model is accurate.

Another geometrical approximation concerns the shape of the tyre supposed to be perfectly circular. In reality indeed, the tyre belt is deformed by the vehicle load (around 250 kg per wheel for a light passenger car), which has for consequence to deform the tyre / road interface and to modify substantially the horn effect amplification factors. However, it has been shown recently in [Graf 2002] that the effect of the loading deformation could be reproduced to a large extent by using an undeformed tyre while shifting the position of the noise source inside the horn.

The last critical point of the model, which can be by no means compensated for, is the acoustical property of the road surface. Due to the model design, the road is acoustically rigid and an eventual absorption of sound by the road is not included in the present implementation. Alternative methods, presented in Chapter 4, section 4.1, could be thought of but they result in a very limited range of applications.

Instead the elected method should be numerically efficient and should still be able to account for the elaborated acoustical properties of road surfaces. In this respect, an original model for the sound propagation of arbitrary sound fields, which is based on the *ES* method, has been designed and is presented in the next chapter.

Chapter 3

Ground Effects Modelling Using the *ES* Method

A complete model for the tyre / road noise must include the acoustical properties of the road surface. After having described the source field in the previous chapter, the modelling of its propagation over arbitrary surfaces is proposed here.

In this respect, the present approach, which is based on the *ES* method, describes the radiation of an arbitrary, *2D* sound source over a piece-wise constant impedance ground. The aim is that the resulting model for the ground effects could be coupled to the previous *ES* model for the tyre radiation.

First, the technique is derived and its numerical implementation is presented. The resulting model is then validated on the basis of comparisons with analytical solutions and measurements. Finally, the features of the present approach are emphasised and addressed to the tyre / road noise modelling.

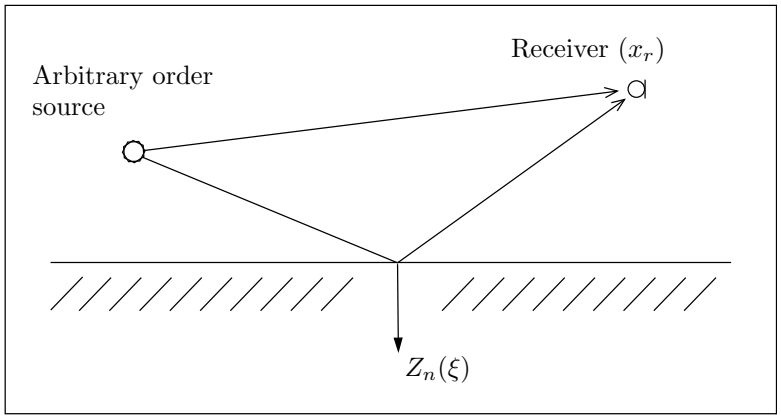

Figure 3-1: *Source radiating over a arbitrary impedance surface.*

3.1 Principle and description

In this chapter, attention should be paid to the chosen time convention, even though, the present derivation holds whatever the time dependence. In order to compare with analytical solutions available from literature, a time dependence in $e^{-j\omega t}$ is assumed in this chapter. The consequences of this choice compared to using $e^{+j\omega t}$ are mentioned in the text when appropriate.

Theoretical basis

The *ES* method has been suggested as an accurate technique to model the sound radiated by vibrating structures. It was also proved to be an efficient tool to simulate the scattering of sound by objects of arbitrary shape (see *Appendix I*). Normally sources are placed inside the object body and the amplitudes of these sources are adjusted in such a way that a given boundary condition on the object surface is fulfilled.

The basic idea of the technique proposed here is to replace the boundary by sources fulfilling the prescribed condition even though these sources are located directly on the surface. This approach, also used in [Kropp 1998], can be viewed as controlling the boundary impedance by means of active sources at the points where the impedance value differs from that of the surrounding medium. The use of physical sources clearly distinguishes this approach from integral equation based approaches which use single or double layer potentials, although this difference might be more academic.

The situation, two-dimensional, is that of an incident sound source radiating over a flat surface

of arbitrary acoustical impedance (see Fig. 3-1). The source is of arbitrary type; it can have monopolar characteristics or more complicated radiation patterns. The sources on the ground are set to be monopoles. Therefore, the total pressure at a point x_r of the half space above the ground can be written as the superposition of the sound field due to the original source, denoted p_0, and the sound field due to the sources on the ground surface, denoted p_Γ :

$$\begin{aligned} p_{tot}(x_r) &= p_0(x_r) + p_\Gamma(x_r) \\ \text{or} \quad p_{tot}(x_r) &= p_0(x_r) + \int_\Gamma Q(\xi)\, G(\xi \mid x_r)\, \mathrm{d}\xi \end{aligned} \tag{3-1}$$

In this equation, $Q(\xi)$ is the unknown source density associated with the sources on the ground; $G(\xi \mid x_r)$ is the Green function for the pressure calculated at the point x_r due to a source at a point ξ of the ground surface Γ.
The total velocity in the direction $\vec{n}$ is expressed as previously by introducing the Green functions for the velocity $G^{(v,n)}$

$$\begin{aligned} v_{tot,n}(x_r) &= v_{0,n}(x_r) + v_{\Gamma,n}(x_r) \\ \text{or} \quad v_{tot,n}(x_r) &= v_{0,n}(x_r) + \int_\Gamma Q(\xi)\, G^{(v,n)}(\xi \mid x_r)\, \mathrm{d}\xi \end{aligned} \tag{3-2}$$

The boundary condition is expressed using the value of the acoustical impedance of the ground in the normal direction, $\vec{n}$, pointing inside the ground. The impedance at a point x of the surface Γ is expressed as

$$Z_n(x) = \frac{p_{tot}(x)}{v_{tot,n}(x)} \tag{3-3}$$

By combining Eq. 3-1 and Eq. 3-2 written at a point x of the surface Γ, the previous equation becomes

$$p_0(x) + \int_\Gamma Q(\xi)\, G(\xi \mid x)\, \mathrm{d}\xi = Z_n(x)\, v_{0,n}(x) + Z_n(x) \int_\Gamma Q(\xi)\, G^{(v,n)}(\xi \mid x)\, \mathrm{d}\xi$$

By re-arranging the terms, the boundary value problem can be written as

$$\begin{aligned} \int_\Gamma Q(\xi)\, G(\xi \mid x)\, \mathrm{d}\xi - Z_n(x) \int_\Gamma Q(\xi)\, G^{(v,n)}(\xi \mid x)\, \mathrm{d}\xi &= \\ -p_0(x) + Z_n(x)\, v_{0,n}(x) & \end{aligned} \tag{3-4}$$

This is an integral equation which can be solved numerically by discretising the boundary. However, some difficulties arise due to the singularities included in the Green functions G and $G^{(v,n)}$ when $x = \xi$, i.e. when the receiver is placed directly at the source position. To overcome this, the integrals containing the singularities are isolated and worked out separately.

The previous equation can be written as

$$I_p(x) \; - \; Z_n(x) \; I_v(x) \; = \; -p_0(x) + Z_n(x) \; v_{0,n}(x)$$

where I_p, resp. I_v, is an integral for the pressure, resp. for the velocity. Let us denote by E_j the element of the ground surface on which the receiver x lies. Then Γ can be expressed as $\Gamma' \cup E_j$ where Γ' embraces the whole surface except the element E_j. Thus both I_p and I_v contains an integral which is said to be regular over Γ', and a singular integral over the element E_j :

$$\begin{aligned} I_p(x) &= \int_{\Gamma'} Q(\xi') \; G(\xi' \mid x) \; \mathrm{d}\xi' \quad + \quad \int_{E_j} Q(\xi_j) \; G(\xi_j \mid x) \; \mathrm{d}\xi_j \\ I_v(x) &= \underbrace{\int_{\Gamma'} Q(\xi') \; G^{(v,n)}(\xi' \mid x) \; \mathrm{d}\xi'}_{\text{regular integrals}} + \underbrace{\int_{E_j} Q(\xi_j) \; G^{(v,n)}(\xi_j \mid x) \; \mathrm{d}\xi_j}_{\text{singular integrals}} \end{aligned}$$

The singularity is encountered when ξ_j "meets" x. Rigorously, the integrals should be evaluated at all points of the element surface. Instead in this study, as usually done in standard numerical integration schemes, the integral is evaluated only for values of x at the element's mid point. This is done while assuming that the source density function Q is slowly varying over the element length. This assumption is valid only if the impedance is also slowly varying over the element length, and the discretisation is fine enough.
Therefore, it is sufficient to compute the source density merely at the element mid point. Furthermore Q can be taken out of the integrals in the previous equations and Eq. 3-4 becomes

$$\begin{aligned} Q(x) \Bigg[\int_{\Gamma'} G(\xi' \mid x) \; \mathrm{d}\xi' + \; \int_{E_j} G(\xi_j \mid x) \; \mathrm{d}\xi_j \\ - \; Zn_(x) \int_{\Gamma'} G^{(v,n)}(\xi' \mid x) \; \mathrm{d}\xi' + \; \int_{E_j} G^{(v,n)}(\xi_j \mid x) \; \mathrm{d}\xi_j \Bigg] \\ = \; -p_0(x) \; + \; Z_n(x) \; v_{0,n}(x) \end{aligned} \qquad (3\text{-}5)$$

This is a "simple" boundary equation from which the unknowns $Q(x)$ can be determined using for instance a standard Gaussian elimination. Once it is done, the pressure at any point of the half space above the ground can be calculated using Eq. 3-1.

Green functions' integration

This paragraph presents the expression of the Green functions and the calculation of the integrals contained in Eq. 3-5. In fact, this computation represents the main critical point of the model.

The Green functions for a point source radiating over a flat, rigid or soft plane can easily be found by introducing a mirror image source at $\overline{x}_s$. For the chosen time convention[1], it is written

$$G(x_s \mid x_r) \;=\; -\frac{\mathrm{j}}{4}\left[\mathrm{H}_m^{(1)}(k \mid x_r - x_s \mid)\mathrm{e}^{\mathrm{j}m\varphi} \;\pm\; \mathrm{H}_m^{(1)}(k \mid x_r - \overline{x_s} \mid)\mathrm{e}^{\mathrm{j}m\overline{\varphi}}\right] \tag{3-6}$$

where m is the order of the source and φ, resp. $\overline{\varphi}$, is the angle with the horizontal direction from the source, resp. from the image source, to the receiver. The plus sign corresponds to a rigid ground whereas the minus sign corresponds to a perfectly soft ground.

Pressure and velocity Green functions are connected by[2]

$$G^{(v,n)}(x_s \mid x_r) \;=\; +\frac{1}{\mathrm{j}\omega\rho}\nabla G(x_s \mid x_r)\cdot\vec{n}$$

In this study, the ground sources are set to be only monopoles embedded in a rigid baffle. Hence, the Green functions for the ground sources can be written

$$\begin{aligned} G(x_s \mid x_r) &= -\frac{\mathrm{j}}{2}\,\mathrm{H}_0^{(1)}(k \mid x_r - x_s \mid) \\ \text{and}\quad G^{(v,n)}(x_s \mid x_r) &= \frac{1}{2\rho c}\,\mathrm{H}_1^{(1)}(k \mid x_r - x_s \mid)\,\vec{u}_r\cdot\vec{n} \end{aligned}$$

where $\vec{u}_r$ is the radial direction of the source contribution.

The integration of these expressions can be performed numerically with arbitrary accuracy on the length Γ' of ground. In particular, if the sources are on the ground, the integral for the velocity vanishes : the vector $\vec{u}_r$ is always perpendicular to the surface normal $\vec{n}$, and their product is indeed zero. Thus

$$\int_{\Gamma'} G^{(v,n)}(\xi' \mid x)\;\mathrm{d}\xi' = 0 \qquad \forall x \neq \xi'$$

The computation of the singular part needs more attention. It has been shown in [Bécot 2002] that these integrals could be estimated by calculating the Cauchy principal value. It is also proved in *Appendix III* that asymptotic expressions of the Hankel functions could be used to

[1] Hankel function of second kind are used for a time dependence as $\mathrm{e}^{+\mathrm{j}\omega t}$.

[2] A minus sign is required if one uses $\mathrm{e}^{+\mathrm{j}\omega t}$.

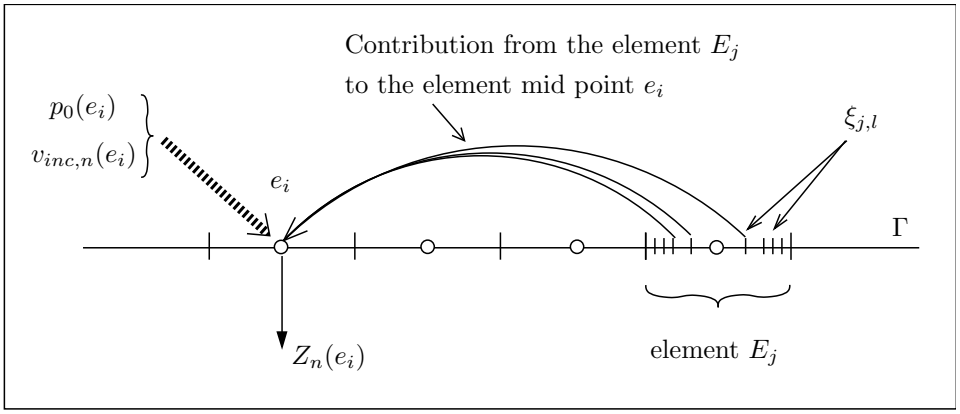

Figure 3-2: *Ground discretisation used for numerical integration.*

yield the same results. According to these, the contributions from the singularities to the pressure and the velocity fields are

$$\begin{aligned} \int_{E_j} G(\xi_j \mid e_j)\ \mathrm{d}\xi_j &= \frac{\Delta}{\pi}[\ln(\frac{k\Delta}{4}) - 1 + \gamma] - \mathrm{j}\frac{\Delta}{2} = I_\Delta \\ \int_{E_j} G^{(v,n)}(\xi_j \mid e_j)\ \mathrm{d}\xi_j &= -\frac{\mathrm{j}}{\rho\omega} \end{aligned}$$

where Δ is the length of the element E_j and γ is the Euler constant.

Numerical implementation

To solve numerically the unknown source amplitudes, the ground surface needs to be discretised. The surface is divided into N elements E_j $(j = 1, \ldots, N)$. The elements mid points are denoted by e_i $(i = 1, \ldots, N)$. The index i is used for the evaluation points of the integral and the index j is used for the integration variables.

With these notations, Eq. 3-5 can be written at an element mid point e_i of the ground surface $(i = 1, \ldots, N)$

$$\sum_{j=1}^{N} Q(e_j) \int_{E_j} G(\xi_j \mid e_i)\ \mathrm{d}\xi_j \ +\ Q(e_i)\ \mathrm{j}\frac{Z_n(e_i)}{\rho\omega} = -p_0(e_i) \ +\ Z_n(e_i)\ v_{0,n}(e_i) \qquad (3\text{-}7)$$

This equation can be written for all element mid points. This forms an equation system which can be expressed using matrix notations as

$$[\ \mathbf{I}_p \ -\ \mathbf{Z}_n \times \mathbf{I}_v\ ]\ \mathbf{Q} \ =\ -\ \mathbf{P}_0 \ +\ \mathbf{Z}_n \times \mathbf{V}_0 \qquad (3\text{-}8)$$

where

$$\mathbf{I}_p = \begin{bmatrix} I_\Delta & \int_{E_2} G(\xi_2 \mid e_1)\ \mathrm{d}\xi_2 & \dots & \int_{E_N} G(\xi_N \mid e_1)\ \mathrm{d}\xi_N \\ \int_{E_1} G(\xi_1 \mid e_2)\ \mathrm{d}\xi_1 & I_\Delta & \ddots & \vdots \\ \vdots & \ddots & I_\Delta & \int_{E_N} G(\xi_N \mid e_{N-1})\ \mathrm{d}\xi_N \\ \int_{E_1} G(\xi_1 \mid e_N)\ \mathrm{d}\xi_1 & \dots & \int_{E_{N-1}} G(\xi_{N-1} \mid e_N)\ \mathrm{d}\xi_{N-1} & I_\Delta \end{bmatrix}$$

$$\mathbf{I}_v = \begin{bmatrix} -\mathrm{j}/\rho\omega & 0 & \dots & 0 \\ 0 & -\mathrm{j}/\rho\omega & \ddots & \vdots \\ \vdots & \ddots & -\mathrm{j}/\rho\omega & 0 \\ 0 & \dots & 0 & -\mathrm{j}/\rho\omega \end{bmatrix}$$

$$\mathbf{Z}_n = [\ Z_n(e_1), \dots, Z_n(e_N)\ ]^T$$

$$\mathbf{Q} = [\ Q(e_1), \dots, Q(e_N)\ ]^T$$

$$\mathbf{P}_0 = [\ p_0(e_1), \dots, p_0(e_N)\ ]^T$$

$$\mathbf{V}_0 = [\ v_{0,n}(e_1), \dots, v_{0,n}(e_N)\ ]^T$$

The largest part of the computational work is required for the computation of the integrals contained in $\mathbf{I}_p$. However, it only depends on the ground discretisation. Therefore, it is possible to reduce the computational effort for different impedance distributions on an invariant geometry.

The numerical integration is also a critical part of the method also because it determines to a large extent the accuracy of the results. In the present work, the numerical integration is performed using a Gauss-Legendre quadrature. The principle of such a procedure is to approximate an integral by a weighted summation. This summation consists of weighted values of the integrand, calculated at different points of the interval of integration. According to this technique [Abramowitz 1972], the integral of the above equation can be written, for $i \neq j$

$$\int_{E_j} G(\xi_j \mid e_i)\ \mathrm{d}\xi_j = \frac{\Delta}{2} \sum_{l=1}^{L} w_l\ G(\xi_{j,l} \mid e_i) + R_L \qquad \text{where} \quad \xi_{j,l} = e_j + \frac{\Delta}{2} x_l$$

x_l and w_l are the abscissae and the weights of the quadrature of order L. R_L is the remainder of the quadrature, which is a measure of the error made using such a procedure. The resulting ground discretisation used to perform the numerical integration is shown in Fig. 3-2.

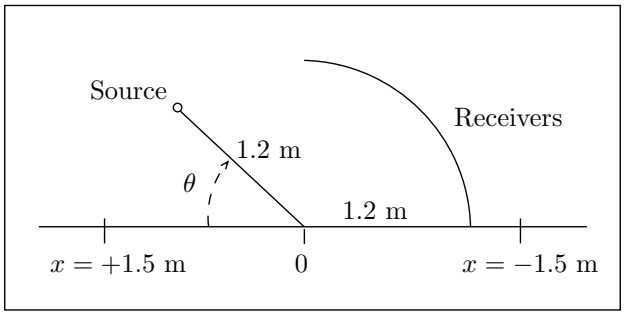

Figure 3-3: *Geometry used for the numerical examples of this chapter.*

Finally, Eq. 3-7 can be simplified by introducing the mirror image of the original source. If the amplitudes of both sources are equal, then the total velocity due to these sources is zero and the pressure is doubled on the ground. This corresponds to fulfill a rigid boundary condition, which can be seen as a primary boundary impedance when Q is zero. In this case, the boundary equation becomes

$$[\ \mathbf{I}_p\ -\ \mathbf{Z}_n \times \mathbf{I}_v\ ]\ \mathbf{Q}\ =\ -\ 2 \times \mathbf{P}_0 \tag{3-9}$$

On the contrary, if the amplitudes have opposite signs, the pressure on the ground vanishes and the velocity is doubled. This corresponds to a totally soft boundary condition and Eq. 3-7 becomes

$$[\ \mathbf{I}_p\ -\ \mathbf{Z}_n \times \mathbf{I}_v\ ]\ \mathbf{Q}\ =\ 2 \times \mathbf{Z}_n \times \mathbf{V}_0$$

As a consequence, in both cases, the layer of ground sources only compensate for the difference between the desired boundary impedance and the impedance value achieved by the original source and its mirror image.

3.2 Model validation

In order to demonstrate the accuracy of the proposed method, some examples are shown in this section. For all the predictions shown below, the implemented Green function includes an image source, which fulfills together with the original source a rigid primary boundary condition on the ground surface (see Eq. 3-9). Details of the ground discretisation are given in each paragraph.

The results are compared in terms of the relative sound pressure levels to remove the influence of the source strength. For this, the pressure level of the source in the presence of the absorbing

surface is normalised by the pressure level of the same source in the free field.
Numerical examples for homogeneous surfaces are presented in the first two paragraphs. The last paragraph presents an experimental validation of the present *ES* model by comparisons to measurements over surfaces having more complex impedance distributions[3].

Trivial case : Dirichlet boundary condition

The geometry for the numerical examples in the first two paragraphs is shown in Fig. 3-3. The geometry is chosen to cover a wide range of angles from grazing incidence to very steep. Two values of the angle θ between the ground plane and the source, as seen from the origin, are used in the examples: $\theta = 5°$ and $\theta = 45°$. These angles are chosen to represent a low source and a high source respectively. The region on the ground where the surface is discretized is between $x = -1.5$ m and $x = +1.5$ m, and a value of 10 elements per wavelength is used in order to ensure good convergence. The results are compared in terms of the sound pressure level relative to the free field. In all the following figures a receiving angle equal to 90° means a receiving point on the ground.
The first comparison is made for the case of the so-called Dirichlet boundary condition. A *2D* monopole is radiating over a totally soft surface, which means that the impedance is zero on the ground. In this case, the exact pressure field can be determined by introducing an image source of opposite source strength as

$$\begin{aligned} & p_{exact}(x_r) &=& \; Q_0\, G(x_s \mid x_r) \;-\; Q_0\, G(\overline{x_s} \mid x_r) \\ \text{or} \quad & p_{exact}(x_r) &=& -\frac{\mathrm{j}}{4}\, Q_0 \left[\mathrm{H}_0^{(1)}(k \mid x_r - x_s \mid) \;-\; \mathrm{H}_0^{(1)}(k \mid x_r - \overline{x_s} \mid) \right] \end{aligned}$$

according to Eq. 3-6. As previsouly mentioned, the influence of Q_0 is removed by comparing relative pressure levels.
In the implementation of the present *ES* model, the primary impedance is infinite on the ground; this corresponds to a totally rigid surface. Therefore, to achieve the desired impedance value, that is $Z_n = 0$, the ground sources are expected to contribute to their largest extent. As seen in Fig. 3-4, the agreement is very good for both source positions. Calculations, which are not shown here, at other frequencies and for other source and receiver positions demonstrate a similarily high accuracy of the present method, at both low and high frequencies as well as for

[3]Some of these results can be found in [Bécot 2002]

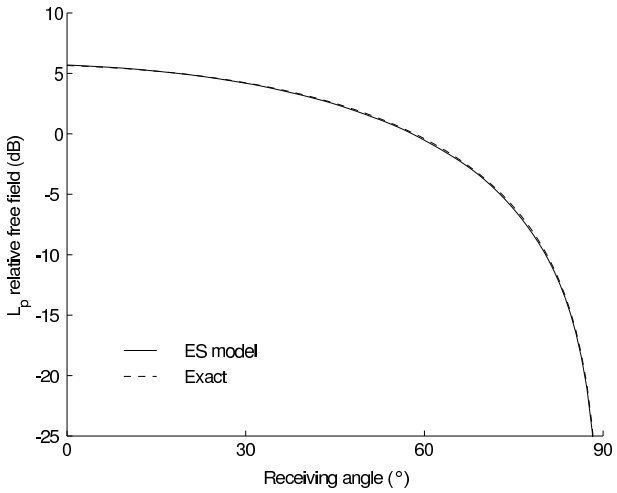

(a) Low source position ($\theta = 5°$)

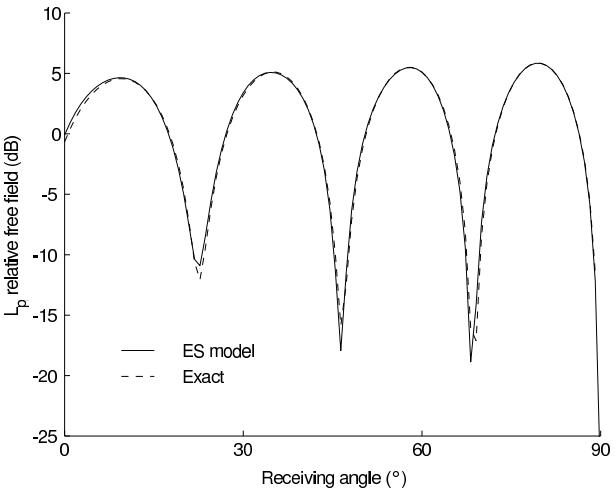

(b) High source position ($\theta = 45°$)

Figure 3-4: *Results for the Dirichlet boundary condition – $Z_n = 0$, $f = 1$ kHz.*

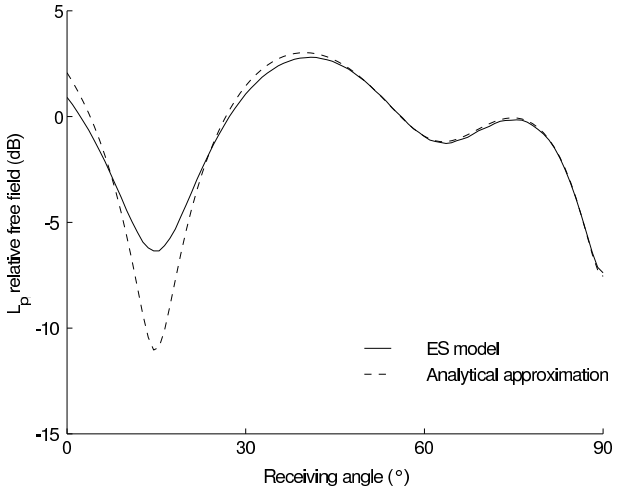

(a) Low source position ($\theta = 5°$)

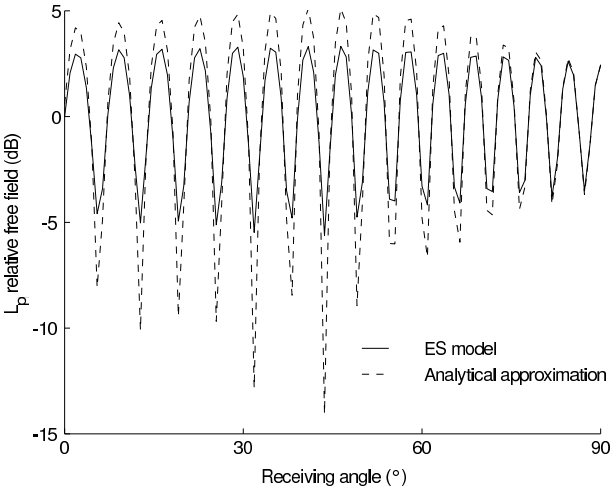

(b) High source position ($\theta = 45°$)

Figure 3-5: *Results for Robin boundary conditions – $\beta = 0.2$, $f = 4$ kHz.*

a large range of geometries.

Robin boundary condition : Homogeneous absorbing surfaces

This paragraph presents numerical examples of sound propagation over finite ground impedance.

The ground absorption is considered in terms of dimensionless normalised admittances, i.e. $\beta = \rho c/Z_n$. The geometry used here is the same as in the previous paragraph (see Fig. 3-3).

In this case, results are compared with results from the model presented in [Chandler-Wilde 1995]. In this latter approach, the total pressure above the ground is expressed as the superposition of the direct sound field and the field reflected at the ground surface. As in the present *ES* model, the Green functions for the direct sound field include the field of an image source, thus fulfilling a rigid boundary condition on the ground. The authors propose to evaluate the reflected sound field by expanding it in plane waves. The resulting expession is however not suitable for direct numerical evaluation. By means of the steepest descent method they obtained an analytical approximation valid for grazing incidence and for limited values of the ground impedance. This method is accurate for medium to low admittance values ($\beta < 0.7$) and for admittance values close to one ($|1 - \beta| < 0.1$).

Given these limitations, the case $\beta = 0.2$, which represents a rather rigid ground, is examined. Results are presented in Fig. 3-5(a) for a low source position and in Fig. 3-5(b) for a high source position. It is clear that the agreement between the models is good at grazing incidence, a condition which is assumed in the analytical approximation. As expected for steeper angles of incidence, the difference increases due to errors in the analytical approximation. Comparisons for softer grounds impedances were also made, but the agreement was not satisfying because of the limitations in the analytical approximation.

Experimental validation

To be able to compare measurements to model calculations, a *2D* omnidirectional source would be needed. Since such a source is difficult to realise, a *3D* point source was used. This might seem inappropriate for our purpose. However, it has been shown in [Duhamel 1996] that sound pressure levels relative to the free field are equal for coherent line source and for a point source, provided that the angle between the ground reflection path and the surface normal is rather high. Therefore it is safe to compare measurements of attenuation for such a source with predictions using the present model.

The source used for the measurements is an electrodynamic driver with a flexible hose attached. The hose was made sufficiently long to be able to remove eventual reflections at the opening inside the flexible tube by windowing the time signals. Considering its power output and its directivity, the useful frequency range of this source lies between 200 Hz and 6 kHz. Measure-

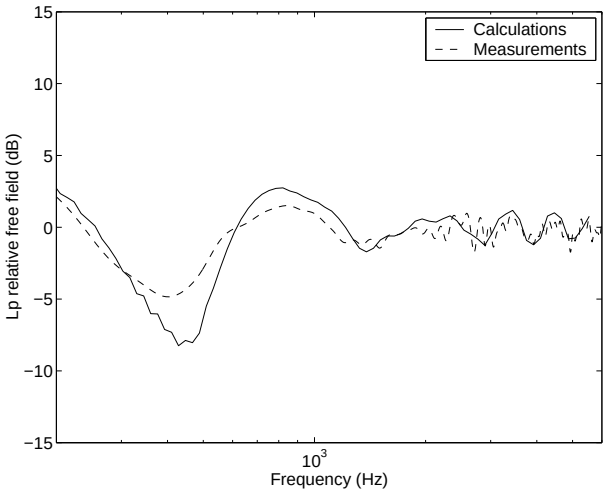

Figure 3-6: *Measured and calculated relative pressure fields over a homogeneous absorbing surface – Source height: 0.3 m, receiver height: 0.3 m, horizontal distance: 0.5 m.*

ments were performed using the MLS[4] technique ensuring that the influence of the background noise could be minimized. Note that some of the following results can be found in [Bécot 2002]. For the impedance ground, panels of mineral wool employed for thermic insulation were used. In all configurations, the flat panels of absorbing material were put directly on a rigid concrete floor. Thus, the material of interest is a hardbacked absorbing material. The acoustic impedance was chosen to characterize the absorbing material. The impedance distribution was determined experimentally using the Level Difference technique (see *Appendix IV* for the details).

With the obtained data, three propagation situations were tested : propagation over an absorbing plane, over a plane with an impedance step and over a strip of absorbing material in a rigid baffle. Within the frequency range of interest, all geometrical configurations were assumed to be two-dimensional. The propagation direction was always perpendicular across the impedance discontinuities.

Results for the sound radiation over a homogeneous absorbing surface are shown in Fig. 3-6. For all frequencies, the agreement between measurements and calculations is good. The largest difference, about 3 dB, found around 500 Hz, might be due to the fact that the value of the relative pressure field is very sensitive to errors in the area of the interference minimum. The

[4]Maximum Length Sequence

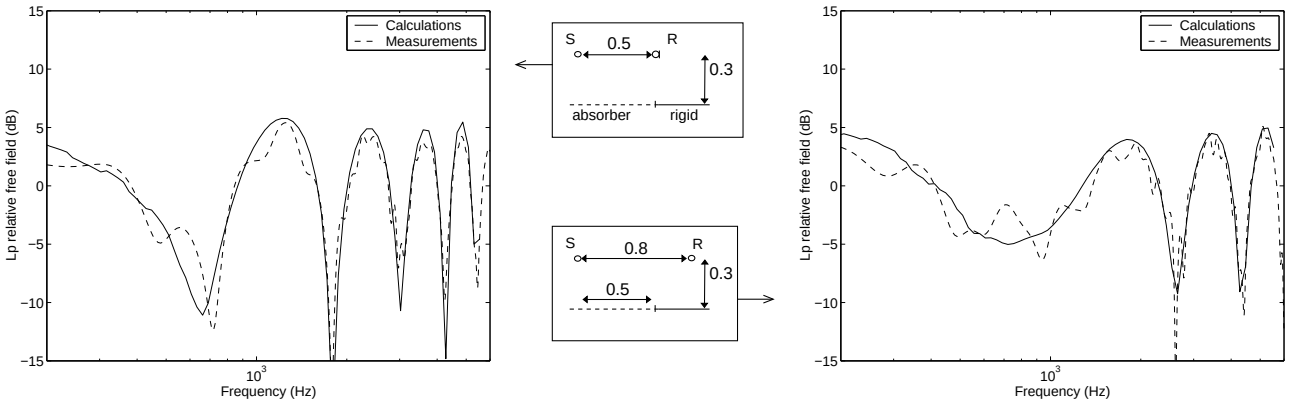

(a) Receiver above discontinuity (b) Geometries (c) Receiver away from discontinuity

Figure 3-7: *Measured and calculated relative pressure fields over a step impedance surface.*

errors can also be caused by the absorbent panels being to small. Besides this, predictions and measurements are within about 1.5 dB. Moreover, the frequencies at which interference maxima and minima occur are well predicted by the model. Measurements for other geometries (not presented here) also showed good concordance with calculations. Results averaged over third octave bands of frequencies presented in [Bécot 2002] also showed very good concordance with the measured values.

Measurements over a surface having one discontinuity of impedance were also performed. In this configuration, a sheet of mineral wool is placed jointly to a large rigid plane. The source is radiating above the rigid surface and the receiver is located above the absorber. This situation is similar to typical traffic noise measurements, where the noise source radiates above a rigid surface (the road surface) while the propagation occurs in most cases above softer grounds like earth or grass lands. Fig. 3-7 shows the measured and predicted values for two different geometries. The exact geometries are drawn in Fig. 3-7(b). In the *ES* model, the ground is discretised from 1.5 m on the left of the source to the impedance step. Significant deviations are observed between measurements and calculations below 1 kHz. However, values in third octave band of frequencies shown in [Bécot 2002] correspond well (less than 3 dB difference). The deviations probably come from diffraction at the side edges of the rigid panel. Above this frequency the predictions are good; the calculations follow the measurements well.

Finally, the sound radiation over a strip of absorbing material embedded in a rigid baffle is investigated (see Fig. 3-8). The width of the strip is 0.43 m. The two geometries used in the

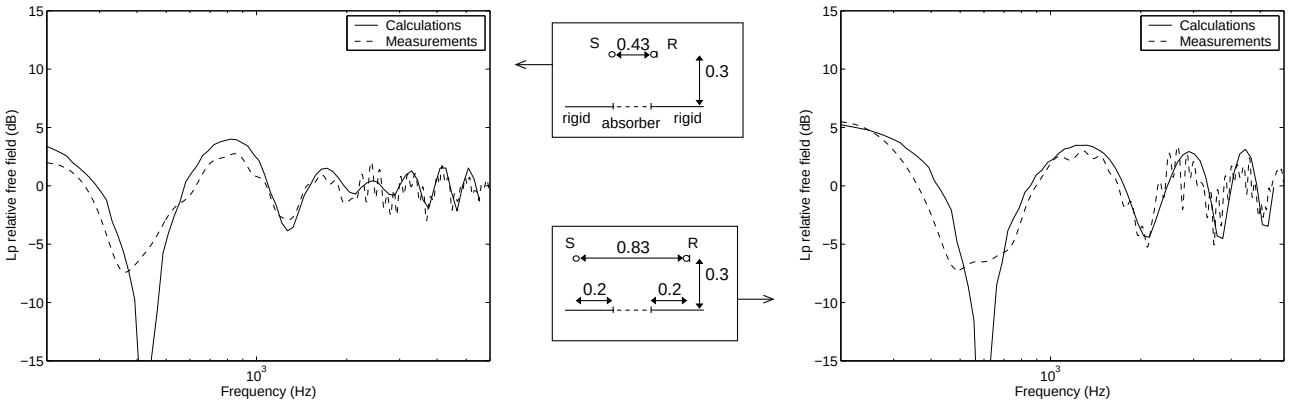

(a) Source and receiver above the discontinuities

(b) Geometries

(c) Source and receiver away from the discontinuities

Figure 3-8: *Measured and calculated relative pressure fields over a strip of absorbing material in a rigid baffle.*

measurements are drawn in Fig. 3-8(b). For the *ES* model implementation, only the ground length corresponding to the strip of absorbing material is discretised. Due to the Green functions used for the incident sound field, the presence of the rigid baffle is automatically accounted for. Large discrepencies are observed between 400 Hz and 600 Hz. It has been checked in [Bécot 2002] that predicted and measured values in third octave band of frequencies correspond well in this frequency range. The deviations are caused by the fact that the pressure levels are very sensitive in this area of minimum interferences. Beyond this frequency range, predictions are in good concordance with the measurements.

In conclusion, the numerical examples and the comparisons with measurements presented in this section prove the method to be suitable for the sound radiation of an omnidirectional sound source over an arbitrary impedance ground. The other features and limitations of the model are examined in the next section.

3.3 Other directional sources

Dipole source over impedance ground

Omnidirectional sources, as examined in the previous section, may represent a heavy shortcoming in real traffic noise situations. As far as tyre noise is concerned, the characteristics of the emitted sound field, which are strongly modified by the horn effect, are shown to be

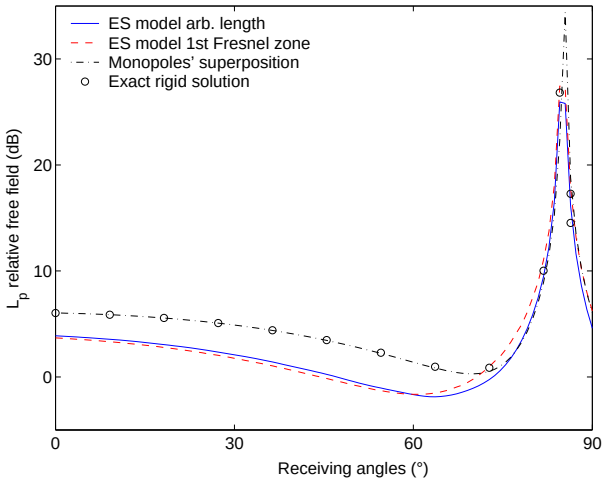

Figure 3-9: *Comparison of different ground discretisations for a dipole source radiating over a homogeneous absorbing ground – $\beta = 0.2$, $f = 1$ kHz, low source position. (Also in [Bécot 2001])*

strongly directional (see for instance Fig. 2-12). As a consequence, it might be difficult to decide how much ground must be included in the surface discretisation. Therefore, the aim of the following calculations is to determine if a reduction of the calculation time is possible by decreasing the length of the discretised ground, under satisfactory accuracy. The possibilities are briefly investigated as the actual optimisation is outside the scope of the present work.

First, the situation of a dipole source radiating over a homogeneous absorbing surface is examined. The geometry is that of Fig. 3-3. Besides integral equation based methods which can handle any kind of situation but are very computationally demanding, no simple reference solutions are available for multipole sources radiating over a finite impedance ground. Therefore, the pressure field from a dipole over an impedance surface is reproduced by the superposition of two monopoles' pressure fields. Each monopole field over the impedance surface is calculated separately according to [Chandler-Wilde 1995]. The two obtained fields are then added to obtain the field of the equivalent dipole radiating over the impedance ground. The representation of such a dipole is valid only if the distance between the monopoles, say a, is small in comparison to the wavelength of interest. Therefore, the reference calculations using the principle of monopole' superposition are run for a separation distance yielding a dimensionless wave number ka around 10^{-5}.

For the implementation of the present *ES* model, two different ground lengths are used. Results are obtained using 10 elements per wavelength either for a ground length corresponding to the

first Fresnel zone[5], or for an arbitrary ground length, namely from x = -1.5 m to x = +1.5 m. Results for the two ground lengths are shown in Fig. 3-9 together with the reference calculations. As in indication, the solution for a dipole radiating over a totally rigid surface is also shown. Application of the Fresnel zone principle gives results which are in accordance with those obtained using an arbitrary ground length. Note that the size of the Fresnel zones depends on the source and the receiver position and on the frequency. In this case, the length of the first Fresnel zone corresponds to at most 80 % of the arbitrary length. The correspondence with the solution using the monopole superposition is good at and near the grazing incidence, which is the condition assumed in the computation of the individual source fields. Therefore, an optimisation of the computational time by considering a limited portion of discretised ground seems to be possible in this case.

However, the solution using such a monopole superposition is limited to the case of low order sources. At a given frequency, the simulation of a high order source implies the presence of several monopoles in a small region of space, dominantly cancelling each others fields. As a consequence, the reproduction of the interference pattern is not accurate numerically. Practically, it has been found that the simulation of such a multipole field is limited to around a 10-th order source approximately. Also, the interaction between the fields due to the monopoles constituting the dipole is not correctly predicted using such a superposition method. Discrepencies due to this deficiency are expected to increase with the order of the source.

Therefore, in the following, the radiation of multipole sources is examined only over totally soft surfaces because an exact solution is available in this case and is used as the reference.

High order source

To further examine if an optimisation of the discretised ground length is possible, the following numerical examples deal with multipole sources radiating over totally soft surfaces. The *ES* model has been run for different ground lengths obtained by introducing an increasing number of Fresnel zones. For a 5-th order source (see Fig. 3-10(a)), including the first five Fresnel zones gives predictions which correspond well with the exact solution. If one takes the five first Fresnel zones, this corresponds to cover around 110 % of the horizontal distance between the source and the receiver placed at 45° of incidence. If ones includes only the first Fresnel zone,

[5]Details on the Fresnel zone principle can be found in [Picaut 2000].

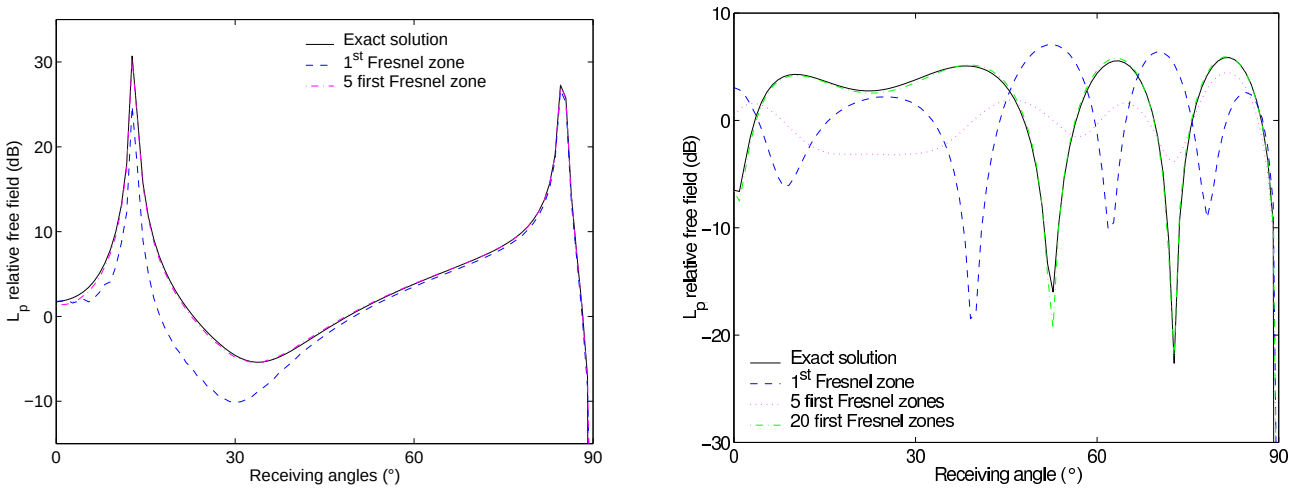

(a) 5-th order source – $f = 1500$ Hz, low position

(b) 60-th order source – $f = 5$ kHz, high position

Figure 3-10: *Comparison of different ground discretisations for multipole sources radiating over a totally soft ground* $Z_n = 0$.

then it corresponds to only half of the distance between the source and the receiver. For a source of order 60 (see Fig. 3-10(b), also in [Bécot 2002]), one must include at least the first twenty Fresnel zones to obtain a good correspondence with the exact solution. In this case, for the receiver placed at 45° of incidence, the size of the first Fresnel zone represents about 30 % of the distance source to receiver projected on the ground, the 5-th Fresnel zone corresponds to 70 % and the 20-th Fresnel zone to 140 %.

Therefore, these two examples prove that the present *ES* model is accurate in the case of high order sources too, provided that the ground length included is large enough. An optimisation of this length depending on the source order seems to be possible. However, the determination of such an optimisation criteria is beyond the scope of this work.

3.4 Summary

To deal with the sound propagation over a flat, arbitrary impedance ground, an original method, which is based on the *ES* method, has been developped and is presented in this chapter. This method can handle arbitrary radiating sources, i.e. omnidirectional sources as well as strongly

directional sources.
The basic idea is to place a layer of physical sources on the ground surface, which can be seen as active sources controlling the ground impedance on a certain portion of the surface. Therefore, it is assumed that the ground is locally reacting; any sound propagation inside the ground is omitted. However, the impedance distribution is defined from point to point, allowing the study of the effects of piece-wise constant impedance distributions and impedance discontinuities.
When determining the ground sources' amplitudes, singularities are encountered due to the fact that the sources are placed directly on the boundary. This problem is overcome here by using the approximations of the Hankel functions for small argument, so that the contribution from the singularity is calculated analytically[6]. Once this is done, the field can be estimated at any point above the ground surface.
Results obtained with the present technique fit well with the exact solutions available for the radiation over totally soft surfaces, and also in the case of a strongly directional incident field. In the presence of impedance surfaces, the predictions from the present model correspond well with the solutions given previously by other authors. Lastly, comparisons with measurements proved the method to be accurate in the presence of impedance discontinuities also.
Due to its numerical efficiency, the present model is of interest for traffic noise purposes because it allows one to include both the directivity of the sound source and the presence of surfaces having different acoustical properties. More generally, this model could be used for the sound propagation from complicated structures over inhomogeneous grounds.

In particular, the present model for the ground effects can be coupled to the model derived in *Chapter 2* for the prediction of tyre noise above impedance surfaces. Its implementation is presented in the next chapter together with comparisons with measurements of horn effect amplifications over arbitrary impedance surfaces.

[6]It has also been shown in [Bécot 2002] that the Cauchy principal value could be used to estimate the singularity contribution.

Chapter 4

Tyre / Road Noise Over Arbitrary Impedance Surfaces

An efficient prediction of tyre / road noise requires an accurate modelling of the tyre emission but also the introduction of the acoustical properties of the road surface. In this respect, this chapter proposes different methods for introducing the presence of an arbitrary impedance surface into the tyre noise model presented in *Chapter 2*. The surface is assumed to be locally reacting.

In the first section, solutions using the image source technique and a reflection coefficient are investigated. Besides that for plane waves, a reflection factor for cylindrical waves of arbitrary order is derived. To model the tyre radiation over arbitrary impedance surfaces, an original implementation based on the combination of the models presented in *Chapter 2* and *Chapter 3* is proposed. The functioning and the validity of the model is then discussed on the basis of comparisons to measurements.

4.1 Preliminary

This section examines the introduction of the ground effects into the *ES* model, which is derived in *Chapter 2*, in the form of a reflection coefficient. The adaptation of the reflection coefficient for plane wave to the *ES* model is first discussed. The exact solution in the form of a reflection factor for cylindrical waves is examined at the end of this section.

Use of a reflection coefficient

In outdoor propagation studies, a widely used solution to include the reflection on the ground surface consists in introducing an image source, the amplitude of which is proportional to the amplitude of the incident source. The factor of proportionality, the so-called *reflection coefficient*, is defined as follows

$$p_{total} = p_{direct} + p_{ref} = p_{direct} + R_{coef}\ p_{image} \qquad \text{with} \quad R_{coef} = \frac{p_{direct}}{p_{total}}$$

where p_{direct} represents the direct pressure field, p_{ref} the pressure field reflected on the ground surface. R_{coef} depends on the type of waves that are propagating.
If cylindrical waves are propagating , given the geometry of Fig. 4-1, at a point $x_r(r, \varphi)$ above the road surface and outside the tyre body

$$\begin{aligned} p(r,\varphi) &= p_1(r_1,\varphi_1) + R_{coef}(r,\varphi)p_2(r_2,\varphi_2) \\ &= \sum_{m=-N_{max}}^{m=+N_{max}} A_m \left[\mathrm{H}_m^{(2)}(kr_1)\mathrm{e}^{\mathrm{j}m\varphi_1} + R_{coef}(r,\varphi)\mathrm{H}_m^{(2)}(kr_2)\mathrm{e}^{\mathrm{j}m\varphi_2} \right] \end{aligned} \tag{4-1}$$

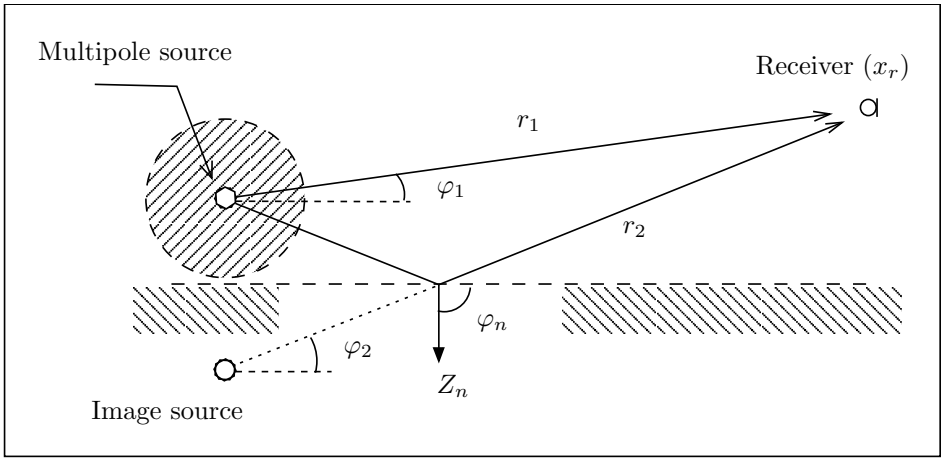

Figure 4-1: *Geometry used in the reflection coefficient definition. The broken lines represent excluded domains.*

In this equation, the reflection coefficient depends *a priori* on the position of the receiver x_r; for the sake of brevity, it is denoted R_{coef} in the following.

The velocity field in the direction $\vec{n}$, deduced from the pressure field, is expressed as

$$v_n(r,\varphi) \;=\; -\frac{1}{\mathrm{j}\omega\rho}\vec{\nabla}p_1\cdot\vec{n} \;-\; \frac{1}{\mathrm{j}\omega\rho}\vec{\nabla}(R_{coef}\;p_2)\cdot\vec{n}$$

According to the expression of the gradient in cylindrical coordinates (see Eq. 2-4), it can be written

$$\begin{aligned} v_n(r,\varphi) \;=\; & -\frac{1}{\mathrm{j}\omega\rho}\sum_{m=-N_{max}}^{m=+N_{max}} A_m\left[\; k\mathrm{H}_m^{(2)'}(kr_1)\cos(\varphi_1-\varphi_n)+\frac{\mathrm{j}m}{r_1}\mathrm{H}_m^{(2)}(kr_1)\sin(\varphi_1-\varphi_n)\right]\mathrm{e}^{\mathrm{j}m\varphi_1} \\ & -\frac{1}{\mathrm{j}\omega\rho}\sum_{m=-N_{max}}^{m=+N_{max}} R_{coef}\;A_m\left[\; k\mathrm{H}_m^{(2)'}(kr_2)\cos(\varphi_2-\varphi_n)+\frac{\mathrm{j}m}{r_2}\mathrm{H}_m^{(2)}(kr_2)\sin(\varphi_2-\varphi_n)\right]\mathrm{e}^{\mathrm{j}m\varphi_2} \\ & -\frac{1}{\mathrm{j}\omega\rho}\sum_{m=-N_{max}}^{m=+N_{max}} A_m\mathrm{H}_m^{(2)}(kr_2)\mathrm{e}^{\mathrm{j}m\varphi_2}\left[\frac{\partial R_{coef}}{\partial r_2}\cos(\varphi_2-\varphi_n)+\frac{1}{r_2}\frac{\partial R_{coef}}{\partial\varphi_2}\sin(\varphi_2-\varphi_n)\right] \end{aligned} \quad (4\text{-}2)$$

This equation differs fondamentally from the expression for the velocity in the presence of a rigid surface (see Eq. 2-5 and Eq. 2-7) : two additional terms are included, which contain the partial derivatives of the reflection coefficient.

In the case where plane waves or spherical waves are propagating, expressions for the reflection coefficient are available from the literature; they are fully used nowadays in outdoor propagation studies (see *Section 1.3* for references). By definition, these solutions are not suited for two-dimensional geometries.

However, besides its obvious limitations, the reflection factor for plane waves is of interest for our purpose because its implementation is effortless. The next paragraph examines the application of this latter solution to the *ES* model for the tyre radiation. In the last paragraph of this section, the derivation of the exact solution, i.e. in the form of a reflection factor for cylindrical waves, is investigated.

Plane wave approximation

At an infinite distance from the source, the wave front of an omnidirectional cylindrical wave becomes close to a plane. Therefore, the solution described in this paragraph can be seen as an approximation of the true solution in the case where only omnidirectional cylindrical waves are propagating and when the source is far from the ground surface.

According to [Morse 1968], the reflection coefficient for plane waves is defined as

$$R_p = \frac{\sin\varphi - \rho c/Z_n}{\sin\varphi + \rho c/Z_n} = \frac{\sin\varphi - \beta}{\sin\varphi + \beta} \tag{4-3}$$

where φ is defined in Fig. 4-1 and $\beta = \rho c/Z_n$, Z_n is the normal acoustical impedance of the road surface. This solution only holds for impedance surfaces, which are homogeneous.
Therefore, in the expression of the velocity field Eq. 4-2, one has

$$\frac{\partial R_{coef}}{\partial r_2} = 0 \qquad \text{and} \qquad \frac{\partial R_p}{\partial \varphi_2} = \frac{2\beta\cos\varphi_2}{(\sin\varphi_2 + \beta)^2}$$

By including this expression in Eq. 4-2 and after rearranging the terms, the total velocity at a point $x_r(r,\varphi)$ above an homogeneous impedance plane can be expressed as[1]

$$\begin{aligned} v_n(r,\varphi) &= -\frac{1}{\mathrm{j}\omega\rho}\sum_{m=-N_{max}}^{m=+N_{max}} A_m\left[\, k\mathrm{H}_m^{(2)'}(kr_1)\cos(\varphi_1-\varphi_n) + \frac{\mathrm{j}m}{r_1}\mathrm{H}_m^{(2)}(kr_1)\sin(\varphi_1-\varphi_n)\right]\mathrm{e}^{\mathrm{j}m\varphi_1} \\ &-\frac{1}{\mathrm{j}\omega\rho}\sum_{m=-N_{max}}^{m=+N_{max}} R_p \times A_m\; k\mathrm{H}_m^{(2)'}(kr_2)\mathrm{e}^{\mathrm{j}m\varphi_2}\cos(\varphi_2-\varphi_n) \\ &-\frac{1}{\mathrm{j}\omega\rho}\sum_{m=-N_{max}}^{m=+N_{max}} A_m\frac{1}{r_2}\mathrm{H}_m^{(2)}(kr_2)\mathrm{e}^{\mathrm{j}m\varphi_2}\left[\frac{\mathrm{j}m(\sin^2\varphi_2-\beta^2)+2\beta\cos\varphi_2}{(\sin\varphi_2+\beta)^2}\right]\sin(\varphi_2-\varphi_n) \end{aligned} \tag{4-4}$$

Note that this equation also provides a measure of the error when using the reflection coefficient in normal incidence. Though, this calculation is not examined further because of the more important, inherent deficiencies of this approach.
To examine to what extent the solution using reflection factor for plane waves is reliable, horn effect amplification factors are compared to measured ones over a rather soft surface.
The absorbing material used in the experiment is a panel of mineral rock wool, normally employed for thermic insulation, layed on top of a concrete surface. The normal acoustical impedance of the material was measured in a Kuntd's tube (the measured impedance values are shown in *Appendix IV*). Due to practical reasons, the domain of validity of the measurements ranges from 200 Hz to 2 kHz. The measurement procedure is the same as for horn effect measurements over rigid surfaces, i.e. the reciprocity principle is applied (see Fig. 2-1). Sound pressure levels are first recorded in the presence of the tyre and the absorbing layer and in a second stage, when the tyre is removed. The microphone is mounted flush with the absorbing

[1]This expression can be found in [Kropp 2000b]; besides the different angle dependency, mistakes have been corrected in the present study regarding Eq. (10) of the mentioned work.

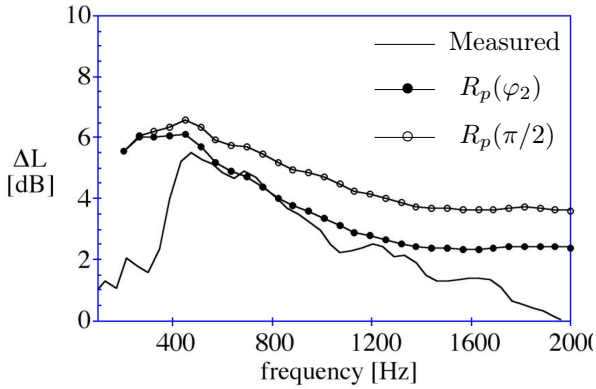

Figure 4-2: *Measurements of amplification factors over an impedance surface compared to prediction from the ES model using plane wave reflection coefficient.*

panel at a distance $d = 20$ mm from the horn centre, and at the middle of the contact area (see Fig. 2-7). The sound source, a standard loudspeaker positioned one meter ahead of the microphone, is directed toward the microphone so that all sound reflections occur in the geometrical plane which contains the tyre, the microphone and the loudspeaker.

Results from the *ES* model shown in Fig. 4-2 are denoted $R_p(\varphi_2)$. As expected, the amplification factors obtained are overestimated at low frequencies due to the two-dimensional character of the model. Above 500 Hz, the proposed solution corresponds fairly well with measurements. The deviations between measurements and calculations increase again at frequencies above 1.5 kHz, probaby due to incertainties in the impedance measurements. In total, this yields a frequency range of usability from 500 Hz to 1.5 kHz, which corresponds to the dominant frequency range of the A-weighted noise levels used in pass-by measurements.

In the same figure, the solution using a reflection factor only for normal incidence has been plotted; it is indicated as $R_p(\pi/2)$. At very low frequencies, this solution gives results, which are very similar to the solution including the angle dependence. However, as the frequency increases, the solution deviates from the measurements due to an incorrect velocity field expressed on the tyre surface.

In conclusion, the solution using the plane wave reflection coefficient predicts amplification factors, which fit well with the measurements over an absorbing surface; a better correspondence would certainly be achieved for harder surfaces. However, it is not mathematically correct to use the plane wave reflection coefficient together with cylindrical harmonics. It does not include

the correct wave front and the "geometrical divergence" that occurs when cylindrical waves are propagating. In fact, the impedance obtained when using the reflection coefficient for plane waves is not the correct one, that is the one given as input to the model. This means that the calculated sound field includes only partially the presence of the impedance plane. Therefore, the next paragraph examines the expression and the application of a reflection coefficient for cylindrical waves.

Cylindrical wave assumption

The idea of the following derivation is to design a reflection coefficient which gives the correct impedance value given on the ground. The normal acoustical impedance at one point of the surface is the ratio between the pressure and the normal velocity at this point. Therefore, let us derive the expression of the pressure and velocity fields on the surface. Note that the following derivation holds for any ground impedance but zero impedance. However, the solution in this case is known : the reflection coefficient equals -1.

For all points of the ground surface, the symmetry of the construction imposes $r_1 = r_2$ and $\varphi_1 = \varphi_2$. Let us denote r and φ the co-ordinates of one point of the ground surface. Therefore, according to Eq. 4-1, the total pressure field impinging at one point (r, φ) of the surface is

$$p(r,\varphi) = \sum_{m=-N_{max}}^{m=+N_{max}} A_m \mathrm{H}_m^{(2)}(kr) \mathrm{e}^{\mathrm{j}m\varphi} \ (1 + R_m)$$

where R_m is the reflection factor for cylindrical waves. It depends *a priori* on the variable r and φ, and on the order m of the source.

The total velocity field in the normal direction to the surface is obtained from Eq. 4-4 :

$$\begin{aligned} v_n(r,\varphi) = & \\ & -\frac{1}{\mathrm{j}\omega\rho} \sum_{m=-N_{max}}^{m=+N_{max}} A_m \left[\ k\mathrm{H}_m^{(2)'}(kr)\sin\varphi \ - \ \frac{\mathrm{j}m}{r}\mathrm{H}_m^{(2)}(kr)\cos\varphi \right] \mathrm{e}^{\mathrm{j}m\varphi} \ (1 - R_m) \\ & +\frac{1}{\mathrm{j}\omega\rho} \sum_{m=-N_{max}}^{m=+N_{max}} A_m \mathrm{H}_m^{(2)}(kr) \mathrm{e}^{\mathrm{j}m\varphi} \left[\frac{\partial R_m}{\partial r}\sin\varphi - \frac{1}{r}\frac{\partial R_m}{\partial \varphi}\cos\varphi \right] \end{aligned}$$

One can thus express the impedance boundary condition as

$$p(r,\varphi) = Z_n \ v_n(r,\varphi)$$

using the two previous equations. The obtained equation must hold for each order m of the Green function. Therefore, the summation can be removed. Moreover, because they appear on

both sides of the equation, the modal amplitude A_m and the exponential term can be removed also. By doing so, one obtains, for each harmonic order m

$$\begin{aligned} \mathrm{H}_m^{(2)}(kr)\ (1+R_m) &= -\frac{Z_n}{\mathrm{j}\omega\rho}\ \left[\ k\mathrm{H}_m^{(2)'}(kr)\sin\varphi - \frac{\mathrm{j}m}{r}\mathrm{H}_m^{(2)}(kr)\cos\varphi\right]\ (1-R_m) \\ &\quad + \frac{Z_n}{\mathrm{j}\omega\rho}\ \mathrm{H}_m^{(2)}(kr)\ \left[\frac{\partial R_m}{\partial r}\sin\varphi - \frac{1}{r}\frac{\partial R_m}{\partial\varphi}\cos\varphi\right] \end{aligned}$$

After rearranging the terms, one can write the differential equation which must be satisfied by R_m at one point (r,φ) of the surface :

$$\left[\frac{\partial R_m}{\partial r}\sin\varphi - \frac{1}{r}\frac{\partial R_m}{\partial\varphi}\cos\varphi\right] + \left[\ a_m(r,\varphi) - \frac{\mathrm{j}\omega\rho}{Z_n}\right] \times R_m = \left[\ a_m(r,\varphi) + \frac{\mathrm{j}\omega\rho}{Z_n}\right]$$

where

$$a_m(r,\varphi) \ = \ k\frac{\mathrm{H}_m^{(2)'}(kr)}{\mathrm{H}_m^{(2)}(kr)}\sin\varphi - \ \frac{\mathrm{j}m}{r}\cos\varphi \tag{4-5}$$

The differential equation above is always valid as the Hankel function never takes on zero values. The derivation can therefore proceed.

For the points of the ground surface, the variables r and φ are connected through $r\sin\varphi = h$, where h is the height of the incident source (see Fig. 4-1). Hence, one has

$$\frac{\partial R_m}{\partial\varphi} = -\frac{-r^2\cos\varphi}{h}\ \frac{\partial R_m}{\partial r}$$

and

$$\begin{aligned} \sin\varphi - \frac{\cos\varphi}{r}\ (-\frac{-r^2\cos\varphi}{h}) &= \frac{r}{h}\ (\ \frac{h}{r}\sin\varphi + \cos^2\varphi) \\ &= \frac{r}{h}\ (\sin^2\varphi + \cos^2\varphi) \ = \ \frac{r}{h} \ = \ \frac{1}{\sin\varphi} \end{aligned}$$

Thus, the previous partial differential equation, i.e. involving two independent variables, becomes an ordinary differential equation involving only the variable r

$$\frac{\partial R_m}{\partial r} \ + \ f_m(r)\times R_m \ = \ g_m(r) \tag{4-6}$$

with

$$\left\{\begin{array}{rcl} f_m(r) &=& [\ a_m(r,\varphi) \ - \ \mathrm{j}\omega\rho/Z_n\ ]\ h/r \\ g_m(r) &=& [\ a_m(r,\varphi) \ + \ \mathrm{j}\omega\rho/Z_n\ ]\ h/r \end{array}\right. \tag{4-7}$$

and a_m defined in Eq. 4-5.

In the above expressions, the dependency upon the angle of incidence φ is included implicitely because the variables r and φ are not independent.

At this point, one can check the validity of the approach. As r tends to ∞, Eq. 4-6 can be written

$$\left.\frac{\partial R_m}{\partial r}\right|_{\infty} + 0 \times R_m(\infty) = 0 \qquad \text{which gives} \qquad \left.\frac{\partial R_m}{\partial r}\right|_{\infty} = 0$$

One then obtains

$$R_m(\infty) = \frac{g_m(\infty)}{f_m(\infty)} = \frac{-\mathrm{j}k\sin\varphi + \mathrm{j}\omega\rho/Z_n}{-\mathrm{j}k\sin\varphi - \mathrm{j}\omega\rho/Z_n}$$

which can also be written

$$R_m(\infty) = \frac{\sin\varphi - \rho c/Z_n}{\sin\varphi + \rho c/Z_n} = R_p(\infty) = -1$$

Therefore, as expected, the cylindrical wave reflection coefficient tends to the reflection coefficient for plane waves at infinity. In addition, this value is found to be -1 at infinity, or at grazing incidence, which is a known result from outdoor sound measurements[2].

Eq. 4-6 is the differential equation that must satisfy, if it exists, the reflection coefficient for cylindrical waves. This is a first order, linear differential equation of one variable, the solution of which, according to [Ince 1956], is known. As the equation holds for any points of the ground surface, it has the following general solution

$$R_m(r) = \mathrm{e}^{-\int_r^{r_0} f_m(\nu)\,\mathrm{d}\nu}\left[\int_r^{r_0} g_m(\nu)\mathrm{e}^{\int_\nu^{r_0} f_m(\mu)\,\mathrm{d}\mu}\,\mathrm{d}\nu + R_m(r_0)\right] \tag{4-8}$$

where μ, ν are dummy integration variables, and r_0 a bound fixed arbitrarily.
Clearly, the choice of r_0 is crucial for the computation of the solution. As one knows the solution at infinity, one may be willing to set r_0 to infinity. However, the computation of the integrals contained in the above equation are troublesome and has not solved yet. This will be the subject of future works.

[2]Experimentally, the value of the reflection factor is always -1 at grazing incidence, and this, whatever the ground impedance because the impedance, in reality, has always a finite value.

4.2 Iterative *ES* model of the tyre radiation over impedance surfaces

To overcome the lack of solution for a cylindrical reflection coefficient, this section presents a solution, which is based on the combination of the models of *Chapter 2* and *Chapter 3*. However, contrary to the derivations of *Chapter 3*, a time dependence as $e^{+j\omega t}$ is assumed in the following.

After the presentation of the general principle of the method, the implementation of the model is explained in this section. The general functioning of the model and its validation are presented in *Section 4.3*.

Solving principle

The present model consists of two sub–models : one for the tyre radiation and one for the ground effects. The unknowns of the problem are, on one hand, the amplitude of the multipole source, which stands for the tyre radiation, and on the other hand, the amplitudes of the ground sources, which control the value of the impedance on the ground surface. The sources included in the complete model are illustrated in Fig. 4-3.

The key point of the model, and of the *ES* method in general, is that all sources have to fulfill together the boundary conditions. There are two boundary conditions in our case : one on the

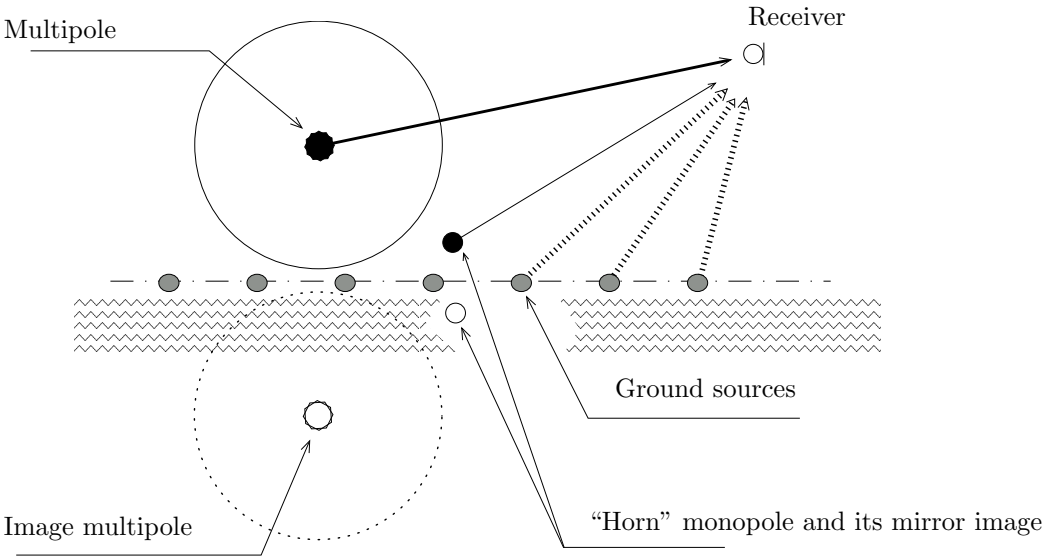

Figure 4-3: *Illustration of the sources included in the iterative ES model.*

tyre surface and one on the ground surface.
A straigthforward and somewhat rough method consists in putting up the entire equation system and solving it for the different sources' amplitudes. The system is then a concatenation of the equations issued from the boundary condition on the tyre belt and of the equations resulting from the impedance condition on the ground. However, such an equation system is found to be ill–conditionned because of the too different order of magnitude of the two sub–systems. The resulting set of amplitudes is not accurate enough to ensure a good reproduction of the sound field.

Another approach consists in considering the multiple reflexions occuring inside the horn between the rigid tyre and the ground surface. In this approach, the amplitudes of the sources are solved through an iterative process.
At the first stage, the amplitude of the multipole is tuned to fulfill the prescribed velocity on the tyre surface. This results in a certain pressure field impinging on the road surface. Given this incident pressure, the source strengths of the ground monopoles are tuned to reproduce the prescribed impedance value on the ground. These monopoles produce a velocity distribution on the tyre surface, in addition to the velocity originally prescribed as a tyre boundary condition. Therefore, an additional multipole amplitude is computed to compensate for this unwanted velocity. However, this new multipole amplitude creates an additional pressure field on the ground. This perturbation is counteracted by computing new monople amplitudes, which themselves create a new velocity field on the tyre surface...
The process stops when the achieved velocity on the tyre surface and the achieved impedance value on the ground are lower than a given error value. At this point, an additional field from one of the system of sources does not perturb the other system's behaviour. Finally, the total amplitudes of the multipole and of the ground monopoles, are the sum of all the amplitudes computed during the iterative process.
Once the amplitudes of the sources are determined, the pressure or the velocity field can be computed at any point above the ground surface and outside the tyre body. This field represents the field radiated by the vibrating tyre in the presence of an impedance plane.

Mathematical derivation

The mathematical basis of the present model can be found in *Chapter 2* and in *Chapter 3*. For clarity, the notations used respectively in these two chapters are used in this chapter too as often as possible. The different stages of the iterative process are indicated in the text below; this notation will also be used in the coming numerical implementation.

To reproduce the horn effect sound amplification, the prescribed velocity on the tyre surface is given by a monopole source and its mirror image, which are located respectively at x_0 and $\overline{x_0}$; this situation corresponds to a "scattering" problem (the derivation below also holds in the case a "radiation" problem is expressed, see *Chapter 2*). The velocity at a point of the tyre surface is given in Eq. 2-12.

A multipole and its mirror image are used to fulfill the previously prescribed velocity. These two multipoles have equal source strength in order to achieve zero velocity (infinite impedance value) on the ground surface[3]. The multipole amplitudes are called A_m. Mathematically, the boundary condition on the tyre is expressed as (stage 1)

$$-\frac{1}{\mathrm{j}\omega\rho}\sum_{m=-N_{max}}^{m=+N_{max}} A_m^*\left[\, k\ \mathrm{e}^{\mathrm{j}m\varphi_1} \;+\; k\ \frac{r_1+b\sin\varphi_1}{r_2}\ \frac{\mathrm{H}_m^{(2)'}(kr_2)}{\mathrm{H}_m^{(2)'}(kr_1)}\ \mathrm{e}^{\mathrm{j}m\varphi_2} \;+\; \mathrm{j}m\frac{b\cos\varphi_1}{{r_2}^2}\ \frac{\mathrm{H}_m^{(2)}(kr_2)}{\mathrm{H}_m^{(2)'}(kr_1)}\ \mathrm{e}^{\mathrm{j}m\varphi_2}\right] = -\Big[v_{scat}(x_0 \mid x_{tyre}) + v_{scat}(\overline{x_0} \mid x_{tyre})\Big] \tag{4-9}$$

r_1 and φ_1, resp. r_2 and φ_2, are the distance and the angle from the multipole, resp. from the image multipole, to the point x_{tyre} of the tyre surface. The actual multipole amplitudes A_m are then calculated using Eq. 2-8.

Next, the pressure field due to these multipoles impinges on the ground. In order to control the impedance value on the surface, monopole sources are placed directly at the ground level. Given the incident pressure field, the source strengths $Q^{(1)}$ of the ground monopoles are calculated according to (stage 2)

$$\int_\Gamma Q^{(1)}(\xi)\ G(\xi \mid x)\ \mathrm{d}\xi \;-\; Z_n(x)\int_\Gamma Q^{(1)}(\xi)\ G^{(v,n)}(\xi \mid x)\ \mathrm{d}\xi \;= -\left[\sum_{m=-\infty}^{m=+\infty} A_m\left[\mathrm{H}_m^{(2)}(kr_g)\mathrm{e}^{\mathrm{j}m\varphi_g} + \mathrm{H}_m^{(2)}(kr'_g)\mathrm{e}^{\mathrm{j}m\varphi'_g}\right] + p_{scat}(x_0 \mid x) + p_{scat}(\overline{x_0} \mid x)\right] \tag{4-10}$$

[3]Other Green functions, which fulfill e.g. a pressure release condition on the ground, may be considered for the incident field; the implementation in this case is similar to the present one and is therefore not examined.

where r_g and φ_g, resp. r'_g and φ'_g, are the distance and the angle from the multipole source, resp. from the multipole image, to a point x of the ground surface. $Z_n(x)$ is the value of the prescribed impedance at the point x of the ground.

Note that, since multipole and image multipole of equal source strength are used, the incident field does not contribute to the velocity on the ground surface. Another consequence is that the set of ground sources of amplitude $Q^{(1)}$, only compensate for the difference between the impedance value fulfilled by the incident field, i.e. infinite impedance, and the prescribed impedance distribution.

At this point, we have two sets of amplitudes, denoted A_m for the multipole and $Q^{(1)}$ for the ground sources, which are such that the two boundary conditions of the problem are fulfilled separately. Therefore, one "just" has to counteract the perturbations due to one system of sources with the other, to obtain the final solution to the problem.

The perturbations on the tyre surface are due to the field from the ground sources in the form of an additional velocity. The new multipole amplitudes, denoted $B_m^{(1)}$, which counteract this unwanted velocity, are determined according to (stage i)

$$-\frac{1}{\mathrm{j}\omega\rho}\sum_{m=-N_{max}}^{m=+N_{max}} B_m^{(1)*}\; k\; \mathrm{e}^{\mathrm{j}m\varphi_1} \;=\; -\int_\Gamma Q^{(1)}(\xi)\; G^{(v,n)}(\xi \mid x_{tyre})\; \mathrm{d}\xi \tag{4-11}$$

As before, the actual multipole amplitudes $B_m^{(1)}$ are then obtained using Eq. 2-8. In fact, the field from the image multipole should not be included at this stage. If it was included, the impedance value on the ground woud be re-set to infinity and this would annihilate the benefit of the ground sources previously placed on the surface.

This new set of multipole amplitudes $B_m^{(1)}$ create a new incident field on the ground surface so that the impedance condition is not fulfilled any longer. Given the fact that the incident field contributes now to both the pressure and the velocity, a new set of ground source amplitudes, say $Q^{(2)}$, is computed according to (stage $i+1$)

$$\begin{aligned}&\int_\Gamma Q^{(2)}(\xi)\; G(\xi \mid x)\; \mathrm{d}\xi \;-\; Z_n(x)\int_\Gamma Q^{(2)}(\xi)\; G^{(v,n)}(\xi \mid x)\; \mathrm{d}\xi \\ &= -\sum_{m=-N_{max}}^{m=+N_{max}} B_m^{(1)}\mathrm{H}_m^{(2)}(kr_g)\end{aligned}$$

$$+ \; Z_n(x) \sum_{m=-N_{max}}^{m=+N_{max}} B_m^{(1)} \left[k\mathrm{H}_m^{(2)'}(kr_g)\sin\varphi_g - \frac{\mathrm{j}m}{r}\mathrm{H}_m^{(2)}(kr_g)\cos\varphi_g \right] \mathrm{e}^{\mathrm{j}m\varphi_g} \qquad (4\text{-}12)$$

Next, additional source amplitudes for the multipole and for the ground sources are determined using successively Eq. 4-11 and Eq. 4-12; in a general form, they are denoted $B_m^{(i)}$ and $Q^{(i)}$ for $i = 1, \ldots, i_{conv}$.

At the end of the iterative process, i.e. at $i = i_{conv}$, the two boundary conditions are fulfilled together by the two systems of sources, the mutlipole and the ground monopoles.

Amplification factors

Once the boundary conditions are fulfilled, the pressure field at any point above the road surface and outside the tyre body can be determined. It is written, at a point x_r

$$\begin{aligned} p_{tot}(x_r) \;=\; & \sum_{m=-\infty}^{m=+\infty} A_m \left[\mathrm{H}_m^{(2)}(kr_1)\mathrm{e}^{\mathrm{j}m\varphi_1} + \mathrm{H}_m^{(2)}(kr_2)\mathrm{e}^{\mathrm{j}m\varphi_2} \right] \;+\; p_{scat}(x_0 \mid x_{tyre}) + p_{scat}(\overline{x_0} \mid x_{tyre}) \\ & + \sum_{i=1}^{i=i_{conv}} \left[\sum_{m=-\infty}^{m=+\infty} B_m^{(i)} \mathrm{H}_m^{(2)}(kr_1)\mathrm{e}^{\mathrm{j}m\varphi_1} \;+\; \int_\Gamma Q^{(i)}\; G(\xi \mid x_r)\; \mathrm{d}\xi \right] \end{aligned}$$

For the calculation of the horn effect amplification factors, the reference pressures are

– when removing the road :

$$p_{ref_1}(x_r) \;=\; \sum_{m=-\infty}^{m=+\infty} \widetilde{A}_m \left[\mathrm{H}_m^{(2)}(kr_1)\mathrm{e}^{\mathrm{j}m\varphi_1} + \mathrm{H}_m^{(2)}(kr_2)\mathrm{e}^{\mathrm{j}m\varphi_2} \right] \;+\; p_{scat}(x_0 \mid x_{tyre})$$

where $\widetilde{A}_m$ is the multipole amplitude calculated for the prescribed velocity given by the original monopole only (see *Chapter 2*);

– when removing the tyre :

$$p_{ref_2}(x_r) \;=\; p_{scat}(x_0 \mid x_{tyre}) + p_{scat}(\overline{x_0} \mid x_{tyre}) \;+\; \int_\Gamma \widetilde{Q}(\xi)\; G(\xi \mid x_r)\; \mathrm{d}\xi$$

where $\widetilde{Q}$ is the amplitude of the ground source calculated for an incident field due to the "horn" monopole and its image only.

Numerical implementation

The implementation of the iterative process is summarized in the following using matrix notations. The matrix elements can be identified easily from the equations above.

Stage 1

The prescribed tyre velocity, which is given by a monopole source placed inside the horn, is fulfilled by the multipole and its image (see Eq. 4-9) :

$$\mathbf{A}^* \;=\; \mathbf{M}^{-1} \times \Big[\; -\mathbf{V}_{scat} \Big]$$

The set of multipole amplitudes $\mathbf{A}$ are then calculated according to Eq. 2-8.

Stage 2

Given the incident pressure field, the ground sources are "switched on" so that the prescribed impedance value Z_n is achieved on the ground surface (see Eq. 4-10) :

$$\mathbf{Q}^{(1)} \;=\; [\; \mathbf{I}_p \;-\; \mathbf{Z}_n \times \mathbf{I}_v \;]^{-1} \times \Big[\; -(\mathbf{P} \;+\; \mathbf{P}_{scat}) \; \Big]$$

The matrix $\mathbf{P}$ contains the pressure contributions from the multipole and its image.

The iteration process starts here.

Stage i

Additional multipole amplitudes are computed to annihilate the undesired velocity on the tyre due to the ground monopoles. For the iteration numbered i, this is expressed as (see Eq. 4-11)

$$\mathbf{B}^{(i)*} \;=\; \mathbf{M}_1^{-1} \times \Big[\; -\mathbf{V}_\Gamma \times \mathbf{Q}^{(i)} \; \Big]$$

On the contrary to the matrix $\mathbf{M}$, the matrix $\mathbf{M}_1$ only includes the contribution from the original multipole.

Stage $i+1$

As the impedance condition might not be fulfilled any longer, additional ground source amplitudes are calculated according to (see Eq. 4-12) :

$$\mathbf{Q}^{(i+1)} \;=\; [\; \mathbf{I}_p \;-\; \mathbf{Z}_n \times \mathbf{I}_v \;]^{-1} \times \Big[\; -\; \mathbf{P}_1 \times \mathbf{B}^{(i)} \; \Big]$$

where $\mathbf{P}_1$, contrary to $\mathbf{P}$ in the previous equation, includes the pressure and the velocity field due to the original multipole only. The iteration is stopped when the boundary conditions of the tyre and on the ground are both satisfied.

At this point, the boundary conditions are
– on the tyre :

$$\mathbf{M} \times \mathbf{A}^* \; + \; \mathbf{M}_1 \times \left[\sum_{i=1}^{i=i_{conv}} \mathbf{B}^{(i)*} \right] \; + \; \mathbf{V}_\Gamma \times \left[\sum_{i=1}^{i=i_{conv}} \mathbf{Q}^{(i)} \right] \; \equiv \; -\mathbf{V}_{scat} \qquad (4\text{-}13)$$

– on the ground :

$$[\, \mathbf{I}_p \; - \; \mathbf{Z}_n \times \mathbf{I}_v \,] \times \left[\sum_{i=1}^{i=i_{conv}} \mathbf{Q}^{(i)} \right] \; \equiv \; -\, (\mathbf{P} \; + \; \mathbf{P}_{scat}) \; - \; \mathbf{P}_1 \times \left[\sum_{i=1}^{i=i_{conv}} \mathbf{B}^{(i)} \right] \qquad (4\text{-}14)$$

Note that the symbol '≡' is used here because, from the numerical point of view, these equations are satisfied within an error interval defined arbitrarily by the user.

For the optimisation of the calculation time, the matrices $\mathbf{M}_1^{-1}$ and $[\, \mathbf{I}_p \; - \; \mathbf{Z}_n \times \mathbf{I}_v \,]^{-1}$ are computed only once, before the iteration. Therefore, only matrix multiplications are performed during the iteration itself, which is much faster than successive matrix inversions.
Moreover, by construction, the conditioning number of the matrix $\mathbf{M}_1$ is always close to unity. Thus, the inversion of such a matrix is computationally effortless. Finally, this yields calculation times, which are mainly governed by the inversion of the matrix $[\, \mathbf{I}_p \; - \; \mathbf{Z}_n \times \mathbf{I}_v \,]$.

4.3 Model functionning

This section examines the functionning of the iterative model presented above. First, the characteristics of the iterative process are discussed. Then, the evolution of the amplitudes of the sources is presented. The validity of the model is discussed in the next section.

In order to test the model, absorbing materials were needed. The impedance surfaces consisted of panels of mineral rockwool placed on an acoustically rigid support. As a result, the structure was considered as a hardbacked absorbing material, the impedance of which could be accurately modelled using the impedance model proposed in [Delany 1970]. The model parameters were determined using the level difference technique, which is described in *Appendix IV*.
According to the resulting impedance distribution shown in this appendix, an absorbing material built in this way is rather soft. Therefore, in the model, since the incident field gives an infinite impedance value on the ground, the ground sources are expected to contribute significantly to the total field. In general, the difference between the impedance value fulfilled by the

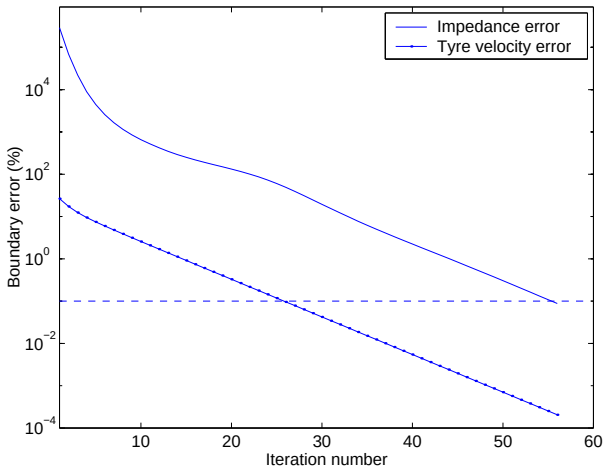

(a) Boundary errors along the iterations. f = 420 Hz, $Z_n = 625 - 3178$j. Geometry of Fig. 4-7(b)

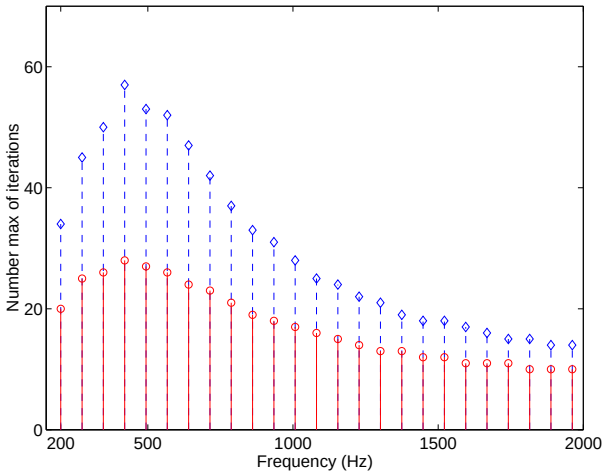

(b) Value of i_{conv} as a function of the frequency. $\diamond$: gap = 0.8 cm (see Fig. 4-7) – $\circ$: gap = 1.85 cm (see Fig. 4-6)

Figure 4-4: *Characteristics of the iterative process : boundary errors and value of* i_{conv}.

incident field and the prescribed impedance value, determines to a large extent the number of iterations needed and the relative importance of the ground sources' contribution.

The iterative process

The iterative process is stopped when the two boundary conditions of the problem are fulfilled simultaneously. From a numerical point of view, this means that the error made is lower than an arbitrary threshold value. In this work, it was set to 0.1 %. The error criteria used for this is the relative surface velocity error proposed in [Schaaf 1982]; it is defined as

$$error \;=\; \frac{\int_S \mid value_{prescribed} \;-\; value_{achieved} \mid^2}{\int_S \mid value_{prescribed} \mid^2}$$

Note that for the tyre surface boundary error, the prescribed value was set to be that given by the monopole source located inside the horn.

One can observe that both boundary errors decrease almost constantly along the iterative process. The impedance error shows some variations at the beginning of the iterative process while the error on the tyre surface uniformly diminishes. The general behaviour depicted in this figure also holds at other frequencies and for other system geometries, which are not shown

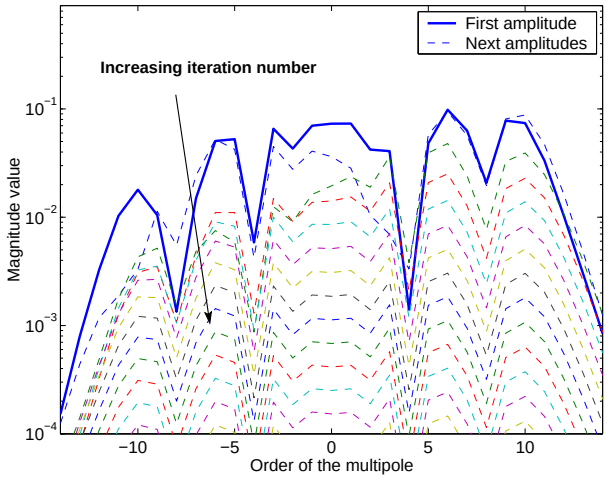

(a) Multipole amplitudes

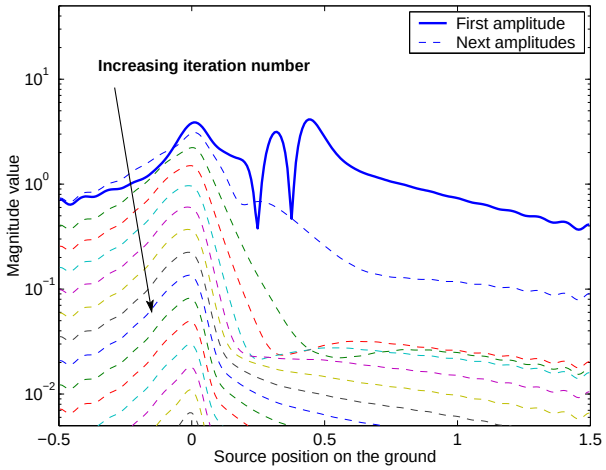

(b) Ground sources amplitudes. The arrow indicates the position of the "horn" monopole (the reciprocity principle is used).

Figure 4-5: *Successive amplitudes of the multipole and of the ground sources.* $f = 1595$ *Hz,* $Z_n = 727 - 738\text{j}$. *Geometry corresponding to Fig. 4-7(b).*

here. Therefore, it is clear that one can compute the source amplitudes with an arbitrary accuracy.

It is also interesting to examine the evolution of the maximum number of iterations, denoted i_{conv} in Eq. 4-13 and Eq. 4-14, as a function of the frequency (see Fig. 4-4(b)). The boundary errors are those defined above. The results, which are shown for two different gap values, are very similar. This is due to the fact that the required number of iterations depends only on the initial difference between the impedance value given the incident field and the prescribed impedance value.

Concerning the general evolution of i_{conv}, it appears that there exists a particular frequency, i.e. impedance value, at which the interaction between the two systems is the largest. It is situated here around 400 Hz; i_{conv} is around 150. Above this frequency, the maximum number of iterations decreases and reaches around 20 at 2000 Hz.

Sources' amplitudes

An example of the successive amplitudes of the multipole and of the ground sources is shown in Fig. 4-5. The results shown here are computed for a single frequency and the correspond-

ing impedance value of the absorbing material described above. In this case, a number of 20 iterations were needed to achieve the prescribed boundary values. It is observed for both the multipole and for the ground sources, the successive sources' amplitudes decrease along the iteration process. This means that the correction is less and less important as new amplitudes are calculated. Moreover, the first computed amplitude globally dominates the next ones. This means that the initial system of sources is already quite reliable. After that, the successive amplitudes "adjust" the field so that an energy balance is reached between the two systems of sources.

4.4 Results and discussion

For the discussion of the model validity, horn effect amplification factors obtained with the present model are compared to measured ones over absorbing surfaces. The measurement procedure and the model implementation is first presented. Then predicted and measured values are compared in the case of homogeneous and inhomogeneous surfaces. The results are discussed in a last paragraph.

Measurement and modelling procedure

The absorbing material used is that described above. The measurements were performed by making use of the reciprocity principle, as it was done for the measurements shown in *Chapter 2*. This means that the source was located in front of the tyre and that the receiver, a 1/4 inch electret microphone, was placed inside the horn, close to the contact area. The source was the same as the one used for the measurements shown in *Chapter 3*, i.e. an electrodynamic driver with a flexible hose attached. This source was used for both the determination of the material impedance and of the amplification factors. This source showed a good directivity diagram between 200 Hz and 2000 Hz, thus restraining the measurements to this frequency range. The tyre used was a non-commercial smooth tyre; its perimeter was 2 m (radius of $1/\pi$) and its belt width was 16 cm. The tyre was suspended over the absorbing surface, which might explain some of the discprencies observed in the measurements. *SPL* were recorded when the tyre was placed above the absorber and when removing the tyre, both using the *MLS* technique.
For the model implementation, the actual positions of the source and of the receiver are used. This means that the receiver is located inside the horn region, whereas the monopole source,

which provides the prescribed velocity on the tyre surface, is located ahead of the tyre outside the horn. In fact, concerning the simulation of the tyre radiation, it was shown in *Chapter 2* that such a configuration leads to a good stability in the field predictions. It also allows the use of a lower order, multipole source for the simulation of the tyre radiation, which yields lower calculation times. For the calculations shown below, numerical tests have shown that a multipole of order $N_{max} = 64$ yields stable field predictions. The tyre surface is discretised into $2N_{max} + 1 = 129$ elements so that the collocation technique can be applied to solve the resulting equation system.

Concerning the ground surface discretisation, a minimum of 10 elements per wavelength is assured, with the constraint that the resulting element length should not be larger than the gap between the tyre and the road. If this is the case, the element length is set to the gap value. It should be underlined that if this additional criteria is not respected, the stability of the system of sources is not ensured, i.e. the boundary error may not decrease along the iterative process. This is due to the fact that if the discretisation is not fine enough, the assumption that the source strength is a slowly varying function on the element is violated (see the derivation of Eq. 3-5), and the model is not accurate anymore. Finally, the numerical integration of the Green functions is performed using a Gauss-Legendre quadrature of order 10.

Homogeneous surfaces

First, the tyre radiation over homogeneous impedance surfaces is examined. Results are shown for two different gap values, and for two different positions of the receiver inside the horn. In the *ES* model, preliminary numerical investigations proved that a ground discretisation spanning from x = -0.5 m to x = +1.5 m yields stable field predictions for the geometry considered here. For a gap of 1.85 cm (see Fig. 4-6), the correspondence between the measured values and the predicted ones is globally statisfactory. The levels of amplifications are well estimated and the frequency behaviour is also well reproduced. This holds for almost all the frequency range available in the measurements, i.e. from 500 Hz to 2000 Hz.

For a smaller gap value (see Fig. 4-7), predictions fit well to the measured values as long as the receiver is not too close to the horn centre. When the receiver is very close to the horn centre, as in Fig. 4-7(a), the *ES* model predicts somewhat lower amplification factors than those measured, in the frequency range between 500 Hz to 1200 Hz. The corrrespondence is however still satisfactory since the error do not exceed 2 dB in this frequency range.

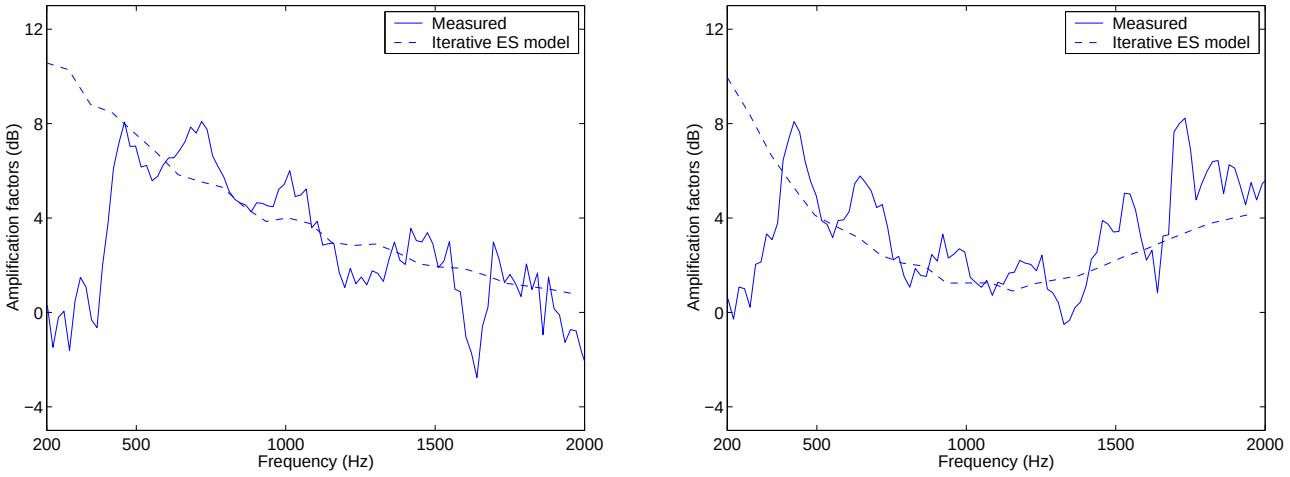

(a) Distance horn centre/receiver = 4.2 cm

(b) Distance horn centre/receiver = 18.2 cm

Figure 4-6: *Horn effect amplification factors over homogeneous impedance surfaces. Gap = 1.85 cm – Source height = 19.7 cm – Distance horn centre/source = 98 cm.*

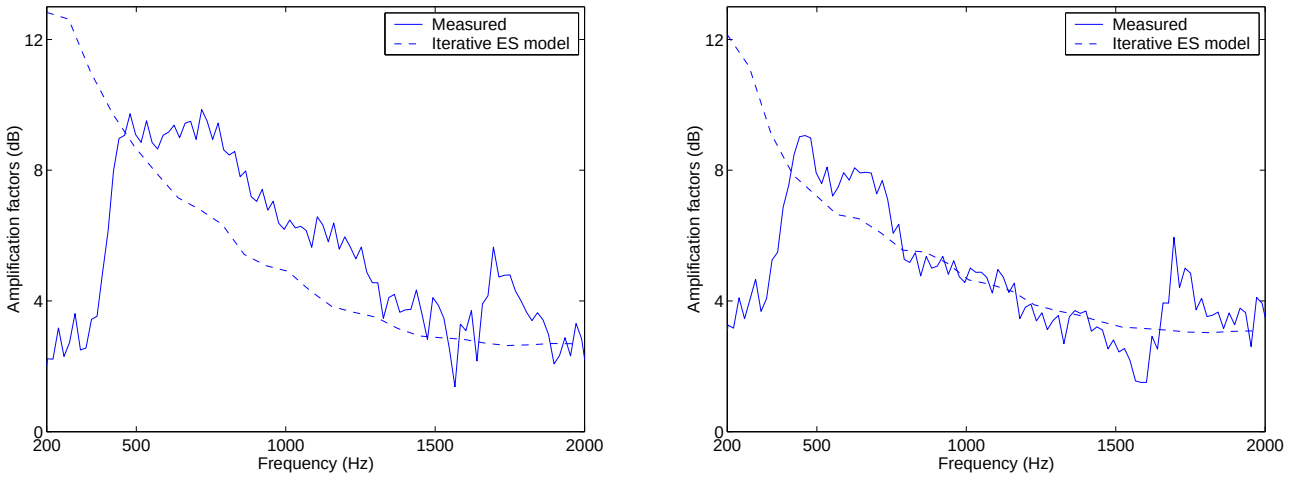

(a) Distance horn centre/receiver = 4.2 cm

(b) Distance horn centre/receiver = 12.2 cm

Figure 4-7: *Horn effect amplification factors over homogeneous impedance surfaces. Gap = 0.8 cm – Source height = 4.7 cm – Distance horn centre/source = 48 cm.*

In total, the present model gives horn effect amplification factors which correspond within 2 dB to the measured values, and this from frequencies as low as 500 Hz to 2000 Hz, maximum frequency available in the measurements. The model seems therefore accurate for the prediction of the tyre radiation over homogeneous surfaces on the main frequency range of interest

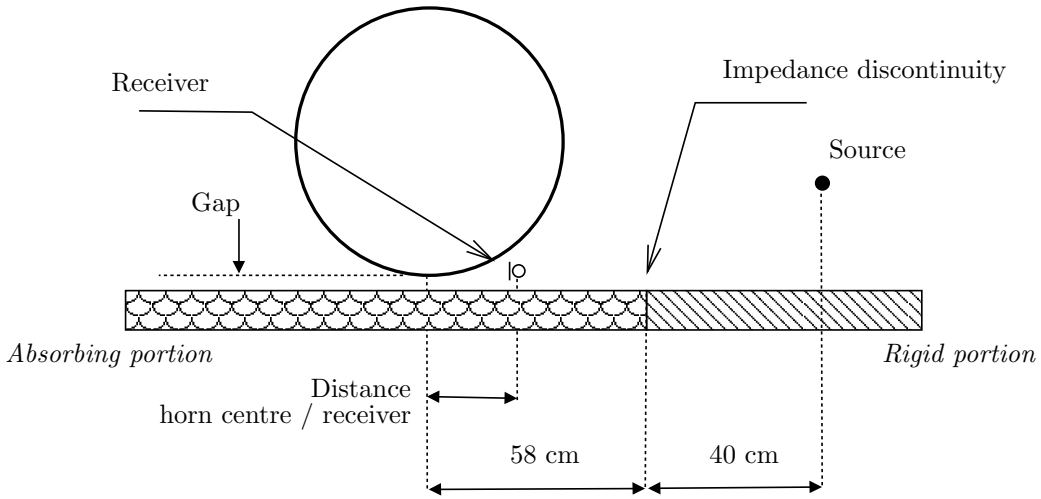

Figure 4-8: *Geometry of the measurement over inhomogeneous surfaces. Case where the tyre and the receiver are located above the absorbing portion and the source is placed over the rigid portion.*

for tyre noise purposes.

Inhomogeneous surfaces

An interesting feature of the present *ES* model is that it handles possible impedance discontinuities of the ground surface. Therefore, measurements of horn effect amplification factors were performed over surfaces having one discontinuity of impedance. Two cases are examined. First the receiver, which lies inside the horn, is placed over an absorbing surface and the source is placed over a rigid plane. Secondly, the source radiates over the absorbing portion and the receiver is located over a rigid plane.

From an experimental point of view, a panel of the absorbing material desribed previously was placed jointly to an acoustically rigid panel. In both situations, the impedance discontinuity was located at a 58 cm distance from the horn centre and at a 40 cm distance from the source (see Fig. 4-8). The impedance discontinuity was always perpendicular to the propagation path from the source to the receiver. In the *ES* model, monopole sources are placed at the ground level, on the length of ground corresponding to the absorbing portion.

In the case the tyre is above the absorbing material, the ground surface is discretised from behind the tyre (x = -0.5 m) up to the impedance discontinuity. Results are shown in Fig. 4-9

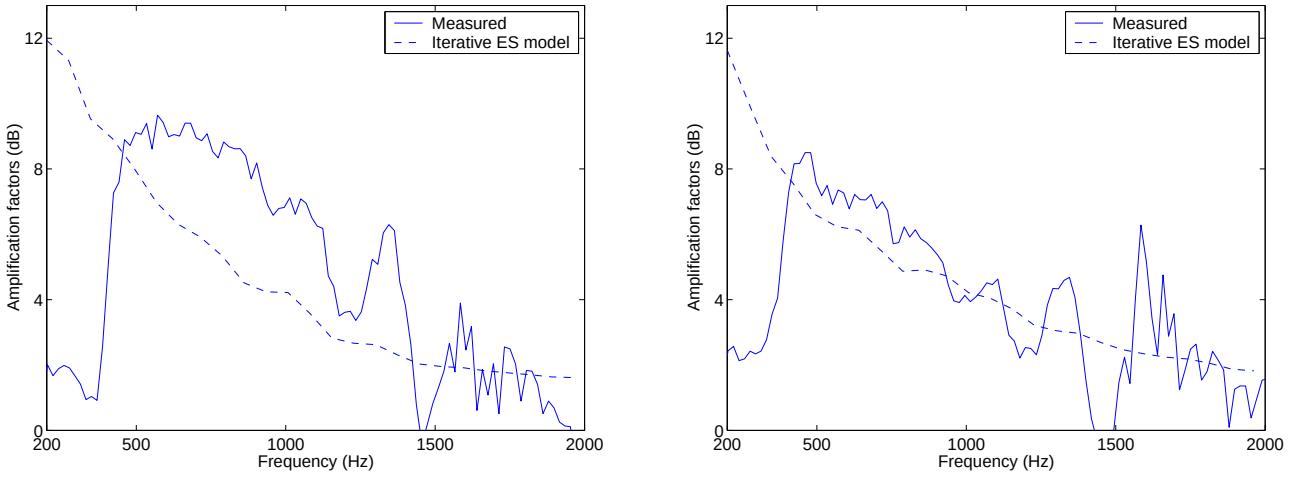

(a) Distance horn centre/receiver = 4.2 cm

(b) Distance horn centre/receiver = 12.2 cm

Figure 4-9: *Horn effect amplification factors over inhomogeneous impedance surfaces. Tyre and receiver over absorbing material and source over rigid surface. Gap = 0.8 cm – Source height = 19.7 cm – Distance horn centre/source = 98 cm.*

for two different receiver positions inside the horn. It can be observed that the amplification factors in this case are very similar to those obtained over a homogeneous surface (see Fig. 4-7). In the present situation too, a decent correspondence is observed as long as the receiver is not too far inside the horn. If this is the case, predicted amplification factors are around 2 dB lower than the measured ones at frequencies between 500 Hz to around 1200 Hz.

The second case examined is when the tyre and the receiver are placed over the rigid portion of ground and that the source is radiating over the absorbing portion of ground. In the *ES* model, the ground surface is discretised from the impedance discontiniuty to a little farther from the actual receiver position ($x = +1.5$ m). The geometry is reminded in Fig. 4-10(a). In this case, Fig. 4-10(b) shows measured and predicted amplification factors with solid lines and broken lines respectively. Results are shown in this figure for three different positions of the receiver inside the horn.

The amplification factors shown here exhibit a pattern, which is very similar to those measured over totally rigid surfaces (see for instance Fig. 2-15). Deviations at low frequencies are undoubtedly ascribed in this case to the two–dimensional character of the *ES* model. At frequencies above 800 Hz, the predictions fit well to the measured values. The levels and the general pattern of the amplification factors are correctly reproduced.

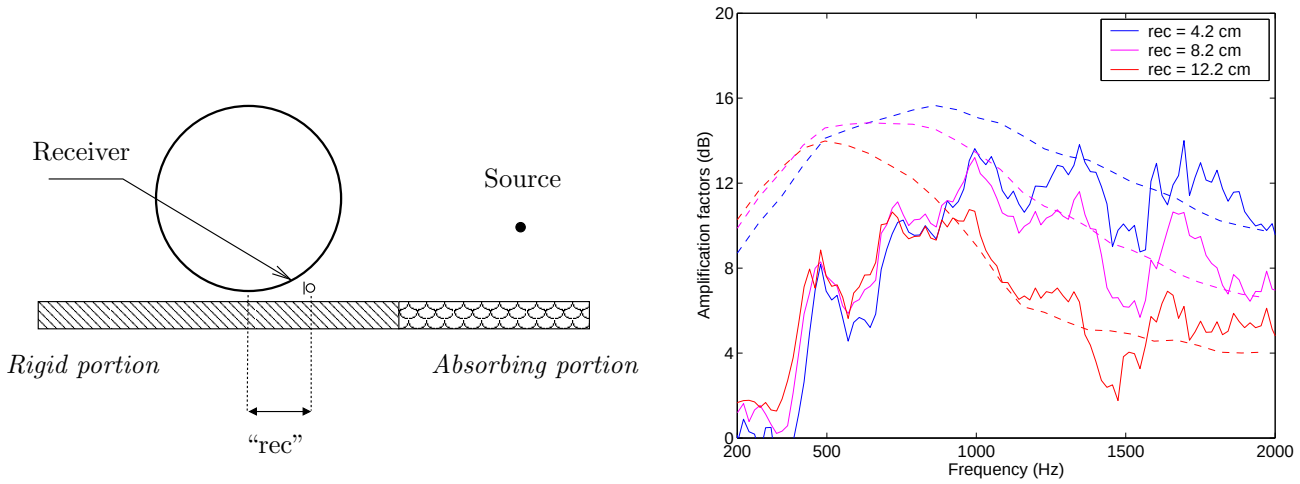

(a) Geometry of the experiment

(b) Measured (solid lines) and calculated (broken lines) amplification factors

Figure 4-10: *Horn effect amplification factors over inhomogeneous impedance surfaces. Tyre and receiver over rigid surface and source over absorbing material. Gap = 0.8 cm – Source height = 19.7 cm – Distance horn centre/source = 98 cm.*

This proves the accuracy of the iterative *ES* model in the presence of inhomogeneous surfaces too. In addition, the frequency range of validity of the model seems to depend on the impedance distribution on the ground surface.

Discussion

The results shown above prove that the present *ES*model is reliable for the prediction of the tyre radiation over homogeneous absobing surfaces from 500 Hz to the 2000 Hz. For inhomogeneous surfaces, the lowest frequency from which the model is accurate appears to be different for different impedance distribution. In particular, if the horn is located over an absorbing portion, the frequency range of validity tends to that obtained in the case of homogeneous absorbing surfaces. In contrast, if the horn is located over the rigid portion, the frequency range where the model is valid is very similar to that obtained in the case the ground is totally rigid (see *Chapter 2*).

These results support the fact that the part of the ground impedance laid in the contact region is expected to determine to a large extent the effect of the horn. However, some of the results may be discussed.

In particular, it is remarkable that in Fig. 4-6 and Fig. 4-7(b), calculated amplification factors correspond well to the measured values, yet from frequencies as low as 500 Hz. This is contradictory with the fact that the present model is two–dimensional, leading to an over–estimation of the horn amplification at these frequencies. It might also be questionned why these results fit well with the measurements if the receiver is not too far inside the horn, but do not correspond to the same extent if the receiver is close to the horn centre ? Finally, where do these deviations come from : experimental deficiencies or inaccuracy of the model ? The answer is probably a combination of both but the following hypotheses may be thought of.

As a matter of fact, the largest deviations observed in Fig. 4-7(a) and Fig. 4-9(a) between 500 Hz and 1200 Hz occur when two conditions are gathered : the receiver is close to the horn centre and the gap is very small. In this situation, the horn may be assumed to be totally closed at its apex, and thus to have its maximum efficiency. Particularly, the horn may considered as closed for the low frequencies, whereas the high frequencies may still "see" this small gap. Moreover, the horn has its major effect on the path which lies in the plane of the tyre. Because of the sound attenuation due to the absorbing material, the contribution from this path may be masked by other contributions lying out of the plane of the tyre, which are not influenced in the same manner by the presence of the horn. These contributions may increase significantly the sound pressure levels measured in the plane of the tyre. This effect is clearly not included in the present *2D* model.

Over rigid surfaces, the *2D* model over–estimates the amplification factors at low frequencies. In the case the horn has substantial absorbing properties, the model may over–estimates the attenuation, thus leading to amplification factors which are too low compared to the measured values. This effect is expected to be very pronounced when the horn has its maximum efficiency, i.e. when the receiver is close to the horn centre and the apex is almost closed.

A last hypothesis is that the model implementation considers that the ground surface is locally reacting. This might be only partially true for the absorbing material used here at low frequencies. If waves in the absorbing material were to be considered, it is likely that the horn effect might enhance their contribution to the radiated field. The horn effect is increased if the apex is closed and so would be the contribution from surface waves.

4.5 Summary

The present chapter examines the problem of the tyre radiation over locally reacting, impedance surfaces. Different solutions are proposed, which are adapted to the type of impedance distribution of the ground surface.

In the case where the surface is homogeneous, that is where the impedance is constant along the ground, simple solutions are presented. One of the solution is based on the well–known reflection factor for plane waves. Due to its ease of implementation, it was shown that such a solution, though not mathematically correct, could be a useful tool to predict general trends of the tyre noise over impedance surfaces.

Moreover, an exact expression of a reflection coefficient for cylindrical waves of arbitrary order is derived in this chapter. The principle consists in using a mirror image source, the amplitude of which is multiplied by a reflection factor. The basic idea of the derivation is that the total field above the ground must give the correct value of the acoustical impedance at any point of the ground surface. Mathematically, this boundary condition takes the form of a linear differential equation, the general solution of which is known from the literature. Finally, a solution for such a reflection factor is expressed as a function of complex integrals and of the value of the reflection factor for plane waves at infinity. The numerical implementation of such a reflection factor is however difficult and will be the subject of future works.

A model for the tyre radiation over arbitrary impedance grounds is proposed. In particular, this model can handle discontinuities of the impedance distribution on the ground. Based on the *ES* method, it combines advantageously the numerical efficiency of a *2D* model for the tyre radiation and the large features of a *BE* alternate technique for the ground effects reproduction. A multipole source is in charge of the simulation of the tyre radiation while monopole sources are placed on the ground to control the impedance at the surface. This results in a large set of amplitudes, which must be tuned in order to fulfill both the tyre boundary condition and the impedance condition. Solving the whole set of amplitudes using a (large) matrix inversion is not numerically accurate. Instead, the amplitude of the multipole and the amplitudes of the ground sources are successively tuned to account for the multiple reflections occuring between the tyre surface and the road. This is implemented in an iterative process, which is numerically effortless. At the end of the iteration, the two boundary conditions are fulfilled simultaneously. The model validity is tested by comparisons with measurements of the horn effect amplification factors over homogeneous and inhomogeneous impedance surfaces. The model fails to

predict the correct amplification values due to its *2D* character, particularly when the receiver is very close to the horn centre. In fact in this case, propagation paths out of the plane of the tyre, which are not considered in a *2D* model, may contribute significantly to the sound field. Besides these limitations, the predictions correspond well to the measured values over homogeneous and inhomogeneous surfaces; the level of the amplification is correctly estimated by the present model on a wide frequency range where the *2D* simplification is valid.

In conclusion, this chapter presents a number of modelling tools to predict accurately the radiation of the tyre in the presence of arbitrary impedance surfaces. Therefore, it seems possible to examine the possibilities of a reduction of the tyre noise with such models. This is the subject of the parametrical study proposed in the next chapter.

Chapter 5

Parameter Study of the Tyre / Road Interface Properties

In the previous chapter, a model for tyre radiation over arbitrary impedance surfaces was derived. Furthermore, owing to its features, this model seems appropriate for studying the possibilities of a reduction of tyre / road noise. Therefore, in this chapter, a number of experiments, based on measurements or calculations, are presented, which investigate the properties of tyre radiation over impedance surfaces.
The parameter study is organised as follows. First, the influence of the geometrical parameters on tyre noise is examined. Next, the influence of the type of ground impedance is investigated. Finally, the combined effects of geometrical and acoustical parameters on tyre radiation is discussed.

5.1 Geometry and notations

Fig. 5-1 presents the geometry used for the experiments presented in this chapter.

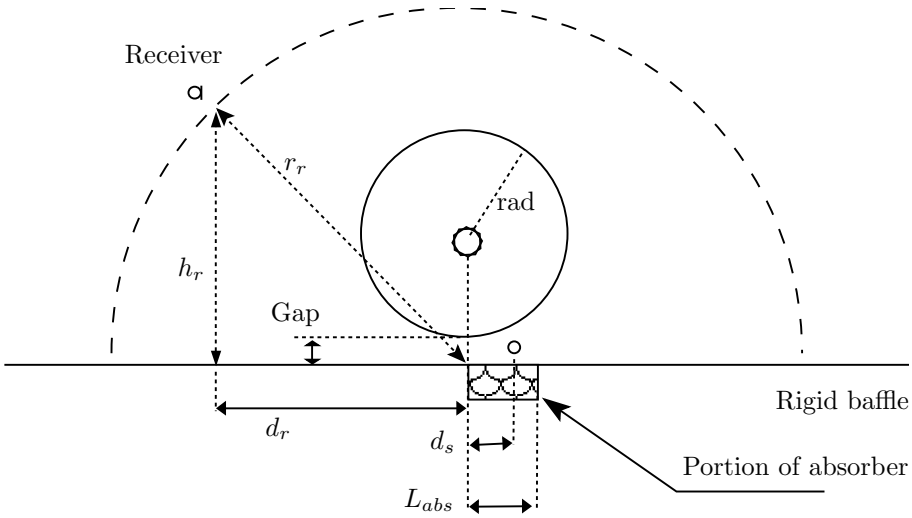

Figure 5-1: *Geometry and notations used for the numerical examples.*

The tyre radius is noted *rad*. The positions of the source and the receiver(s) are given with respect to the position of the horn centre and of the ground surface. Therefore, the position of the noise source is given by $(d_s, 0)$ (the source is always on the ground), and that of the receiver is given by (d_r, h_r). The length of absorbing material laid on the ground is L_{abs}. If "averaged values" is indicated in the figure, it means that *SPL* are calculated and averaged over 100 receivers placed on a semi–circle of radius r_r, to give a single value for each frequency. The influence of the different parameters is examined in terms of horn effect amplification factors. In addition, insertion losses are introduced to measure the reduction (or the increase) of sound amplification. They are defined as

$$IL\ (dB)\ =\ 10\ \log_{10}\left|\ \frac{p_{var}}{p_{ref}}\ \right|^2 \tag{5-1}$$

where p_{ref} is the *SPL* measured or calculated in a reference case, and p_{var} is the *SPL* obtained after the variation of a parameter.

For comparison with the measurements which applied the reciprocity principle, the actual positions of the source and of the receiver are used in the model. However, in the text below, the term "source" refers to noise sources in the contact region inside the horn and the term "receiver" refers to a position in front of the tyre outside the horn.

5.2 Geometrical parameters

In this section, the influence of the following parameters is discussed : the position of the source inside the horn, the position of the tyre height over the reflecting plane of the ground, and the tyre radius.

Position of the source

First, the influence of the source position inside the horn is investigated. Fig. 5-2 shows horn effect amplification factors as a function of the distance from the source to the horn centre. Results are shown for different gap values. A gap value of 0 cm corresponds to the case when the tyre and the road surface are in contact.

Globally, amplification factors here show the same behaviour as in the presence of rigid surfaces. As the source moves out of the horn, the maximum amplification decreases and is shifted towards the low frequencies. Amplification levels decrease with frequency as the absorption

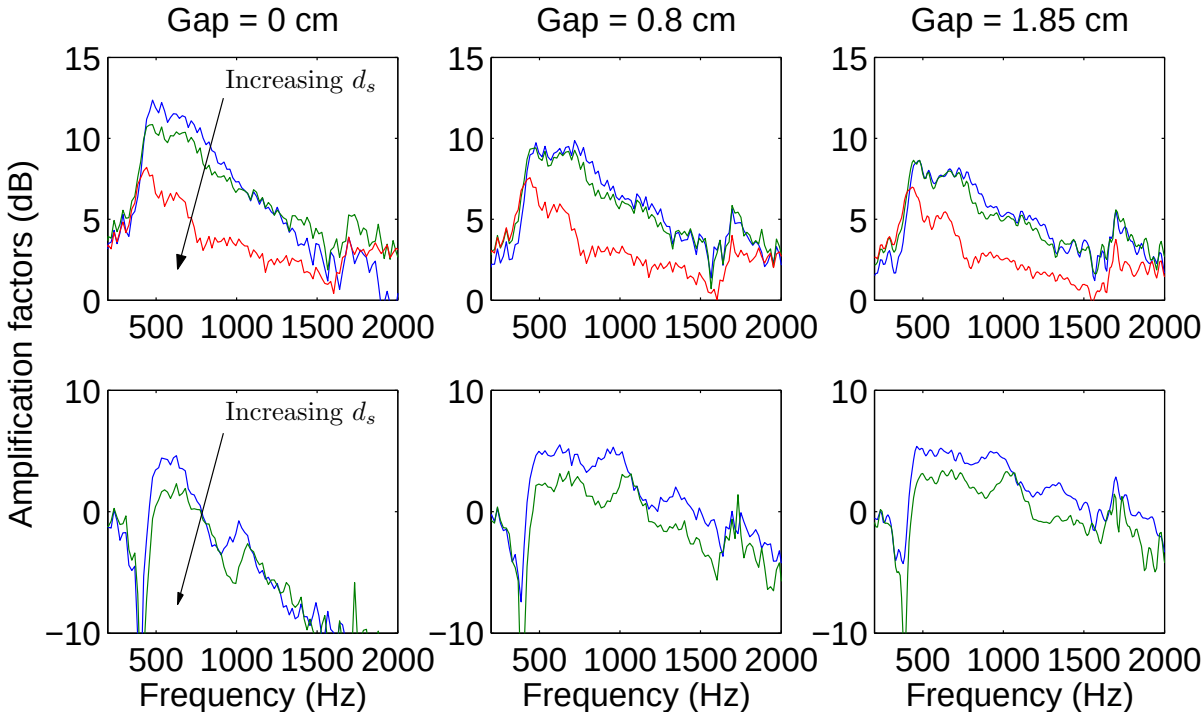

Figure 5-2: *Measured influence of the source position inside the horn for different tyre heights (gap). Top line figures correspond to sources on the front side of the horn : d_s = 4.2 cm, 8.2 cm, 18.2 cm – Bottom line figures for sources on the rear side of the horn : d_s = -5.8 cm, -11.8 cm – d_r = 0.48 m, h_r = 0.20 m.*

properties of the material increase. The maximum amplification is reached around 500 Hz and lies around 12 dB, which is quite substantial. For a gap of almost 2 cm, the maximum still lies around 7 dB for a source very close to the horn centre.

This figure also indicates that the noise sources located on the rear side of the tyre may contribute significantly to the noise perceived in front of the tyre. For a 1.85 cm gap, the amplification reaches around 5 dB at 500 Hz, which is very close to the amplification value for the sources located on the front side of the tyre with the same gap. When the sources moves out of the horn (increasing d_s), the amplification levels decrease, as was observed for the sources placed on the same side of the horn as the receiver.

Position of the reflecting plane

The influence of the tyre height over the reflecting plane is interesting to examine because rolling on very rough roads leads to lifting the tyre above the reflecting plane of the road.

The influence of this parameter may also be investigated from the measurements shown in Fig. 5-2. For an increasing gap value between the tyre and the road, the amplification factors appear to be more influenced when the source is close to the horn centre than when the source is further out from the horn centre. In fact, for a source at a 18.2 cm distance from the horn centre (lower amplification curves in the top line figures), the amplification factors are little influenced by a change in the gap values. If the source is placed at 4.2 cm (larger amplification curves in the top line figures), the maximum amplification drops from 13 dB when the tyre and the ground are in contact, to 7 dB for a 1.85 cm gap. This may be explained by the fact that the change in the horn geometry is more important for a source position close to the horn centre than when the source is farther out of the horn. For sources on the rear side of the horn, their contribution increase as the gap increase, especially at frequencies between 600 Hz to 1200 Hz.

These tendencies are also found at other measurement positions. Results are more cleary shown in Fig. 5-3(a) in terms of insertion loss. The reference case used here is the smallest gap value, i.e. 0.8 cm. Thus, negative values correspond to lower *SPL* when the tyre is further up above the ground than when the tyre is very close to it. Negative values are found on the whole frequency range of the measurements for a gap change from 0.8 cm to 1.85 cm.

For a gap change from 0.8 cm to 10.45 cm, negative values are found only between 400 Hz to

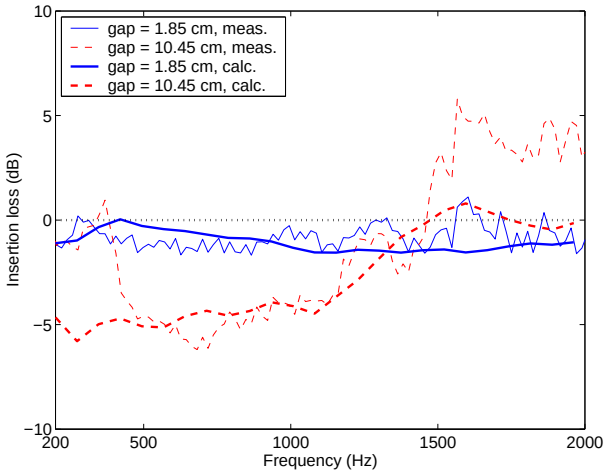

(a) Insertion loss. Reference surface is absorbing with gap = 0.8 cm

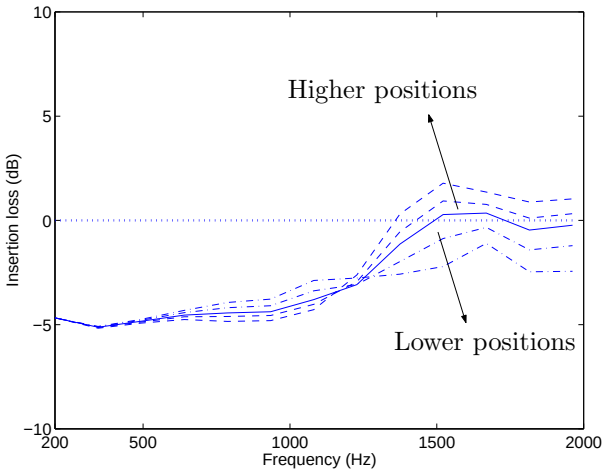

(b) Calculated sensitivity to the receiver position. Changes by steps of 3 cm from the measured position

Figure 5-3: *Measured and calculated influence of the gap over absorbing surfaces.* d_s *= 8.2 cm –* d_r *= 98 cm –* h_r *= 20 cm.*

around 1300 Hz. At higher frequencies, positive values are obtained. This means that higher *SPL* are measured when the tyre is far above the ground compared to when the tyre is close to the ground. This may be due to the fact that, for such a large gap, the high frequencies are no longer sensitive to the presence of the tyre. Lowering the tyre leads to increasing the efficiency of the horn. Since an absorbing material is placed inside the horn, it may thus yield lower amplification factors.

These results are confirmed by the calculations obtained with the iterative *ES* model (thick lines in Fig. 5-3(a)). Predictions lie within 1 dB to the measured values. However, for a gap change from 0.8 cm to 10.45 cm (dashed line), at frequencies above 1400 Hz, the model predicts insertion loss which are lower than those measured. In this frequency range, amplification levels are mainly governed by interferences. The model which is *2D*, is not able to reproduce correctly the interferences due to a cylinder of finite width. As previously mentioned, diffraction at the tyre shoulders is not included. The model sensitivity with respect to the interference pattern is clearly shown in Fig. 5-3(b). It is observed that variations of insertion loss are significant above around 1200 Hz when the receiver position is slightly moved. This supports the fact that a great care should be taken with the interpretation of these results.

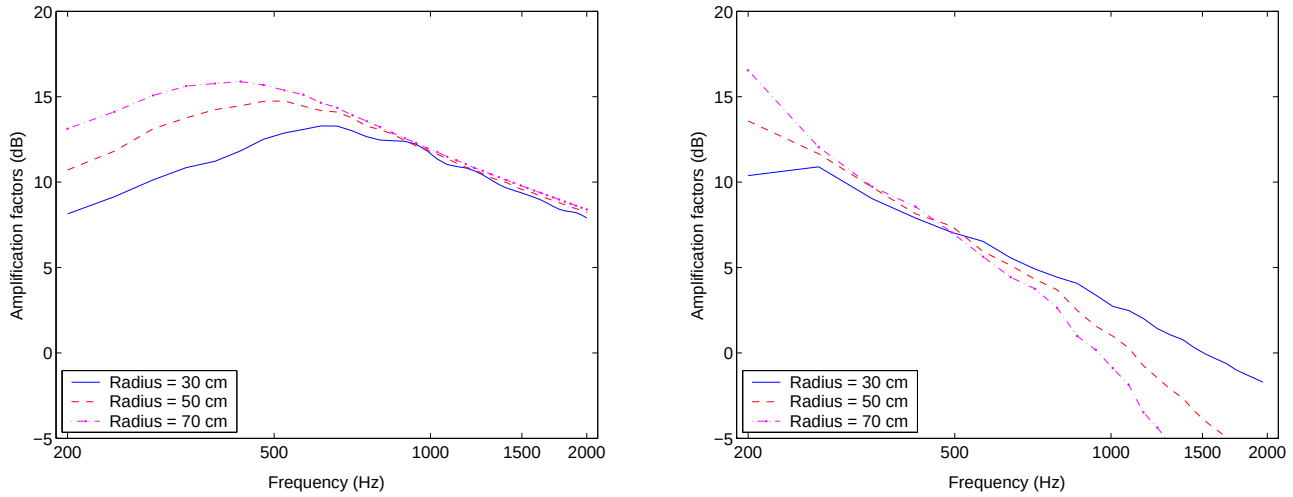

(a) Rigid surface

(b) Absorbing surface used in the previous measurements

Figure 5-4: *Horn effect amplification factors for different tyre radii. Averaged values with* $r_r = 3 \times rad$ *– Gap* $= 1$ *cm –* $d_s = rad/2$*.*

Tyre radius

Another parameter of interest is the influence of the tyre radius on the horn effect sound amplification. In the presence of an absorbing surface, the problem is to know if a given impedance surface has the same effect with tyres having different radii.

First, Fig. 5-4(a) shows horn effect amplification factors calculated for different tyre radii over a rigid surface. Amplification factors obtained over the absorbing surface used in the previous experiments are shown in Fig. 5-4(b). Results are shown in averaged values obtained as described in *Section 5.1*. The distance from the horn centre to the receivers is chosen to be proportional to the tyre radius so that the distance between the receivers and the tyre surface is constant. The gap between the tyre and the road is set to 1 cm to keep low calculation times in the case the surface is absorbing (see the model implementation in *Section 4.4*).
For the radiation over rigid surfaces (Fig. 5-4(a)), amplification factors increase with increasing frequency up to a maximum, the position of which depends on the tyre radius : the larger the tyre radius, the lower the frequency of maximum. In addition, the level of maximum amplification increase with increasing tyre radii. The maximum of amplification lies around

12 dB at 600 Hz for a 30 cm tyre radius; it exceeds 15 dB at 400 Hz for a 70 cm tyre radius. At frequencies above this maximum, the amplification levels decrease and become similar for different tyre radii.
For the tyre radiation over the absorbing surface (see Fig. 5-4(b)), there is no maximum of amplification; levels decrease along the frequency range examined here. At frequencies below 500 Hz, amplification levels are higher with a larger tyre radius, as over rigid surfaces. This is due to the fact that the impedance material has very low absorption properties at these frequencies. Above 500 Hz, a different behaviour is observed. The amplification levels are lower for larger tyre radii.
In conclusion, the effects of an absorbing plane on the tyre radiation appears to depend on the tyre radius. At very low frequencies, below around 300 Hz, introducing an absorbing plane may lead to higher *SPL*. At frequencies above around 500 Hz, the larger the tyre radius, the larger the sound reduction.

5.3 Ground surface impedance

This section examines the effects of the presence of an absorbing surface on the tyre radiation. First, the importance of the type of ground inside the horn is discussed. The spatial re–distribution of sound due to the horn effect is then examined. Numerical examples for various geometries are presented for the determination of the ground impedance value which give the lowest sound amplification.

Ground impedance in the horn region

To be able to control the noise source, it is important to examine the importance of the type of ground in its vincinity, namely inside the horn region. For this, measurements performed over surfaces having a rigid and an absorbing portion are compared to measurements performed over an entirely absorbing surface.

Results are compared in terms of insertion loss as calculated in Eq. 5-1, where the reference surface is entirely absorbing. Insertion losses are displayed for several distances d_s between the horn centre to the source position. Results are shown in Fig. 5-5(a) for the case where the tyre is radiating over the rigid ground and the receiver is placed over the absorbing portion.

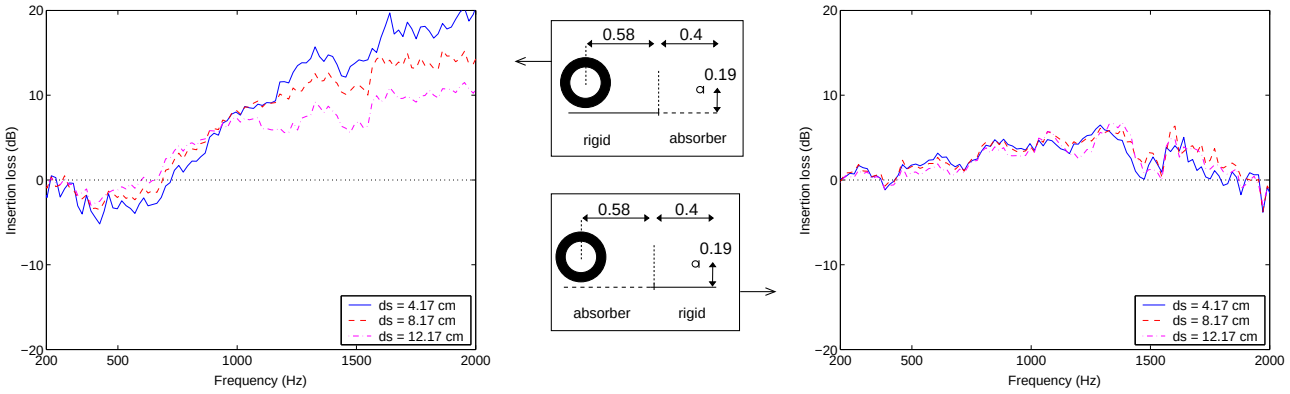

(a) Rigid portion inside the horn and receiver above absorber

(b) Geometries

(c) Absorber inside the horn and receiver above rigid portion

Figure 5-5: *Measured influence of the impedance of the ground inside the horn. Reference surface is entirely absorbing. Results for different source positions inside the horn – Gap = 0.8 cm.*

In Fig. 5-5(c), the reverse situation is examined, that is when the tyre is over the absorbing surface and the receiver is placed over the rigid portion. The exact corresponding geometries are shown in Fig. 5-5(b). In both situations, the impedance surface lying inside the horn is prolongated up to 60 % of the total distance from the horn centre to the receiver.

It is observed in these two figures that the insertion losses are almost always positive, which means that an entirely absorbing surface yields lower amplification factors compared to when the surface is only partially treated. However, this trend, clear in Fig. 5-5(a), is less pronounced when the tyre is radiating directly over the absorbing portion. In this latter case, the situation is worsened only by a few decibels compared to when the surface is entirely absorbing. This means that the main part of the noise reduction is achieved by controlling the impedance in the horn region as expected. This corresponds to controlling the radiation impedance of the noise source inside the horn.

Moreover, positive values of insertion loss are found below around 600 Hz for the tyre radiating over the rigid portion (see Fig. 5-5(a)). This is somehow surprising because it means that the sound amplification when the ground surface inside the horn is rigid is lower than when it is absorbing.

This tendancy is also displayed by the calculations obtained with the iterative *ES* model. Fig. 5-6 shows that the amplifications factors calculated over an entirely absorbing surface may exceed those obtained over a rigid surface at low frequencies. However, the frequency, at which

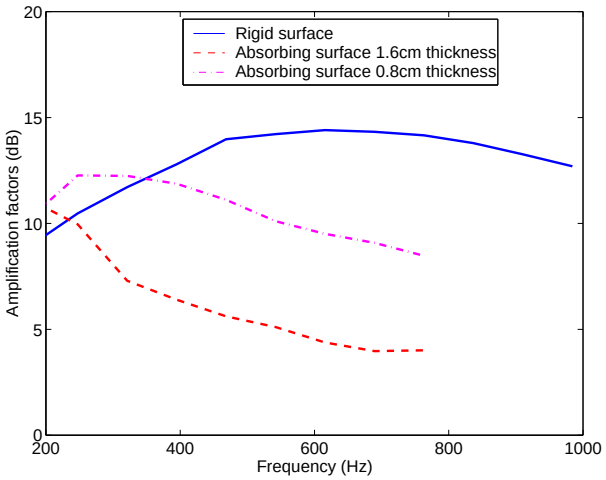

Figure 5-6: *Horn effect amplification factors over a rigid surface compared to over entirely absorbing surfaces of different thicknesses. Geometry of Fig. 5-5(a) – $d_s = 4.2$ cm.*

the amplification factors obtained for the rigid surface become larger than those obtained for the absorbing surface, is not well predicted by the model. If the ground impedance is changed (the absorbing layer thickness is divided by two, see Fig. 5-6), the "cross–over" frequency approaches that obtained in the measurements. Therefore, this somewhat surprising result seems to be confirmed by the calculations; however its explanation still needs to be clarified.

Spatial re–distribution of sound

An important consequence of the horn effect is the re–distribution of sound in space. Calculations presented here investigate qualitatively this property.

SPL are calculated when the tyre is above the road and normalised to *SPL* obtained when the noise source is radiating in the free–field, i.e. without the tyre nor the ground. Three situations are examined : the road is rigid, a strip of absorbing material is placed inside the horn while the rest of the surface is rigid, and the surface is entirely absorbing. In these two latter cases, the material impedance corresponds to that used in the previous measurements (see Fig. IV-4(b)). An excitation signal of 1007 Hz is assumed. It corresponds to the frequency range where the model is accurate; it also corresponds to the dominant frequency range when calculating A–weighted sound levels.
The arrow in the figures indicates the position of the source inside the horn. The length of absorbing material on the ground is also indicated schematically. The gap between the tyre

and the ground is set to 1 cm to keep low calculation times.
Results are presented in decibels where white colors, resp. dark colors, indicate high amplification levels, resp. low amplification levels.

Over a totally rigid surface (see Fig. 5-7), the sound is mainly directed in front and in the rear side of the tyre. Due to the susbtantial gap value used here, sound levels are very similar on both sides of the contact zone. High amplification levels are found, as expected, in the horn and close to the ground. As the receiver height increases, the levels decrease. A shadow zone appears clearly above the tyre. In this region, interferences appear, the pattern of which depends on the frequency of the excitation signal. The lowest levels of amplification are found in this region.
When a strip of absorbing material is introduced inside the horn, Fig. 5-8 shows amplification levels which are globallly lower than for a rigid surface. The highest amplification levels are still found in the horn region and close to the surface. In front of the tyre amplification levels are only slightly lower than for a rigid surface. However, a significant decrease is observed on the rear side of the tyre. Above the tyre, the interference pattern previously observed is modified. First, it is "rotated" towards the rear side of the tyre. Secondly, in contrast to the rigid case, the most contrasted interferences are not found opposite to the source position with respect to the tyre; they are shifted towards the rear side of the tyre.
If the surface is now entirely absorbing (see Fig. 5-9), the directivity of the horn effect is practically the same as for the rigid surface. However, the amplification levels are significantly lower in the case the surface is absorbing. As previously, the maximum levels are found inside the horn and close to the ground surface. In contrast to the two previous situations, amplification levels decrease more rapidly as the receiver moves away from the horn, but still close the ground. The interference pattern observed above the tyre seems to be inverted compared to the rigid case : an increase is observed for the absorbing surface where there was a decrease for the rigid surface, and vice versa. One should keep in mind that the distribution of sound in this region is important because of the presence of the wheelhouse of the tyre.

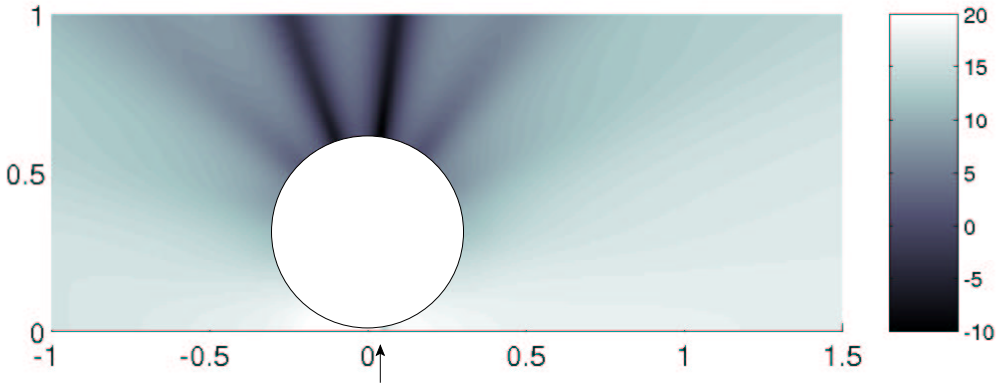

Figure 5-7: *Map of relative SPL over a rigid surface. $f = 1007$ Hz – gap = 1 cm – $d_s = 5$ cm – The arrow indicates the position of the noise source – The scale is in dB.*

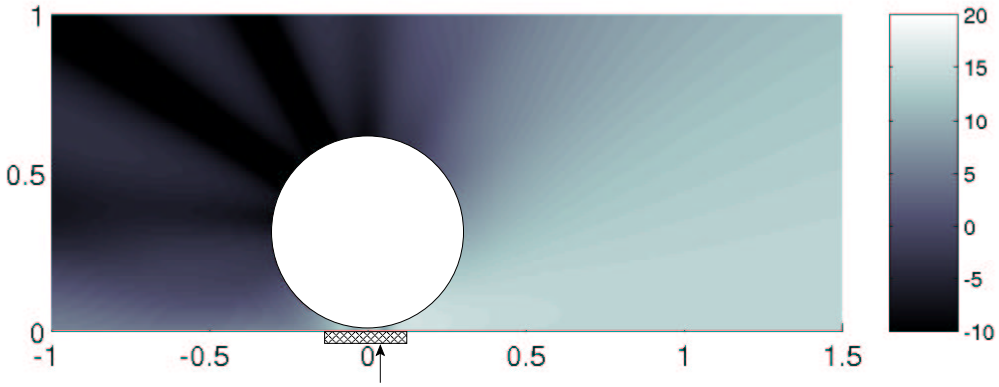

Figure 5-8: *Map of relative SPL over a strip of absorbing material. $L_{abs} = 20$ cm – $Z_n = 720 - 1226\text{j}$ – $f = 1007$ Hz – gap = 1 cm – $d_s = 5$ cm – The arrow indicates the position of the noise source – The scale is in dB.*

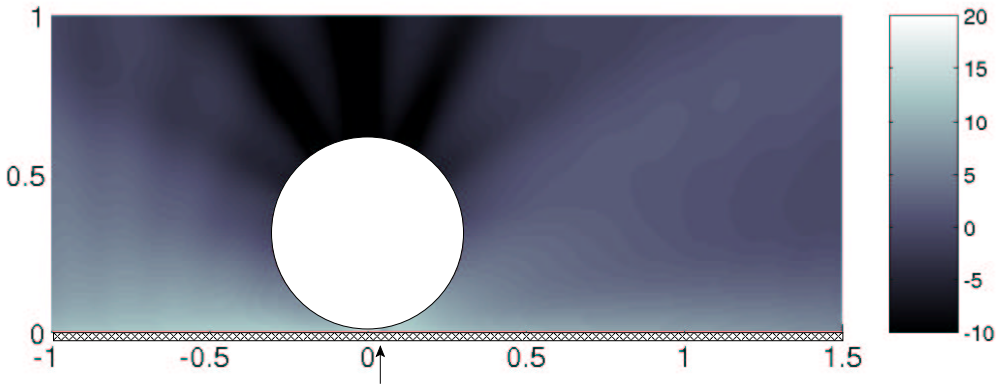

Figure 5-9: *Map of relative SPL over an entirely absorbing surface. $Z_n = 720 - 1226\text{j}$ – $f = 1007$ Hz – gap = 1 cm – $d_s = 5$ cm – The arrow indicates the position of the noise source – The scale is in dB.*

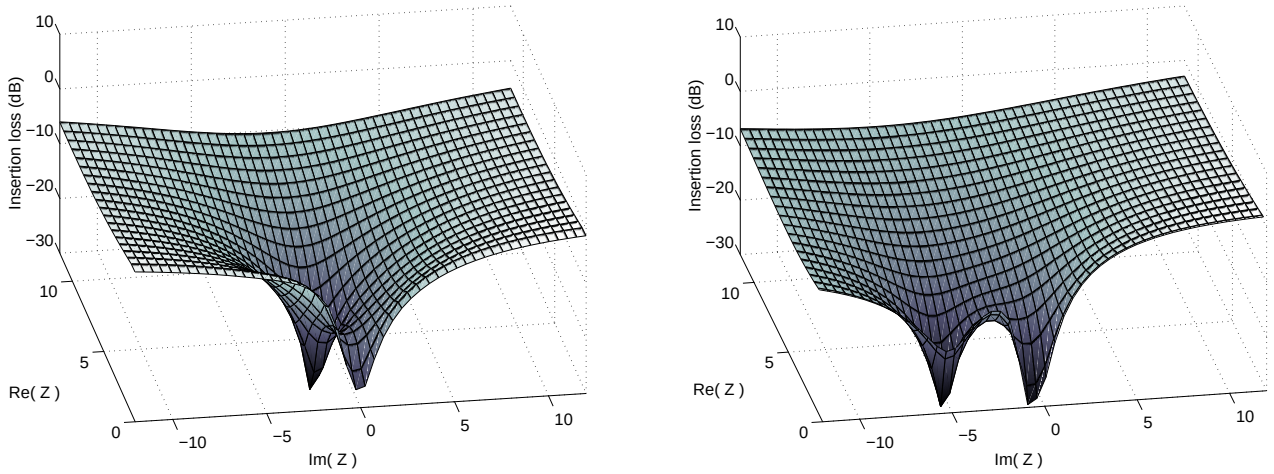

(a) $gap = 0.01$ m – $d_s = 0.05$ m – $rad = 0.3$ m

(b) $gap = 0.01$ m – $d_s = 0.1$ m – $rad = 0.3$ m

Figure 5-10: *Insertion loss for an entirely absorbing surface with varying impedance. Reference surface is rigid – L_{abs} =2×1.2 m centered on the tyre – f = 500 Hz.*

Impedance optimisation

This last paragraph presents a brief attempt to optimise the value of the ground impedance. The tyre is assumed to be radiating over an entirely absorbing surface. The optimisation is performed here for two source positions inside the horn, and for two frequencies, 500 Hz and 1000 Hz.

The value of the normalised impedance of the absorbing material is varied from 0.5 to 12 for its real part, and from -12 to 12 for its imaginary part. Therefore, surfaces having high and low absorption properties are examined. Negative real parts are not considered because this would require introducing active materials; these solutions are not realistic for road surfaces. As a matter of fact, the iterative model rarely converge for these impedance values. Results are shown in terms of averaged values of insertion loss; the reference surface is totally rigid. The optimum impedance will be the one giving the lowest value of the insertion loss.

Results are shown in Fig. 5-10(a) for a 500 Hz signal excitation and for a source position close to the horn centre. In this case, the insertion loss never takes on positive values, which means that all impedance values yield a decrease in the sound amplification in this case. Moreover, two dips can be distinguished. One of these dips gives an impedance value close to zero, which corresponds to the presence of a totally soft surface. This quite trivial solution consists

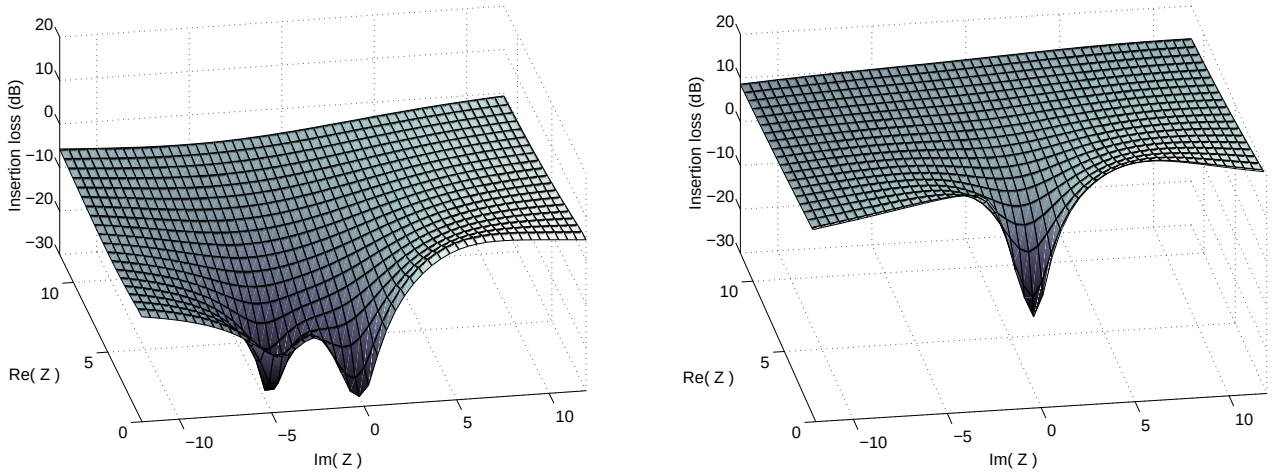

(a) $gap = 0.01$ m – $d_s = 0.05$ m – $rad = 0.3$ m

(b) $gap = 0.01$ m – $d_s = 0.1$ m – $rad = 0.3$ m

Figure 5-11: *Insertion loss for an entirely absorbing surface with varying impedance. Reference surface is rigid – L_{abs} =2×1.2 m centered on the tyre – f = 1000 Hz.*

in reducing the radiation impedance of the source inside the horn. The second dip gives an impedance which has a negative imaginary part and a positive real part. Due to the time dependence in the model as $e^{+j\omega t}$, this is the impedance value of a low damped spring.

If the noise source is moved further out of the horn (see Fig. 5-10(b)), besides zero impedance, an optimum impedance value is found, which has a lower real part and a higher negative imaginary part compared to the previous situation. In total, this impedance has a larger magnitude than that found previously. The physical behaviour of such a surface would correspond to a spring, which would be less damped and have a higher stiffness compared to that found for the previous source position.

For a 1000 Hz excitation signal, the predicted insertion losses shown in Fig. 5-11(a) for a 1 cm gap present two minima, one of which corresponds to zero impedance. The other value of the optimum impedance has a real part different from zero, though very small, and a negative imaginary part. Again, this would physically imply the presence of springs with very little damping on the surface.

If the source is moved further away from the horn centre (see Fig. 5-11(b)), the picture changes considerably : insertion losses are now positive for most impedance values, except for a zero

impedance value. For most impedance values, the increase is about 10 dB, which is quite substantial. This means that for such a system geometry, the presence of an absorbing material would lead to around a 10 dB amplification increase compared to the same system over rigid surfaces, unless this material has zero impedance value. This example shows that the optimisation of the acoustical properties of the ground surface is very sensitive to the exact geometry of the tyre / road interface.

Therefore, for most of the geometries examined here, the model predicts two impedance values, which give a substantial reduction of sound. One optimum impedance value corresponds to a totally soft surface, and the second one corresponds to a material having the characteristics of a low damped spring. These surfaces may be difficult to realise in practice because it is arduous to control the impedance value of the surface on large portion of roads.

5.4 Geometrical and acoustical combined effects

It has been shown in the previous section that the only impedance optimisation could lead to solutions, which may be difficult to realize and to maintain for real road surfaces. Therefore, it is proposed in this section to examine the combined effects of the tyre height above the physical reflecting plane and the presence of an absorbing material. This would correspond in reality to very rough roads having substantial absorption properties, a solution which has already been tested in reality.

Results are shown in Fig. 5-12 in terms of insertion loss with the reference surface as rigid with a 5 mm gap. The impedance value of the absorbing material used here corresponds to the material used in the previous experiments (see Fig. IV-4(b)). In addition, insertion losses calculated over rigid surfaces by varying the gap only are shown in the same figure (thin lines), to estimate the influence of the absorption. The same reference surface is used in this case.
At frequencies below around 400 Hz, positive value of the insertion loss are found, whereas the gap increase over rigid surfaces lead to a decrease in the sound amplification. This result coincides with the result observed in Fig. 5-5(a) which has not been clarified. Beyond this frequency, the decrease in sound amplification is important. At 500 Hz for instance, the insertion loss is around -2 dB for rigid surfaces. The additional effects of the ground impedance make

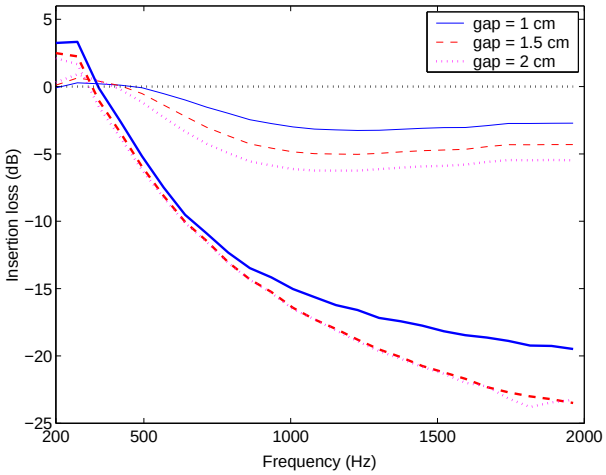

Figure 5-12: *Combined effects of the tyre height and surface impedance on tyre radiation. Averaged values of insertion loss. Reference surface is rigid with 5 mm gap – Solid lines : gap effect only – Thick lines : gap + impedance effect – $d_s = 0.05$ m – $rad = 0.3$ m*

this value drop to -6 dB. The decrease of the insertion loss along the frequency also correponds to increasing absorption properties of the surface modelled here. Insertion losses for all gap changes drop to -15 dB around 1000 Hz. Note that this reduction is achieved even with a 5 mm increase of the tyre height over the road reflecting plane. At 2000 Hz, the decrease lies between -20 dB to -25 dB for 1 cm and 1.5 cm gap increases.

Although these examples do not consider the practical attainability, they show that a substantial noise reduction may come from the combined effects of the acoustical and the geometrical properties of the tyre road interface.

5.5 Summary

This chapter presents a brief parameter study of the tyre / road interface properties. The discussion is based on measurements and on calculations obtained using the model presented in *Chapter 4*. Due to its low computational demands, this model appears to be a convinient tool for such parametrical studies.

The influence of the geometrical parameters on the tyre radiation is first discussed.

As for rigid surfaces, the position of the source inside the horn determines to a large extent the level of sound amplification for absorbing surfaces. As the source moves out of the horn, amplification levels decrease and the frequency of maximum amplification is shifted towards

low frequencies. This also holds for sources placed on the rear side of the horn.

As expected, the contribution from the sources on the rear side of the tyre increases with an increasing gap. For sources on the front side of the tyre, increasing the tyre height leads to a decrease in sound amplification on the whole frequency range. This tendency is well predicted by the iterative *ES* model.

The influence of the tyre radius is also investigated using the model. For rigid surfaces, tyres having larger radii give higher sound amplification at low frequencies. The frequency of maximum amplification is shifted towards lower frequencies as the tyre radius increases. Above this frequency, i.e. around 600 Hz, amplification levels appear to be independent on the radius. The picture is slightly different for the radiation over the absorbing surface. At low frequencies, the same tendency as for rigid surfaces is observed due to the low absorption properties of the impedance material. In the mid and high frequency range, the amplification levels are lower for larger tyre radii.

The influence of the ground impedance on the radiation is also discussed from measurements and from model calculations.

It is shown from the measurements that the sound attenuation due to the presence of an entirely absorbing surface is mainly governed by the ground impedance which lies inside the horn. This result could be expected as it consists in controlling the radiation impedance of the noise source. Measurements also show that amplification levels at low frequencies could be higher over an absorbing surface compared to a rigid surface. This result is confirmed by the calculations but it has not been clarified.

The model allows one to investigate the re–direction of sound due to the horn effect. It is shown that the horn effect over a homogeneous surface leads to a concentration of sound in front and on the rear side of the tyre. However, the amplification levels are significantly lower in the case the surface is absorbing than when the surface is rigid. In addition, amplification levels decrease more rapidly as the receiver moves away from the horn over an absorbing surface than over a rigid surface. Interferences occuring above the tyre, i.e. opposite to the contact zone, are also substantially modified in the presence of an absorbing surface.

Some guidelines for the optimisation of the surface impedance are also given. By construction, the *ES* model is independent of the type of ground impedance. Therefore, besides impedances corresponding to active materials, any impedance value could be implemented in the model.

The model predicts two impedance values which could give a substantial reduction of the sound amplification. One of these is zero impedance, which corresponds to a totally soft surface. The second value of impedance corresponds to a low damped spring. The calculations also prove that the impedance value depends on the exact geometry of the tyre / road interface.

Finally, model calculations show that an efficient sound reduction is achieved by combining the tyre height and the impedance of the road surface. This solution corresponds to surfaces having a large roughness amplitude together with substantial absorption properties.

Chapter 6

Conclusions

Main results

The work presented in this thesis is motivated by the needs to understand and to control the radiation mechanisms of tyre noise. The objective was to design a numerically efficient model for the tyre radiation over impedance surfaces. The thesis describes the work in five chapters.

Chapter 1 presents the main sources of traffic noise. Under normal driving conditions, tyre / road noise is predominant at driving speeds from 50 to 70 km/h for light vehicles or trucks. The models for the prediction of tyre noise are reviewed and classified in three categories : the statistical models, the hybrid models and the deterministic approaches. Whereas the models of the two first groups are mainly addressed to the prediction of A–weighted noise levels, models of the last group allows to optimise the properties of the tyre / road interface.
Deterministic approaches require the modelling of the tyre dynamics, the tyre / road contact and the tyre radiation. In particular, *2D* radiation models give lower computational times compared to *3D* models, but they give an overestimation of the horn effect sound amplification at low frequencies. Hence, they are only accurate at frequencies above around 600 Hz.
Because the road absorption affects both the generation and the radiation of noise, it is important to take these effects into account. Therefore, *Chapter 1* presents a review of the main impedance models. The different techniques to include the ground effects into a model for the tyre radiation are then discussed. Among these techniques, the integral equation–based methods handle any arbitrary incident sound field, which is a prerequisite for handling the field radiated by a vibrating tyre. In addition, these techniques can deal with homogeneous as well as inhomogeneous grounds.

Therefore, to achieve the fixed objectives, the approach presented in this thesis chooses to combine the numerical efficiency of a *2D* radiation model to an integral equation–based method to

include the ground effects.

In *Chapter 2*, a model for the tyre radiation, which has been derived in [Kropp 1992], is implemented on the basis of the *ES* method. Using the basic properties of vibrating cylinders, it is shown that low order modes are responsible for the major part of the radiated sound.
In fact, comparisons with a *BE* code prove that the deviations observed between the measurements and the calculations at frequencies below 600 Hz, are due to the *2D* simplifications of the model. In the mid–frequency range and at higher frequencies, the levels and the interference pattern of horn effect amplification factors are correctly predicted. Moreover, this multipole model is shown to be numerically of advantage compared to *BE* methods. However, the *ES* model does not include correctly the acoustical properties of the road surface.

To model the influence of the ground effects on the tyre sound field, a method which can handle arbitrary sound sources is presented in *Chapter 3*. Based on the *ES* method, it is mainly an alternative to standard integral equation methods. The technique proposed here consists in placing physical sources directly at the ground to control the value of the acoustical impedance at the surface. The main feature of this approach is that the impedance value is controlled point–wise, which means that the model is able to handle any type of ground impedances.
Numerical examples prove this model to be accurate in the case of arbitrary order sources radiating over a homogeneous impedance plane. In addition, comparisons with measurements for homogeneous and inhomogeneous surfaces extend the validity of this approach to arbitrary impedance distributions.

Subsequently, a model for the tyre radiation over impedance surfaces is developed in *Chapter 4*. As an introduction, the exact solution to the problem of an arbitrary order source radiating over an impedance plane is derived. The computation of the solution is, however, subject to numerical difficulties; it will be examined in future works. The model for the tyre radiation over impedance surfaces is developed using the *ES* method, on the basis of the models derived in the two previous chapters.
Therefore, the effects of impedance discontinuities are included in this model. The method is also original in that the source strengths are determined through an iterative process, which is computationally effortless.

This approach is validated by comparisons of horn effect amplification factors measured over homogeneous and inhomogeneous surfaces. It is shown that this iterative *ES* model is accurate at frequencies above around 600 Hz, which corresponds to the frequency range of validity of the multipole model presented in *Chapter 2*.

Finally, *Chapter 5* presents a parametrical study of the properties of the tyre / road interface. This study is based on measurements and calculations using the previous iterative model. The influence of geometrical parameters such as the source position inside the horn, the gap between the tyre and the ground or the tyre radius, is examined and discussed. The influence of the type of ground impedance on the sound amplification is also examined.

In particular, measurements and calculations show that at low frequencies, the sound amplification for absorbing surfaces may exceed that produced for rigid surfaces. This result has not been clearly explained. It is also shown that combining both acoustical and geometrical parameters of the road surface may substantially decrease the sound amplification compared to the optimisation of one of these two parameters only.

Moreover, due to its low computational time, this model is proved to be adapted for the optimisation of the ground impedance. Calculations show however that the value of the impedance which gives the lowest sound amplification is very sensitive to the exact geometry of the tyre / road interface.

Perspectives and future work

The work presented in this thesis ends up with an efficient model for the tyre radiation over arbitrary impedance surfaces. A brief parameter study is presented in *Chapter 5*. A more thorough examination of the tyre radiation conditions is needed in order to fully understand the mechanisms of noise emission.

This iterative *ES* model is aimed to be integrated to a complete model for prediction of tyre / road noise. The next step is thus to use real tyre data together with real road surface data, to predict tyre / road noise over road surfaces having substantial absorption properties. As proved in the last chapter of the thesis, this model can be used for the optimisation of the tyre / road interface properties. Constrains related to the tyre and the road construction could thus be included to yield realistic solutions.

The major drawback of tyre radiation model presented here is its *2D* character. To predict pass-by noise levels, a *3D* model is required. It could be developed using the *ES* method after numerical tests have been performed to optimise the system of sources placed inside the tyre body.

The present *ES* model could also be coupled to other existing *ES* models to include the presence of elastic objects in the neighbourhood of the tyre, such as the wheelhouse. These objects may modify significantly the field radiated by the tyre either by changing its directivity or by contributing directly to the sound field. These effects could be modelled using the *ES* method by placing sources inside the vibrating objects. This model could be implemented in a similar way as the iterative *ES* model presented in this thesis.

Finally, the computation of the reflection coefficient for cylindrical waves presented in *Chapter 4* will be further examined. The interesting feature of the proposed approach is that the solution is expressed as a function of the order of the source, among other parameters. This solution is particularly adapted to traffic noise prediction purposes, the models of which could thus include the so far omitted, directivity of the noise source.

Chapter 7

Appendices

Appendix I **..... The Equivalent Sources (*ES*) method**
Theoretical basis – Numerical implementation – Applications

Appendix II **... Complements on the tyre boundary condition**
Expression of the radiation hypothesis – Boundary velocity in the radiation hypothesis – Comparisons of horn effect predictions

Appendix III **.....Integration over the Green functions' singularities**
Validity of the derivation – Pressure Green function – Velocity Green function

Appendix IV **.....Experimental determination of surface impedance**
Kundt's tube measurements – Level difference technique

Appendix I The Equivalent Sources (*ES*) method

The so–called equivalent sources (*ES*) method is successfully applied to various situations in this thesis. The present appendix aims at establishing a common framework for the functioning and the field of application of this method. Found in the literature under various names, this technique is an alternative to integral equations–based methods, for the radiation and the scattering of sound from objects of arbitrary shape.

The theoretical basis of the method is first presented. Then, some critical considerations concerning the numerical implementation of the method are drawn up based on the author's experience and on other works in other fields of application. A review of these latter works completes this appendix.

Theoretical basis

The *ES* method has been developed independently by many researchers, which explains the fact that several names are given to the same approach in the literature : the source simulation technique, the auxiliary sources method, the substitute sources method, etc. This technique is not restricted to the field of acoustics; for instance, the method is the subject of numerous works in electromagnetics, a good review of which can be found in [Kaklamani 2002].

In the field of acoustics, the theoretical derivation of this technique as well as its physical interpretation can be found in [Bobrovniskii 1980; Ochmann 1995, 2000; Song 1991], among many others. As shown in [Koopmann 1989], the *ES* method is totally equivalent to standard *BE* approaches. Therefore, the *ES* method should be mainly seen as a computationally efficient,

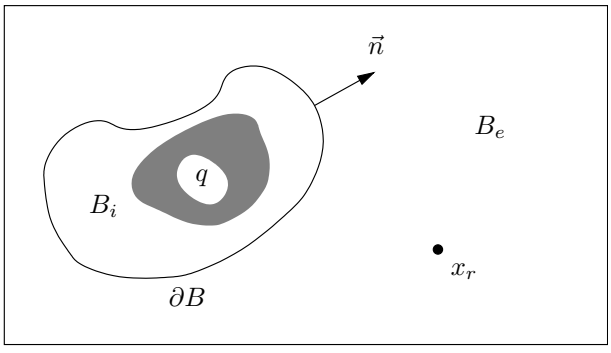

Figure I-1: *Typical geometry for an exterior radiation problem. The gray area represents the source distribution inside the vibating body.*

alternative to BE techniques[1].

The basic idea of this technique is that the radiation of sound due to an arbitrarily shaped vibrating body can be reproduced by a set of acoustic sources placed inside its volume, provided that these sources fulfil a prescribed boundary condition on the body surface.
Given a vibrating object of arbitrary shape, its interior volume is called B_i. The body surface ∂B represents the frontier with the exterior "free space" domain B_e. The situation is depicted in Fig. I-1. The time dependency of the pressure obeys $e^{+j\omega t}$. Therefore at a given frequency f, the pressure p at a receiving point x_r of the free space due a volume source at ξ satisfies the homogeneous Helmholtz equation

$$\Delta p(x_r) \; + \; k^2 p(x_r) \; = \; 0$$

where $k = 2\pi f/c$ is the wave number and c is the speed of sound in B_e. Only outoing waves are of interest here, therefore the solutions of the equation above should also satisfy the Sommerfeld radiation conditions, which express the quite natural concept that "the infinite is absorbent". This latter condition is expressed as

$$\lim_{r\to\infty}\left[\sqrt{r}\left(\frac{\partial p(r)}{\partial r} + jkp(r)\right)\right] \; = \; 0 \qquad \text{with} \quad r = \mid x_r - \xi \mid$$

In practical terms, this ensures that no other sources are present outside the volume B_i.
The solutions to the two above equations are solutions to the exterior radiation problem; they can be written in the form of the Kirchoff-Helmholtz integral equations :

$$\oint_{\partial B}\left(p(\eta)\frac{\partial g(\eta \mid x_r)}{\partial n} - g(\eta \mid x_r)\frac{\partial p(\eta)}{\partial n}\right) \mathrm{d}\eta \; = \; \begin{cases} 0 & \text{if} \quad x_r \in B_i \\ p_e(x_r)/2 & \text{if} \quad x_r \in \partial B \\ p_e(x_r) & \text{if} \quad x_r \in B_e \end{cases}$$

where η describes the surface ∂B and $g(\eta \mid x_r)$ denotes the free space Green function of the problem. According to the above equation, the pressure p_e at a point x of B_e is the superposition of an infinite number of contributions due to a continuous layer of sources placed directly on the border ∂B. Note at this point that a straightforward numerical implementation of the above equation would yield the standard boundary element (BE) method.

[1]The reader interested in an in–depth mathematical discussion of the method basis should refer to [Krutitskii 2003].

Let us now examine the interior radiation problem. A distribution of sources $q(x_i)$ is located in B_i, that is inside the vibrating body. The solution of the inhomogeneous Helmholtz equation is now given as

$$-\int_{B_i} q(\xi)g(x|\xi)\ \mathrm{d}\xi - \oint_{\partial B}\left(p(\eta)\frac{\partial g(\eta \mid x_r)}{\partial n} - g(\eta \mid x_r)\frac{\partial p(\eta)}{\partial n}\right)\ \mathrm{d}\eta\ =\ \begin{cases} p_i(x_r) & \text{if} \quad x_r \in B_i \\ p_i(x_r)/2 & \text{if} \quad x_r \in \partial B \\ 0 & \text{if} \quad x_r \in B_e \end{cases}$$

Moreover, the surface integral for the interior radiation problem equals the surface integral for the exterior radiation problem. By combining the two previous equations for a receiver x_r in B_e, one obtains

$$p_e(x_r)\ =\ -\int_{B_i} q(\xi)\ g(\xi \mid x_r)\ \mathrm{d}\xi$$

This equation shows that the pressure in the free space can be reproduced by a distribution of volume sources inside the vibrating body. To be able to replicate the radiation pattern of the object correctly, additional boundary conditions must be given. The boundary condition can be of any type : Dirichlet, Neumann or Robin boundary condition. As a consequence, the solution to this boundary value problem is unique. Furthermore, this solution is *exact* provided that the boundary condition is *exactly* fulfilled.
From the numerical point of view, the boundary condition is always fulfilled within a confidence interval, the choice of which might influence the accuracy of the prediction. Moreover, the theoretical derivation presented above does not provide any information concerning the placement of discrete sources inside the volume B_i. These open questions are discussed in the next paragraph.

Numerical implementation

The great advantage of the *ES* method is that it can deal with vibrating objects of an arbitrary shape, where standard *BE* codes become quite cumbersome [Ochmann 1980]. For instance, works in [Miller 1991] showed that the *ES* method is always more efficient numerically than *BE* methods. It should be underlined that these two approaches are equivalent, as shown in [Koopmann 1989]. However, contrary to *BE* methods, it has no global criteria to ensure the accuracy of the results. Hence only a few rules of thumb can be outlined.

The first step when implementing the method is to choose the geometry of the source system, i.e. the shape of the so–called auxiliary surface and the type of sources. These two parameters

are strongly dependent on each other : the placement of a given source should account for its radiation properties (importance of the near field, directivity, shape of the wave front, ...). Often, the "trial and error" technique is the only way of assessing the source system and this may become exhaustive for objects of large dimensions or very complex shape.

Discussions presented, for instance in [Machens 1999], try to draw out some global rules for the functioning of the *ES* method. As a general trend, the use of high order sources is only recommended when the object has a regular geometry. For instance, in the case of a radiating tyre, which has an axis of symmetry around its center, the use of a high order multipole located at its centre appears quite natural. For objects having a narrow geometry or sharp profile like a thin noise barrier or a vibrating plate, the choice of low order sources seems better adapted. Because high order sources have a strong near field, they should be placed at approximately equal distances from all parts of the boundary. If this is not the case, the resulting equation system becomes ill-conditioned and the solutions cease to be accurate.

In order to be complete, one should mention that the work presented in [Papakanellos 2001] proposes to optimise the placement the auxiliary sources according to the complex image theory. Developed for electromagnetic purposes, this theory, which could be extended to acoustics [Li 1996], states that the optimal position of the mirror image source is a function of the dissipation at the surface [Weaver 1971]. However, this approach has not been investigated in the present thesis because of the alternative approach presented in *Chapter 3*, which consists in placing the auxiliary sources directly on the surface.

If the situation does not allow the fulfilment of these general requirements, the use of regularisation techniques such as those reviewed in [Nelson 1999] can stabilize the equation system. Such techniques have mainly been developed for the purpose of pressure field reconstruction by inverse methods, like the Singular Value Decomposition [Press et al. 1986] (see *Chapter 2*). For the specific use of the *ES* method, the use of the Tikhonov's technique was proposed in [Kress 1986]. Ochmann in [Ochmann 1999] further extends the use of weighting functions originally proposed in [Cremer 1988], to handle non-full rank systems.

Once the source system is chosen and optimally placed, there is still no guarantee that the prediction of the radiation will converge towards the true field. Although the convergence of the method has been proven theoretically, it was shown in [Machens 1999] that the deviations in the field predictions are not directly related to the error made on the boundary. In other words, the boundary condition can be entirely fulfilled although this will not ensure that the

pressure field is correct. The validity of the modelisation should therefore be confirmed by measurements or comparisons with finite element methods.

Applications

Given the above restrictions, the *ES* method can be applied to various situations. The review below is not exhaustive; it tries to give the reader an overview of the different field of applications of this technique.

In the field of traffic noise prediction, the following applications can be found in the literature. For instance, works presented in [Ögren 2002] propose a model for the propagation of sound from one street to another in a city environment. Due to its numerical efficiency, the *ES* method can be applied to optimise the acoustical treatment of noise barriers, as shown in [Thorsson 2000]. The *ES* method has also been applied to outdoor propagation problems to include the ground effects [Bécot 2002] or the meteorological effects [Forssén 2000, 2002]. An original application can be found in [Kropp 1998, 2000a] for the transmission of exterior sound across balcony openings to the inside of apartments.

A large number of studies refer to the *ES* method to model the radiation sound from vibrating structures. The accuracy of the method was proved in the case of a vibrating tyre [Klein 1998; Kropp 2000b]. The method was also shown to be of advantage compared to pure *BE* models to predict the radiation of vibrating objects having complex vibration patterns [Holste 1997; Tomilina 1993; Too 2001] or for structures made of several parts [Bobrovniskii 1995]. It was also proved that the method is efficient to model the scattering of sound in open spaces [Bouchet 2000] or in enclosures [Johnson 1998]. In particular, the *ES* method can accurately model the scattering of sound from objects with sharp corners [Anastassiu 2002; Karamehmedovic 2001], cases which are often difficult to solve with pure *BE* approaches. This latter study even showed that losses at the object surface could be included in these cases using the *ES* method.

Another field of application concerns the reconstruction of acoustic pressure or velocity fields on the surface of vibrating objects [Magalhaes 2001; Wang 1997]. Because of its flexibility concerning the placement of the equivalent sources, the *ES* method seems particularly convinient to be used together with the experimental technique of acoustical holography [Williams 2001].

Finally, the time domain formulation presented in [Kropp 1995] widens the already large field of application of this approach.

In conclusion, the *ES* method appears to be an efficient alternative to pure *BE* codes in many situations. With regards to the lack of rigorous criteria for the accuracy of the solution, this may be overcome by the experience of the user or by the study of related works, e.g. in electromagnetics.

Appendix II Complements on the tyre boundary condition

Chapter 2 and *Chapter 4* present horn effect predictions in the case a *scattering* problem is expressed. In this case, the tyre surface is rigid. However, if the problem is expressed a a *radiation* problem, a prescribed velocity distribution must be given on the tyre surface as a boundary condition. Depending on the form of the prescribed distribution, different amplification factors are expected.

Therefore, the *radiation* problem is discussed in this appendix. In particular, horn effect amplification factors obtained in this case are compared to those obtained in the case of a *scattering* problem.

Expression of the *radiation* problem

The expression of the *radiation* problem is more intuitive than the *scattering* one because it considers that the tyre belt is vibrating, and therefore, that the noise source is the tyre. In this case, a velocity distribution is given directly on the tyre surface. Mathematically, it can be expressed as, for a point $x_{tyre}(r, \varphi)$ of the boundary

$$v_{rad,n}(x_{tyre}) = \begin{cases} V_0(\varphi) & \text{if } \mid \varphi - \varphi_0 \mid \leq \Delta\varphi_0/2 \\ 0 & \text{otherwise} \end{cases} \tag{II-1}$$

This means that the points vibrating with a velocity V_0 correspond to the angles contained within the aperture $\Delta\varphi_0$ around a given angle φ_0 (see Fig. II-1). Strictly speaking V_0 may be a function of both r and φ. However, since all points of the boundary are at the same distance to the origin of the co-ordinate system, i.e. the tyre centre, it seems reasonable to assume that

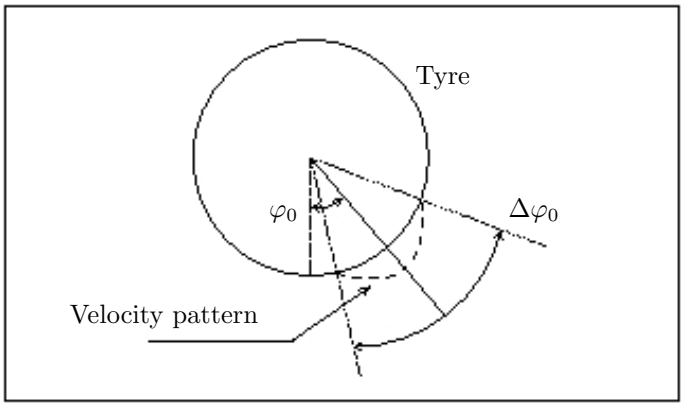

Figure II-1: *Geometry of the boundary condition in the "radiation" problem.*

V_0 is a function of φ only. The boundary velocity can have on any of the forms shown in Fig. 2-5.

For the horn effect calculation, it is necessary to compute the pressure field equivalent to this velocity distribution. The pressure at the receiving point x_r above the road surface and outside the tyre body can be written as

$$p_{rad}(x_r) = \mathrm{j}\omega\rho \cdot q_{rad} \cdot G_0(x_0 \mid x_r) \quad \text{with} \quad G_0(x_0 \mid x_r) = -\frac{\mathrm{j}}{4}\, \mathrm{H}_0^{(2)}(k \mid x_r - x_0 \mid) \qquad \text{(II-2)}$$

$G_0(x_0 \mid x_r)$ is the free space Green's function for the pressure due to a source at x_0, calculated at a point x_r. q_{rad} is the source strength equivalent to the velocity distribution on the boundary. Also called volume flow dues to its dimension, it is defined as

$$q_{rad} = \int_{S_{tyre}} V_0(\varphi)\ \mathrm{d}S_{tyre} \quad \text{and} \quad [q_{rad}] = m^2 \cdot s^{-1} \qquad \text{(II-3)}$$

Note that unlikely q_{scat} (see Eq. 2-11), q_{rad} is homogeneous to a volume flow. The position x_0 of the source is chosen directly on the tyre surface, at an angle φ_0 as defined in Eq. II-1.

In this case, the total pressure field if the superposition of the pressure fields due to the multipole source and its image. The reference pressure field, when the tyre is radiating in the free field, is the superposition of the multipole field as calculated in Eq. 2-14(b). In this equation, the pressure from the monopole source is now that defined in Eq. II-2. If the tyre is removed, the reference pressure is similar to that of Eq. 2-14(c). Given these precisions, the two possible amplification factors in the *radiation* case are, in decibels,

$$\begin{aligned} AF_1 &= 10\log\left|\ \frac{p_1(x_r) + p_2(x_r)}{\widetilde{p}_1(x_r)}\ \right|^2 \\ AF_2 &= 10\log\left|\ \frac{p_1(x_r) + p_2(x_r)}{p_{rad}(x_0 \mid x_r) + p_{rad}(\overline{x_0} \mid x_r)}\ \right|^2 \end{aligned}$$

It should be noted that the reciprocity principle cannot be applied in this case.

Boundary velocity

A crucial point in the *ES* model is to fulfill the boundary condition. In the *radiation* problem, the velocity pattern is arbitrarly given on the tyre belt. The more realistic distributions are Hanning-like and piston-like distributions. Other distributions can be thought of as for instance a "modal" shape (see Fig. 2-5) or a random distribution but they are not examined in the following.

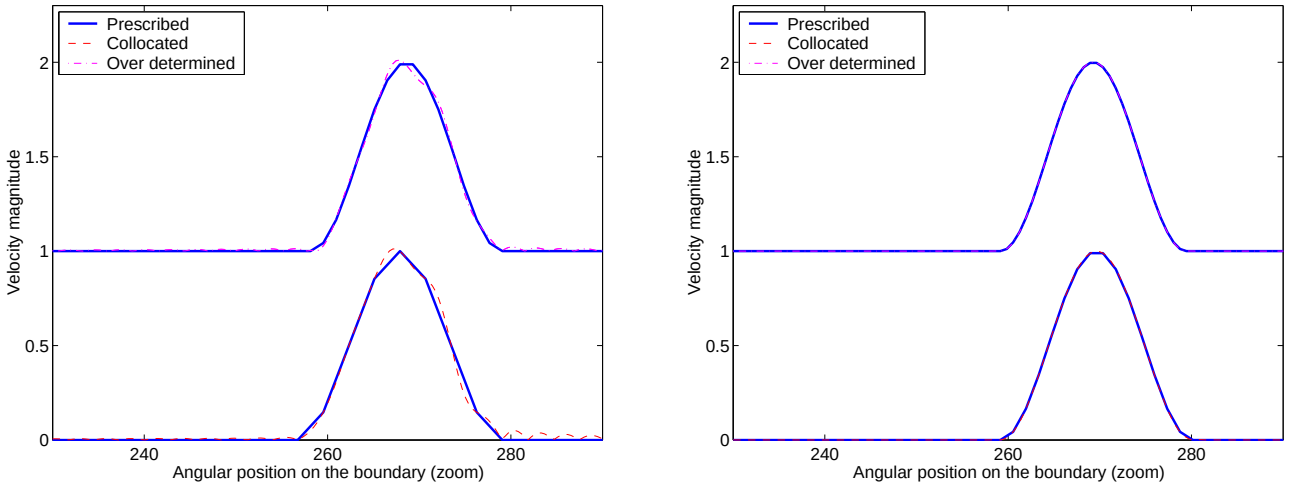

(a) $N_{max} = 64$ (b) $N_{max} = 128$

Figure II-2: *Obtained and prescribed boundary velocities in the case of a Hanning-like boundary condition.*

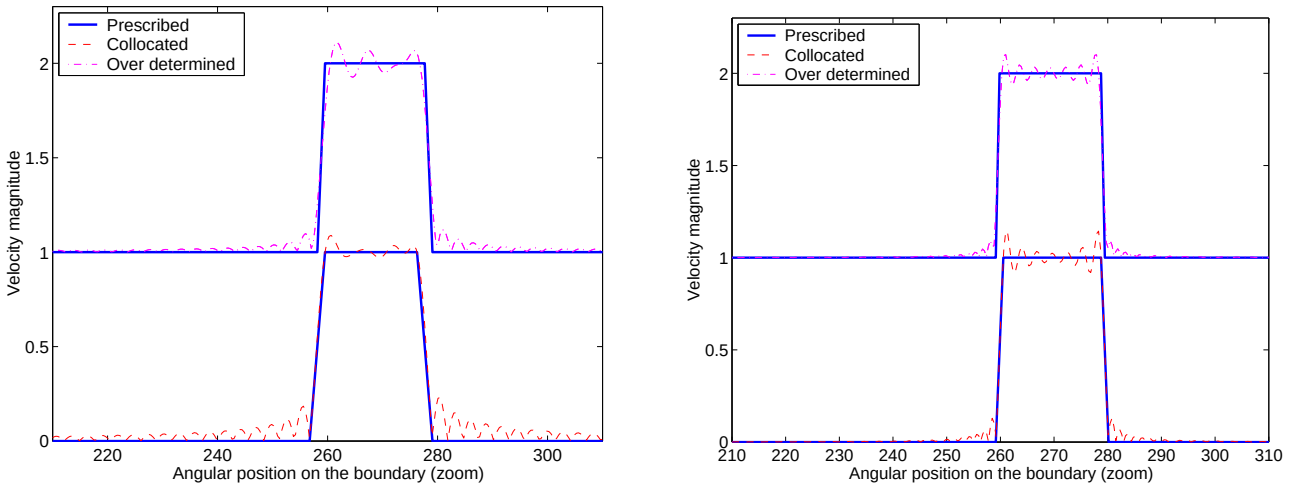

(a) $N_{max} = 64$ (b) $N_{max} = 128$

Figure II-3: *Obtained and prescribed boundary velocities in the case of a piston-like boundary condition.*

Examples of Hanning-like distribution and piston-like distribution are shown respectively in Fig. II-2 and in Fig. II-3. Only the region of maximum velocity is shown in these figures. Velocities achieved using a 64-th and a 128-th order multipole source are compared to the prescribed velocity. Collocated and over-determined systems are used as in *Chapter 2* to obtain the best fulfillment. For both distributions, calculations are performed at a frequency of 800

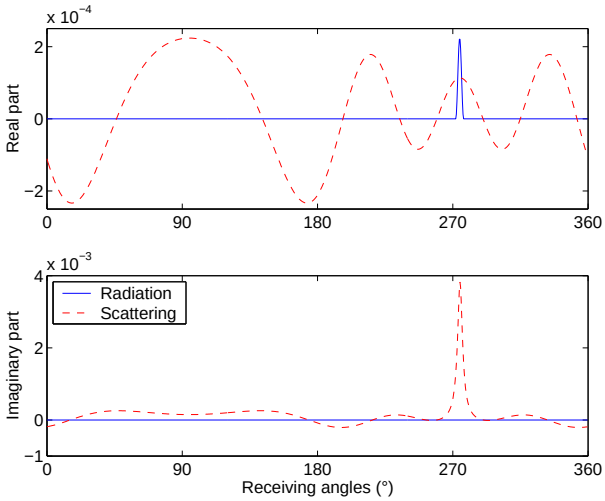

(a) Comparisons of velocity boundary conditions at $f = 1$ kHz

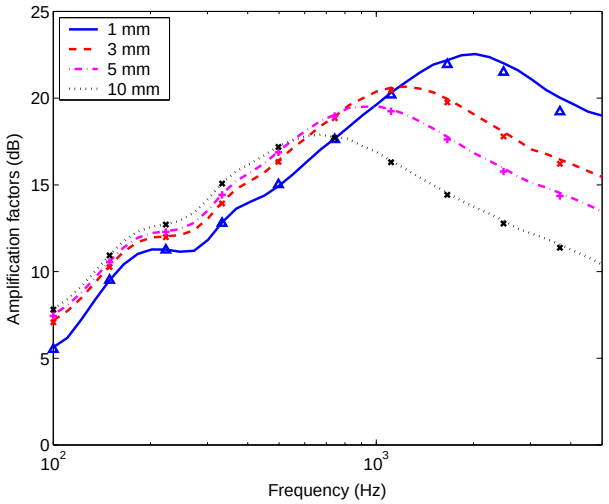

(b) Averaged amplification factors for different gap values; Lines : "radiation", Objects : "scattering"

Figure II-4: *Comparisons of "radiation" and "scattering" hypothesis – Boundary condition and horn effect predictions.*

Hz and for an aperture $\Delta\varphi_0$ of 20°.

Not surprinsigly, Hanning-like distributions are more "easily" reproduced as a 64-th order multipole using an over-determined equation system gives satisfatory prediction of the boundary condition. In the case of a piston-like prescribed velocity, even a 128-th order multipole yields a poor fulfillment of the boundary condition. Higher order sources should be used in this case, the implementation of which would lead to numerical difficulties and to a deterioration of the computational efficiency.

Comparison of horn effect predictions

Besides numerical difficulties which may be faced for particular velocity distributions in the *radiation* case, it is interesting to compare horn effect predictions obtained with the two different approaches.

For this, the *ES* model is run in the *radiation* case using a Hanning-like distribution defined for $\Delta\varphi_0 = 5°$ and $\varphi_0 = 5°$. In this case, a 87-th order multipole is used. On the other hand, the *scattering* problem requires the use of a 64-th order multipole to insure a good reproduction of the prescribed velocity. The monopole that provides with the boundary velocity distribution is

located directly on the tyre belt at the same position as that of the equivalent monopole of the *radiation* problem. In both cases, the boundary is discretised over 900 points. The prescribed velocities of the two approaches are shown in Fig. II-4(a). Note that the real part of the Hanning-like velocity has been scaled to fit the axis (this latter has a unit maximum value).
The pressure is calculated at 100 receiving positions on a 1 meter semi circle centered on the "contact" point between the tyre and the road. The obtained values are then averaged to give one single value of amplification at each frequency (see also *Chapter 5*). This procedure is repeated for the following gap values : 1 mm, 3 mm, 5 mm, 10 mm. Results shown in Fig. II-4(b) are indicated using lines in the *radiation* case and using objects in the *scattering* case. In this latter case, amplification factors are plotted only at few frequencies for sake of clarity.
For all gap values, the two approaches give averaged amplification factors that are very similar if not identical. The amplification increases up to frequency, the value of which depends on the gap value. Beyond this frequency, the amplification decreases with a slope that is identical for all gap values. As a general trend, amplification factors at low frequencies are slighlty larger for larger gaps. Moreover, as expected, the closer the tyre is to the road surface, the stronger the amplification. It reaches 24 dB for a 1 mm gap while it lies around 21 dB for a 3 mm gap; it drops to 17 dB of maximum sound amplification for a 10 mm gap.
Finally, the main difference between the two configurations is the presence of higher modes in the *scattering* case. The great similarity of the compared results further proves that low order modes are responsible for the main part of the sound radiation from tyres.

Appendix III Integration over the Green functions' singularities

The present appendix proposes a calculation of the singular integrals in Eq. 3-5. The difficulty is due to the fact that the Green functions, both for the pressure and for the velocity, are not bounded when the integration variable meets the observation point. The numerical integration of such integrals, using e.g. a Gauss-Legendre quadrature, drastically lacks accuracy.
Mathemetically, singular integrals can be evaluated by calculating the Cauchy principal value[2]. Instead of using this method, the basic idea of the following derivation is to use the approximations of the Hankel functions for very small arguments. The resulting integrals can be performed analytically and evaluated numerically with good accuracy.
The validity of this assumption is briefly discussed in the first paragraph. Then, the integral for the pressure Green function is examined and the integration of the velocity Green function is finally treated.
The reader will note that, as in Chapter 3, a time dependence in $e^{-j\omega t}$ is assumed in the following. This choice implies the use of Hankel functions of first kind in the Green functions' expressions. It is clear that an identical approach can be adopted when using a time dependence as $e^{+j\omega t}$ and therefore, that one uses Hankel functions of second kind; in this case, only the final results of the integration are indicated below.

Validity of the derivation

If all elements of the ground surface have the same length Δ, the maximum argument of the Green functions is

$$\mid e_i - \xi_j \mid_{max} < \Delta/2 \quad \text{or} \quad k \mid e_i - \xi_j \mid_{max} < k\Delta/2$$

If the ground discretization is such that N_{el} elements per wavelength are chosen, one has

$$N_{el}\Delta \equiv \lambda = \frac{2\pi}{k} \quad \text{and hence} \quad k\Delta/2 \equiv \frac{\pi}{N_{el}}$$

For instance, if 10 elements per wavelength are chosen, the maximum value of the argument is $\pi/10 \approx 0.31$. The argument of the Hankel function being always smaller than that value, it is thus safe to use the asymptotic expressions of the Hankel functions for argument values much lower than 1.

[2]This procedure is applied for instance in [Bécot 2002].

Pressure Green function

Using the notations of *Chapter 3*, the integral of the Green function for the pressure is

$$\int_{E_j} G(\xi_j \mid e_i)\ \mathrm{d}\xi_j \ = \ -\frac{\mathrm{j}}{2}\int_{E_j} \mathrm{H}_0^{(1)}(k \mid e_i - \xi_j \mid)\ \mathrm{d}\xi_j$$

where e_i is the element mid point and ξ_j is the variable of integration describing the surface of the element E_j. Let Δ denote the element length. The integrand is an even function of ξ_j on the interval $[-\Delta/2; +\Delta/2]$. If the origin is set at the element mid point, one has $e_i = 0$ and therefore

$$\int_{-\Delta/2}^{+\Delta/2} \mathrm{H}_0^{(1)}(k \mid 0 - \xi_j \mid)\ \mathrm{d}\xi_j = \frac{2}{k}\int_0^{k\Delta/2} \mathrm{H}_0^{(1)}(u)\ \mathrm{d}u \qquad \text{with} \quad u = k \mid \xi_j \mid$$

According to [Abramowitz 1972], the Hankel function of first kind can be written as

$$\forall u < 3 \qquad \mathrm{H}_0^{(1)}(u) \ = \ 1 + \mathrm{j}\frac{2}{\pi}\left[\ln(\frac{u}{2}) + \gamma\right] + \mathcal{O}(u^2 \ln(u))$$

where $\gamma = 0.5777\ldots$ is the Euler's constant. Hence

$$\begin{aligned}\int_{-\Delta/2}^{+\Delta/2} \mathrm{H}_0^{(1)}(k \mid 0 - \xi_j \mid)\ \mathrm{d}\xi_j \ &= \ \frac{2}{k}\left[u + \mathrm{j}\frac{2}{\pi}\left(u\ln(\frac{u}{2}) - u + \gamma u\right)\right]_0^{k\Delta/2} + \mathcal{O}(u^3\ln(u)) \\ &= \ \Delta + \mathrm{j}\frac{2\Delta}{\pi}\left[\ln(\frac{k\Delta}{4}) - 1 + \gamma\right] + \mathcal{O}(u^3\ln(u))\end{aligned}$$

This finally yields

$$\int_{E_j} G(\xi_j \mid e_i)\ \mathrm{d}\xi_j \ = \ \frac{\Delta}{\pi}[\ln(\frac{k\Delta}{4}) - 1 + \gamma] - \mathrm{j}\frac{\Delta}{2} \qquad \text{(III-1)}$$

Therefore, the contribution from the singularity to the pressure field has a finite value, which is denoted I_Δ in the main text of *Chapter 3* [3].

Velocity Green function

Similarly, the integral of the Green function for the velocity is written

$$\int_{E_j} G^{(v,n)}(\xi_j \mid e_i)\ \mathrm{d}\xi_j = \lim_{h\to 0}\ \frac{1}{2\rho c}\int_{E_j} \mathrm{H}_1^{(1)}(k \mid e_i - \xi_j \mid)\ \vec{u}_r \cdot \vec{n}\ \mathrm{d}\xi_j$$

[3] In the case where the time dependence is $\mathrm{e}^{+\mathrm{j}\omega t}$, the contribution from the singularity to the pressure field is

$$\int_{E_j} G(\xi_j \mid e_i)\ \mathrm{d}\xi_j \ = \ -\frac{\Delta}{\pi}[\ln(\frac{k\Delta}{4}) - 1 + \gamma] - \mathrm{j}\frac{\Delta}{2} \qquad \text{(III-2)}$$

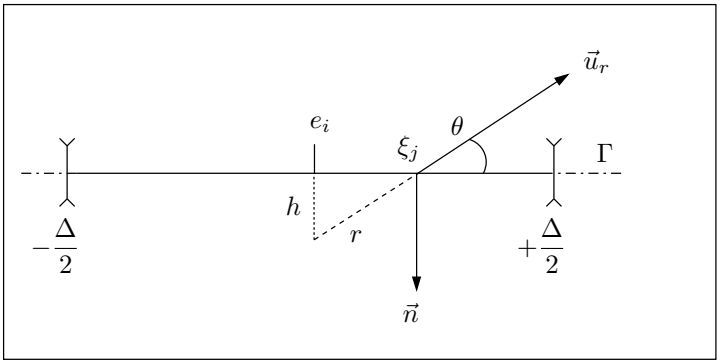

Figure III-1: *Geometry for the analytical calculation of the singular integral for the velocity.*

Using the notations of Fig. III-1, one can write

$$\begin{aligned}\lim_{h\to 0}\int_{E_j} \mathrm{H}_1^{(1)}(k \mid e_i-\xi_j \mid)\ \vec{u}_r\cdot\vec{n}\ \mathrm{d}\xi_j &= \lim_{h\to 0}\ \int_{-\Delta/2}^{+\Delta/2} \mathrm{H}_1^{(1)}(k \mid e_i-\xi_j \mid)(-\sin\theta)\ \ \mathrm{d}\xi_j \\ &= -2\ \lim_{h\to 0}\ \int_{0}^{+\Delta/2} \mathrm{H}_1^{(1)}(k \mid e_i-\xi_j \mid)\sin\theta\ \ \mathrm{d}\xi_j\end{aligned}$$

Again the origin is set at the position $e_i = 0$. Let us introduce the variable r such that $r^2 = {\xi_j}^2 + h^2$. The above equation then becomes

$$\lim_{h\to 0}\int_{E_j} \mathrm{H}_1^{(1)}(k \mid e_i-\xi_j \mid)\ \vec{u}_r\cdot\vec{n}\ \mathrm{d}\xi_j = -2\ \lim_{h\to 0}\ \int_{h}^{\sqrt{\Delta^2/4+h^2}} \mathrm{H}_1^{(1)}(kr)\frac{h}{\sqrt{r^2-h^2}}\ \mathrm{d}r$$

One can make use here of the following asymptotic expression of the Hankel function

$$\mathrm{H}_1^{(1)}(kr) = -\mathrm{j}\frac{2}{\pi}\frac{1}{kr} \qquad \text{for} \quad kr \ll 1$$

One thus obtains

$$\lim_{h\to 0}\int_{E_j} \mathrm{H}_1^{(1)}(k \mid e_i-\xi_j \mid)\ \vec{u}_r\cdot\vec{n}\ \mathrm{d}\xi_j = +\mathrm{j}\frac{4}{k\pi}\ \lim_{h\to 0}\ \int_{h}^{\sqrt{\Delta^2/4+h^2}} \frac{h}{r\sqrt{r^2-h^2}}\ \mathrm{d}r$$

If $v = r/h$, this can be written

$$\begin{aligned}\lim_{h\to 0}\int_{E_j} \mathrm{H}_1^{(1)}(k \mid e_i-\xi_j \mid)\ \vec{u}_r\cdot\vec{n}\ \mathrm{d}\xi_j &= +\mathrm{j}\frac{4}{k\pi}\ \lim_{h\to 0}\ \int_{1}^{\sqrt{1+\Delta^2/4h^2}} \frac{1}{v\sqrt{v^2-1}}\ \ \mathrm{d}v \\ &= +\mathrm{j}\frac{4}{k\pi}\int_{1}^{+\infty} \frac{1}{v\sqrt{v^2-1}}\ \ \mathrm{d}v\end{aligned}$$

The resulting integral is known and from [Abramowitz 1972] one obtains

$$\begin{aligned}\lim_{h\to 0}\int_{E_j} \mathrm{H}_1^{(1)}(k \mid e_i-\xi_j \mid)\ \vec{u}_r\cdot\vec{n}\ \mathrm{d}\xi_j &= +\mathrm{j}\frac{4}{k\pi}\ \left[\arccos\frac{1}{v}\right]_1^{+\infty} \\ &= +\mathrm{j}\frac{4}{k\pi}\ \left[\arccos 0 - \arccos 1\right]\end{aligned}$$

This finally gives

$$\lim_{h\to 0}\int_{E_j} \mathrm{H}_1^{(1)}(k \mid e_i - \xi_j \mid)\ \vec{u}_r \cdot \vec{n}\ \mathrm{d}\xi_j \ = \ +\mathrm{j}\frac{4}{k\pi}\ \left[\frac{\pi}{2} - 0\right] \ = \ +\mathrm{j}\frac{2}{k}$$

Therefore, the integral of the Green function for the velocity is

$$\int_{E_j} G^{(v,n)}(\xi_j \mid e_i)\ \mathrm{d}\xi_j \ = \ +\frac{\mathrm{j}}{\rho\omega} \tag{III-3}$$

This results is in accordance with that presented in [Bécot 2002], for which an error of sign has been noticed [4].

Lastly, the use of such approximations for the Hankel functions also applies to the field calculations whenever the receiver is very close to some surface elements and that the computation of the Green functions requires high accuracy. However, this aspect has not been further examined in this thesis because this situation has never been encountered.

[4] For a time dependence as $\mathrm{e}^{+\mathrm{j}\omega t}$, one obtains the same value of the integral for the velocity. In this case indeed, the opposite sign of imaginary part of the Hankel function approximation is compensated by the opposite sign of the pressure gradient.

Appendix IV Experimental determination of surface impedance

This appendix describes the experimental procedure as well as the impedance distributions of the absorbing materials used in this thesis. Two techniques are reviewed : the Kundt's tube measurement and the level difference technique.

Kundt's tube measurements

A Kundt's tube, also called standing wave tube, can be used to measure the absorption properties of a given material. This type of measurement, widely used nowadays, is described in the standard ISO/DIS 10354. The basic idea of the measurement is to exploit the properties of a standing wave created in a tube, the extremity of which has certain absorbing properties (see Fig. IV-1).

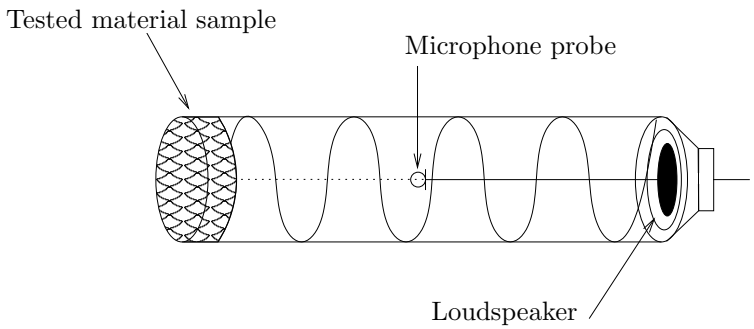

Figure IV-1: *Illustration of an absorption measurement using a standing wave tube.*

A loudspeaker located at one end of the tube gives out a signal, which usually has a sinusoidal form. A sample of the tested material is placed at the other end of the tube so that the incident wave impinges perpendicularly to the sample surface. Thus, two waves co-exist inside the tube : the incident wave, e.g. travelling from the right to the left in Fig. IV-1, and a reflected wave travelling in the opposite direction. The superposition of these waves is a standing wave, which presents a series of local minima and maxima. By measuring the ratio between the maxima and the minima of sound pressure levels, one can determine the acoustical impedance of the sample (see [Brüel 1967]).

The impedance of the material used for the measurements shown in Fig. 4-2 has been determined using this procedure. The impedance values are shown in Fig. IV-2.

It should be mentioned that as far as tyre / road noise is concerned, this method should be considered with extreme care. The acoustical properties of a given road sample, which has been

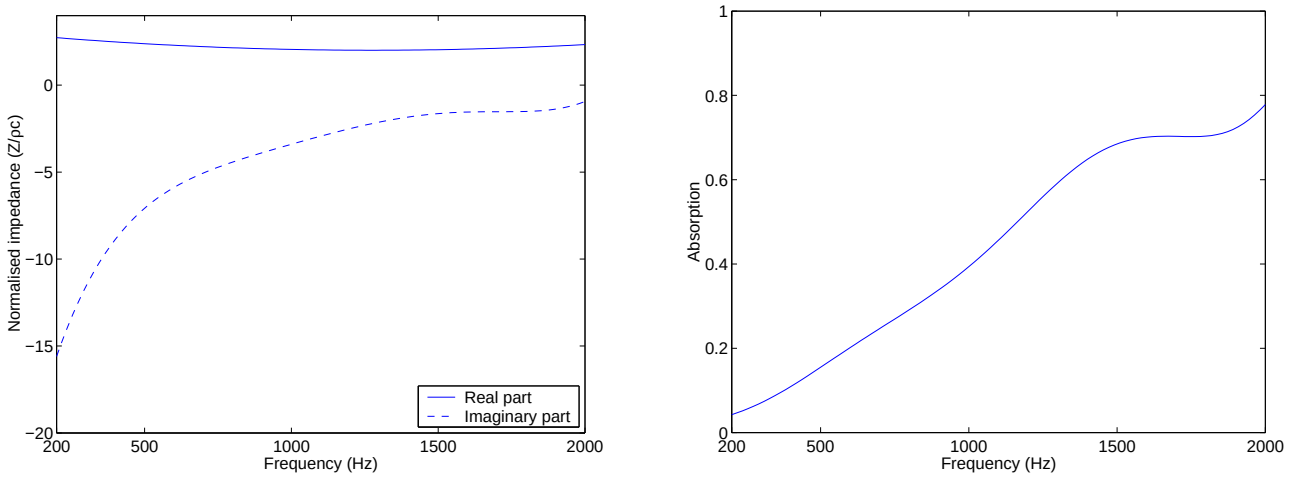

(a) Real and imaginary part of the measured impedance.

(b) Corresponding absorption of the material $(1 - |R|^2)$.

Figure IV-2: *Impedance and absorption values of the material used for Fig. 4-2.*

extracted from the road surface, may not reflect the acoustical behaviour of the all material *in-situ*.

Level difference technique

As mentioned above, impedance measurements using a Kundt's tube are not adapted to the measurements of the acoustical properties of road surfaces. Therefore, a number of non–destructive techniques have been developed, which may be applied to the determination of road impedances. One of these methods is the level difference technique, which has been used for some of the measurements presented in this thesis. The procedure and the impedance values measured are presented in this paragraph.

General guidelines for the measurement can be found in [Ögren 1998]. The method consists in finding the parameters of a given impedance model which give the best fit between the *SPL* differences predicted in this way and the measured ones. Therefore, this method gives the values of the parameters needed for the impedance model, without measuring them. In addition, the chosen impedance model should be adapted to the type of surface considered.

In practical terms, sound pressure levels are measured at different receiver positions over the studied surface (see Fig. IV-3). Thus, each measurement gives a set of parameter values, which can then be averaged to obtain the final value. In particular, the obtained thickness of the

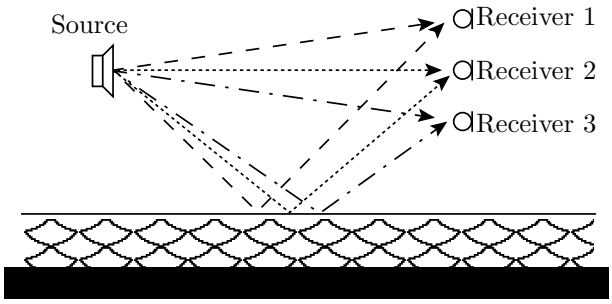

(a) The multiple height measurement.

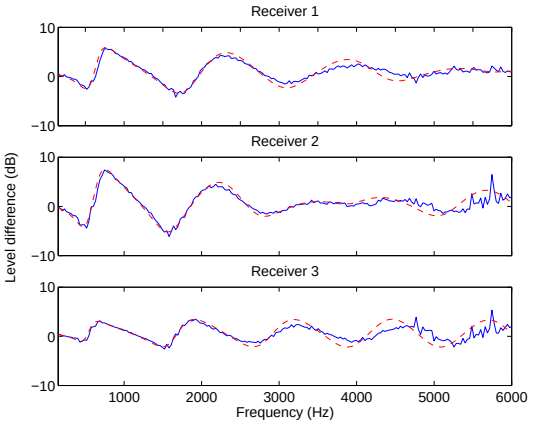

(b) Examples of curve–fitting the measured level difference (solid lines) to predicted ones (broken lines).

Figure IV-3: *Illustration of the principle of the level difference technique.*

absorbing layer should correspond to the thickness measured in reality.

It should be mentioned that the parameter values are optimised for the frequency region where the first minimum and first maximum of interference occur (maximum information on the ground is supposed to be found in this region). However, this value is kept for the whole frequency range of interest, thus assuming that the parameter values are frequency independent. It is clear that this might be partly true for some of the parameters.

This technique has been applied to measure the impedance of the material used for the measurements shown in *Chapter 3* and in *Section 4.2*. For these two measurements, the absorbing material was a panel of mineral rock wool laid on an acoustically rigid surface. Therefore, the material was assumed to be of a hardbacked porous layer. It has been proved in [Attenborough 1985] that the impedance of such a material is accurately described by the model given in [Delany 1970]. This model gives the acoustical impedance in the normal direction to the surface according to

$$\begin{aligned} Z_L &= Z_\infty \times \mathrm{j}\cot(Lk) \\ \text{with} \quad k &= \frac{2\pi f}{c}\left[1 + 10.8\ F_\sigma{}^{-0.70} + \mathrm{j} \times 10.3\ F_\sigma{}^{-0.59}\right], \end{aligned}$$

where L is the thickness and σ the effective flow resistivity, in Ns/m^4, of the material. Z_∞ is

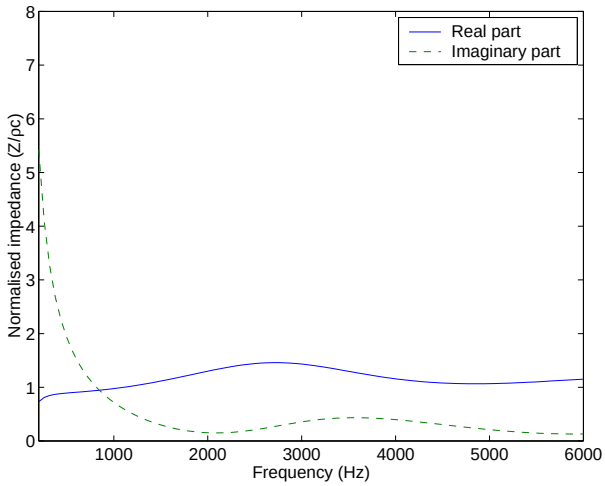

(a) Impedance value for : $\sigma = 22.4$ kNs/m^4 and $L = 0.041$ m.

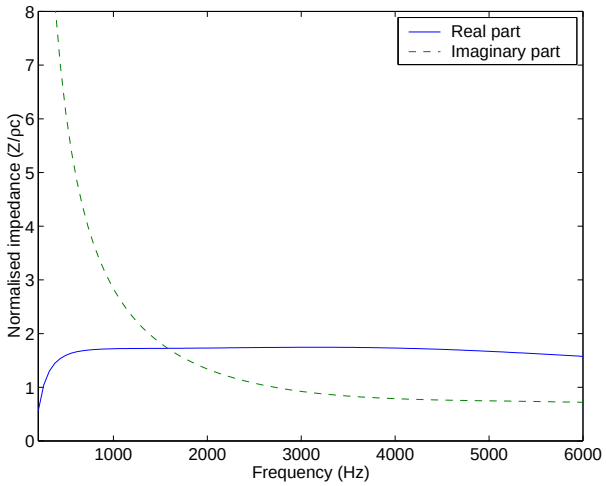

(b) Impedance value for : $\sigma = 124$ kNs/m^4 and $L = 0.016$ m.

Figure IV-4: *Impedance values obtained using the level difference technique.*

the impedance of an infinitely thick layer of the same material. It is given as

$$\begin{aligned} Z_\infty &= 1 + 9.08\ {F_\sigma}^{-0.75} + \mathrm{j} \times 11.9\ {F_\sigma}^{-0.73}, \\ \text{with} \quad F_\sigma &= 1000 f/\sigma. \end{aligned}$$

The impedance values obtained with this procedure are shown in Fig. IV-4. Even though the time dependence used in *Chapter 3* and in *Section 4.2* are not the same, impedance values are shown here in the same assumption, namely $\mathrm{e}^{-\mathrm{j}\omega t}$. The obtained values for the thickness of the absorbing layers correspond well with those measured in reality. For the absorbing material corresponding to Fig. IV-4(a), the obtained thickness is 4.1 cm (4 cm measured); for the absorbing material corresponding to Fig. IV-4(b), the obtained thickness is 1.6 cm (1.5 cm measured).

Finally, the absorption coefficient for the absorbing materials used in this thesis are shown in Fig. IV-5.

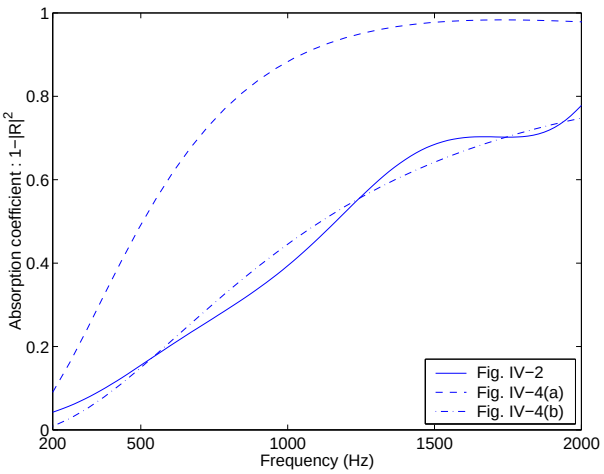

Figure IV-5: *Absorption coefficient of the different impedance materials used in this thesis.*

List of figures

List of figures

Bibliography

Bibliography

M. Abramowitz, I. A. Stegun: Handbook of mathematical functions. Dover Publications, New York, 1972. 2.2, 13, 22, 23

H. T. Anastassiu, D. I. Kaklamani, D. P. Economou, O. Breinbjerg. *Electromagnetic scattering analysis of coated conductors with edges using the method of auxiliary sources (MAS) in conjuction with the standard impedance boundary condition (SIBC). IEEE Transactions on Antennas and Propagation*, 50:59–66, 2002. 21

P. B. U. Andersson. *High frequency tyre vibrations.*. Technical report F 02-04, Department of Applied Acoustics - Chalmers, 2002. 3

F. Anfosso-Lédée. *Application de la méthode des équations intégrales à la modéisation du bruit aux abords des routes - Interaction chaussée / écran antibruit.* PhD thesis, Ecole Nationale des Ponts et Chaussées, Paris, France, 1996. 3

K. Attenborough. *Acoustical impedance models for outdoor ground surfaces.* Journal of Sound and Vibration, 99(4):521–544, 1985. 1.3, Appendix IV

K. Attenborough T. Waters-Fuller. *Effective impedance of rough porous ground surfaces.* Journal of the Acoustical Society of America, 108(3):949–956, 2000. 1.3

K. Attenborough *Developments in modelling ground effects on outdoor sound.* In *Proceedings of I.C.A. 2001*, Rome, Italy, 2001. 1.3

M. Ballie J. Gal. *Noise reduction induced by use of very thin wearing courses and crumb rubber particles.* In *Proceedings of inter.noise 2000*, Nice, France, 2000. (document)

T. Beckenbauer, A.Kuijpers. *Prediction of pass-by levels depending on road surface parameters*

by means of a hybrid model. In *Proceedings of inter.noise 2001*, The Hague, The Netherlands, 2001. 4

F.-X. Bécot, P.J. Thorsson, W. Kropp. *Line source radiation over inhomogeneous ground using an extended Rayleigh integral method.*. In *Proceedings of I.C.A. 2001*, Rome, Italy, 2001. 3-9, Appendix IV

F.-X. Bécot, P.J. Thorsson, W. Kropp. *An efficient application of equivalent sources to noise propagation over inhomogeneous ground*. Acustica - Acta Acustica, 88(6):853–860, 2002. 13, 3, 15, 15, 15, 15, 16, 6, 21, 2, 23

M. C. Bérengier M. R. Stinson G. A. Daigle J. F. Hamet. *Porous road pavements: Acoustical characterization and propagation effects*. Journal of the Acoustical Society of America, 101 (1):155–162, 1997. 1.3

M. Bérengier and M. Garai. *A state-of-the-art of in situ measurement of the sound absorption coefficient of road pavements*. In *Proceedings of I.C.A. 2001*, Rome, Italy, 2001. 1.3

Y. I. Bobrovniskii T. M. Tomilina. *Calculation of radiation from finite elastic bodies by the method of auxiliary sources*. Sov. Phys. Acoust., 36(4), 1980. Appendix I

Y. I. Bobrovniskii T. M. Tomilina. *General properties and fundamental errors of the method of Equivalent Sources*. Acoustical Physics, 41(5):649–660, 1995. 21

J. Borish, J. B. Angell. *An efficient algorithm for measuring the impulse response using pseudorandom noise*. Journal of the Audio Engineering Society, 31:478–487, 1983. 4

L. Bouchet T. Loyau N. Hamzaoui C. Boisson. *Calculation of acoustic radiation using equivalent-sphere methods*. Journal of the Acoustical Society of America, 107(5):2387–2397, 2000. 21

F. Böhm. *Mechanik des Gürtelreifens*. Ing.-Arch., 35:82–101, 1966. 2

Brüel & Kjær. *Instructions and applications for standing wave apparatus Type 4002*. Manual Brüel & Kjær, 1967. Appendix IV

C. B. Burroughs *Applications of nearfield acoustical holography in the research of mechanisms of acoustic radiation*. In *Proceedings of inter.noise 2001*, The Hague, The Netherlands, 2001. 1.1

S. N. Chandler-Wilde D. C. Hothersall. *Sound propagation above an inhomogeneous impedance plane.* Journal of Sound and Vibration, 98(4):475–491, 1985. 6

S. N. Chandler-Wilde D. C. Hothersall. *Efficient calculation of the Green function for acoustic propagation above a homogeneous impedance plane.* Journal of Sound and Vibration, 180(5): 705–724, 1995. 5, 14, 3.3

C. F. Chien W. W. Soroka. *Sound propagation along an impedance plane.* Journal of Sound and Vibration, 43:9–20, 1975. 6

C. F. Chien W. W. Soroka. *A note on the calculation of sound propagation along an impedance surface.* Journal of the Acoustical Society of America, 69(2):340–343, 1980. 6

T. G. Clapp. *Approximation and analysis of tire / pavement contact information resulting from road surface roughness.* PhD thesis, Rayleigh, USA, 1985. 3, 4

J. P. Coyette B. Van De Nieuwenhof. *A conjugated infinite element method for half-space acoustic problems.* Journal of the Acoustical Society of America, 108(4):1464–1473, 2000. 6

L. Cremer, M. Heckl. *Structure-borne sound – Structural vibrations and sound radiation at audio frequencies.* Springer-Verlag New-York, 528p, 1973. 1, 7

L. Cremer M. Wang. *Die synthese eines von einem beliebigen körper in luft erzeugten feldes aus kugelschallfeldern und deren realisierung in durchrechnung und experiment.* Acustica, 65: 53–74, 1988. 21

J. Defrance Y. Gabillet. *A new analytical method for the calculation of outdoor noise propagation.* Applied Acoustics, 57:109–127, 1999. 6

E. Delany E. N. Bazley. *Acoustical properties of fibrous absorbent materials.* Journal of the Acoustical Society of America, 3:105–116, 1970. 1.3, 4.3, Appendix IV

A. Dufour. *Perception du cadre de vie et attitudes sur l'environnement.* Rapport CREDOC 86, 1990. (document)

D. Duhamel. *Efficient calculation of three-dimensional sound pressure field around a noise barrier.* Journal of the Acoustical Society of America, 197(5):547–571, 1996. 14

J. A. Ejsmont U. Sandberg. *Texturing of cement concrete pavements to reduce traffic noise.* Noise Control Engineering Journal, 46(6):231–243, 1998. (document)

A Fadavi, D Duhamel, H.P. Yin. *Tyre road noise : finite element modelling.* In *Proceedings of inter.noise 2001*, The Hague, The Netherlands, 2001. 3

A Fadavi. *Modélisation numérique des vibrations d'un pneumatique et de la propagation du bruit de contact.* PhD thesis, Ecole Nationale des Ponts et Chaussées, Paris, France, 2002. 3, 6

S. Fong. *Tyre noise prediction from computed road surface texture induced contact pressure.* In *Proceedings of inter.noise 98*, Christchurch, New Zealand, 1998. 4

J. Forssén. *Calculation of noise barrier performance in a turbulent atmosphere by using substitute sources above the barrier.* Acustica - Acta Acustica, 86:269-275, 2000. 21

J. Forssén. *Calculation of noise barrier performance using the substitute-sources method for a three-dimensional turbulent atmosphere.* Acustica - Acta Acustica, 88:181-189, 2002. 21

T. Fujikawa H. Hoike Y. Oshino H. Tachibana. *Generation mechanism of tire / road noise - Part 1: Tire vibration caused by road roughness.* In *Proceedings of Internoise 1999*, Fort Lauderdale, Florida, USA, 1999. 3

E. Gerretsen F. de Roo F. van Gorkum. *A prediction model for tyre-road noise emission.* In *International Symposium on Pavement Surface Characteristics*, Christchurch, Australia, 1996. 4

E. Gerretsen, E. H. Mulder. *TRIAS : a comprehensive tyre-road noise model and its validation.* Technical Report, TNO report HAG-RPT-000121a, TNO Delft, The Netherlands, 2001. 4

R. A. G. Graf C. Y. Kuo A. P. Dowling W. R. Graham. *Horn amplification at a tyre/road interface – Part* I*: experiment and amplification.* In *Proceedings of Internoise 1999*, Fort Lauderdale, Florida, USA, 1999. 3

R. A. Graf, C.-Y. Kuo, A. P. Dowling W. R. Graham *On the horn effect of a tyre / road interface, Part I : Experiment and computation.* Journal of Sound and Vibration, 256(3): 417-431, 2002. 3, 2.3, 2.5

D. Habault. *Etude de l'influence des sols sur la propagation sonore.* PhD thesis, Université de Provence Aix–Marseille I, France, 1984. 6

D. Habault. *Sound propagation above an inhomogeneous plane: boundary integral equation methods.* Journal of Sound and Vibration, 100(1):55–67, 1985. 6

J.-F. Hamet, J. M. Clairet, J. C. Bruyère. *Bruit extérieur pneumatique / chaussée - Aménagement et instrumentation du laboratoire de Grenoble.* Rapport MMA 9103, INRETS, 1991. 1.1

J.-F. Hamet. *Modélisation acoustique d'un enrobé drainant - Prise en compte des phénomènes de thermoconductivité dans une nouvelle formulation phénoménologique.* Rapport LTE 159, INRETS, 1992. 1.3

J.-F. Hamet (a), P. Klein. *Use of a rolling model for the study of the correlation between road texture and tire noise.* In *Proceedings of inter.noise 2001*, The Hague, The Netherlands, 2001. 4

J.-F. Hamet (b), P. Klein. *Recherches physiques sur le bruit de roulement dans les projets 'Texture & Bruit' et SI.R.U.US.* In *Proceedings of Journées d'étude Bruit du Trafic Routier*, Nantes, France, 2001. 1.2

J.-F. Hamet (c). *Tire / road noise : Time domain Green's function for the orthotropic plate model.* Acustica - Acta Acustica, 87(4):470–474, 2001. 3

R. E. Hayden. *Road side noise from the interaction of a rolling tire with the road surface.* In *81st meeting of the Acoust. Soc. of America*, Washington, USA, 1971. 1.1, 3

M. Heckl. *Tire noise generating mechanisms - State of the Art Report.* In *International Tire Noise Conference*, pages 41–55, Stockholm, Sweden, 1979. 1.2

M. Heckl. *Tyre noise generation.* In *Seminar on Friction and Contact Noise*, volume 113, pages 157–170, 1986. 1, 1.2

F. Holste. *An equivalent source method for calculation of the sound radiated from aircraft engines.* Journal of Sound and Vibration, 203(4):667–695, 1997. 21

S. C. Huang W. Soedel *Response of rotating rings to harmonic and periodic loading and comparison with the inverted problem.* Journal of Sound and Vibration, 118(2):255–270, 1987. 2

S. C. Huang C. K. Su. *In-plane dynamics of tires on the road based on an experimentally verified ring model.* Vehicle System Dynamic, 21:247–267, 1992. 2

S. Huschek. *Characterization of pavement surface texture and its influence on tyre / road noise.* In *3rd International symposium on pavement surface characteristics*, Christchurch, New Zealand, 1996. 1.2

E. L. Ince. *Ordinary differential equations.* Dover Publications, New York, 1956. 19

U. Ingard. *On the reflection of a spherical sound wave from an infinite plane.* Journal of the Acoustical Society of America, 23(3):329–335, 1951. 6

M. E. McIntyre, J. Woodhouse. *On the fundamentals of bowed–string dynamics.* Acustica, 43 (2):93–108, 1979. 3

P. Jean. *A variational approach for the study of outdoor sound propagation and application to railway noise.* Journal of Sound and Vibration, 212(2):275–294, 1998. 6

K. L. Johnson. *Contact mechanics.* Cambridge University Press, Cambridge, 1985. 3

M. E. Johnson, S. J. Elliot, K-H. Baek, J. Garcia-Bonito. *An equivalent source technique for calculating the sound field inside an enclosure containing scattering objects.* Journal of the Acoustical Society of America, 104(3):1221–1231, 1998. 21

D. I. Kaklamani, H. T. Anastassiu. *Aspects of the method of auxiliary sources (MAS) in computational electromagnetics. IEEE Antenna's and Propagation Magazine*, 118(2):255–270, 2002. Appendix I

M. Karamehmedovic, O. Breinbjerg. *A convergent method of auxiliary sources for two-dimensional impedance scatterers with edges.* In *Conference on Applied Electromagnetic and Communication*, Croatia, 2001. 21

P. Klein. *Effet diàdre – Etude du modàle de Kropp.* Rapport MMA 9807, INRETS, 1998. 3, 2.2, 2.2, 8, 2.3, 9, 21

P. Klein. *Projet PREDIT "Texture/ Bruit" – Etude de la relation bruit/texture sur la base de mesures effectuées dans le cadre de la phase 1.* Rapport LTE 2033, INRETS, 2000. 1.2, 4

P. Klein. *Tyre noise horn effect on an absorbing surface - 2D analytical modelling using the multipole synthesis.* In *Proceedings of Forum Acusticum 2002*, Sevilla, Spain, 2002. 3

G. H. Koopmann L. Song J. B. Fahnline *A method for computing acoustic fields based on the principle of wave superposition.* Journal of the Acoustical Society of America, 86(6): 2433–2438, 1989. Appendix I, 21

J. Kragh *et al. Nordic prediction for road traffic noise. New basic input values due to the tightening of vehicle noise limits?.* Danish Acoustical Institute Report LI 971/91, Lyngby, Danmark, 1991. (document)

J. Kragh. *News and needs in outdoor noise prediction.* In *Proceedings of inter.noise 2001*, The Hague, The Netherlands, 2001. 5

R. Kress A. Mohsen. *On the simulation Source Technique for exterior problems in acoustics.* Mathematical Methods in the Applied Science, 8:585–597, 1986. 21

W. Kropp. *Structure-borne sound on a smooth tyre.* Applied Acoustics, 26:181, 1989. 2, 7

W. Kropp. *Ein Model zur Beschreibung des Rollgeräusches eines unprofilierten Guertlreifens auf rauher Strassenoberfläche.* PhD thesis, Institut für Technische Akustik, Berlin, Germany, 1992. (document), 1, 2, 3, 1.4, 7, 2.2, 6

W. Kropp P. Svensson. *Application of the time domain formulation of the method of Equivalent Sources to radiation and scattering problems.* Acustica, 81:528–543, 1995. 21

W. Kropp, J. Bérillon. *A theoretical model to investigate the acoustic performance of building facades in the low and middle frequency range.* Acustica - Acta Acustica, 84:681-688, 1998. 3.1, 21

W. Kropp (a), J. Bérillon. *A theoretical model to consider the influence of absorbing surfaces inside the cavity of balconies.* Acustica - Acta Acustica, 86:485-494, 2000. 21

W. Kropp (b), F.-X. Bécot, S. Barrelet. *On the sound radiation from tyres.* Acustica - Acta Acustica, 86(5):769–779, 2000. 1, 3, 2-2, 2-3, 7, 2-13, 2-14, 5, 2-15, 1, 21, Appendix IV

W. Kropp, K. Larsson, F. Wullens, P. Andersson. F.-X. Bécot, T. Beckenbauer. *The modelling of tyre / road noise – a quasi three-dimensional model.* In *Proceedings of inter.noise 2001*, The Hague, The Netherlands, 2001. 3

P. A. Krutitskii. *Method of interior boundaries for the impedance problem in scattering theory.* Applied Mathematics and Computation, 135:147–160, 2003. 1

A.Kuijpers, G. J. van Bokland. *Tyre / road noise models in the last two decades : a critical evaluation.* In *Proceedings of inter.noise 2001*, The Hague, The Netherlands, 2001. 1.2

C.-Y. Kuo, R. A. Graf, A. P. Dowling W. R. Graham. *On the horn effect of a tyre / road interface, Part II : Asymptotic theories.* Journal of Sound and Vibration, 256(3):433-445, 2002. 3

K. Larsson (a). *Modelling of dynamic contact – Exemplified on the tyre / road interaction.* PhD thesis, Department of Applied Acoustics, Gothenburg, Sweden, 2002. 3

K. Larsson (b), S. Barrelet, W. Kropp. *The modelling of the dynamic behaviour of tyre tread blocks.* Applied Acoustics, 63(6):659–677, 2002. 3

Y. L. Li, M. J. White. *Near–field computation for sound propagation above ground using complex image theory.* Journal of the Acoustical Society of America, 99(2):755–759, 1996. 21

K. U. Machens. *Approximate solutions for acoustic radiation problems: a critical appraisal of the method of comparative sources.* Acustica - Acta Acustica, 85:764–779, 1999. 2.4, 21

M. B. S. Magalhaes, R. A. Tenenbaum, M. Zindeluk *Application of equivalent sources methods in acoustical holography.* In *Proceedings of inter.noise 2001*, The Hague, The Netherlands, 2001. 21

J. D. Maynard *Near field acoustic holography : a review.* In *Proceedings of inter.noise 2001*, The Hague, The Netherlands, 2001. 1.1

F. P. Mechel. *A line source above a plane absorber.* Acustica - Acta Acustica, 86(2):203–215, 2000. 6

H. M. E. Miedema. *Noise & health: how does noise affect us?.* In *Proceedings of inter.noise 2001*, The Hague, The Netherlands, 2001. (document)

R. D. Miller, E. T. Moyer, H. Huang, H. Überall. *A comparison between the boundary element method and the wave superposition approach for the analysis of the scattered fields from rigid bodies and elastic shells.* Journal of the Acoustical Society of America, 89(5):2185–2196, 1991. 21

P. M. Morse, K. U. Ingard *Theoretical acoustics.* Princeton University Press, 949p, 1968. 4.1

P. A. Nelson. *Some inverse problems in acoustics.* In *Sixth International Congress on Sound and Vibration*, Copenhagen, Denmark, 1999. 21

N.-Å. Nilsson. *Air resonant and vibrational radiation – Possible mechanisms for noise from cross-bar tires.* In *International Tire Noise Conference*, pages 93–110, Stockholm, Sweden, 1979. 1

M. Ochmann. *Calculation of sound radiation from complex machine structures using the multipole radiator synthesis and the boundary element multigrid method.* Internal report, Technische Fashhochule, Berlin, Germany, 1980. 2.4, 21

M. Ochmann. *The source simulation technique for acoustic radiation problems.* Acustica, 81: 512–526, 1995. 2.4, Appendix I

M. Ochmann. *The full-field equations for acoustic radiation and scattering.* Journal of the Acoustical Society of America, 105(5):2574–2584, 1999. 21

M. Ochmann. *Source simulation techniques for the calculation of sound radiation and scattering - An overview.* In *Sixth International Congress on Sound and Vibration*, Garmisch-Partenkirchen, Germany, 2000. Appendix I

P. J. Papakanellos, D. I. Kaklamani, C. N. Capsalis. *Analysis of an infinite current source above a semi-infinite lossy ground using fictitious current auxiliary sources in conjuction with complex image theory techniques. IEEE Transactions on Antennas and Propagation*, 49(10): 491–1503, 2001. 21

J. Périsse. *A study of radial vibrations of a rolling tyre for tyre-road noise characterisation* . Mechanical Systems and Signal Processing, 16(6):1043–1058, 2002. 1.1

J. Picaut. *Contribution à l'étude de la réflexion du son par une façade. Partie* I Bibliographies et considérations qualitatives. Report JP-00-03, Laboratoire Central des Ponts et Chaussées, Nantes, France, 2000. 5

R. J. Pinnington. *A one dimensional wave model for an automotive tyre.* In *Proceedings of inter.noise 2000*, Nice, France, 2000. 3

R. J. Pinnington, A. R. Briscoe. *A wave model for a pneumatic tyre.* Journal of Sound and Vibration, 253(5):941–959, 2002. 3

H. Press et al. *Numerical recipies, the art of scientific computing.* Cambridge University Press, Cambridge, 994p, 1986. 2.3, 21

K. B. Rasmussen. *Sound propagation over grass covered ground.* Journal of Sound and Vibration, 78(2):247–255, 1981. 1.3

J. W. S. Rayleigh. *The theory of sound.* (two volumes), Dover Publication, New York, 1945. 2.1

T. L. Richards. *Finite element analysis of structural-acoustical coupling in tyres.* Journal of Sound and Vibration, 149(2):235–243, 1991. 3

D. Ronneberger. *Towards quantitative prediction of tire / road noise.* In *A workshop on rolling noise generation*, Newport Beach, USA, 1989. 1, 3

D. Ronneberger C. Preuss. *Optimum positions of microphones in trailers.* In *International tire/road noise conference INTROC 1990*, Gothenburg, Sweden, 1990. 1.1

F. de Roo, E; Gerrestsen, E. H. Mulder. *Predictive performance of the tyre-road noise model TRIAS.* In *Proceedings of inter.noise 2001*, The Hague, The Netherlands, 2001. 4

R. J. Ruhala. *A study of tire / pavement interaction noise using nearfield acoustical holography.* PhD thesis, Pennsylvania State University, USA, 1999. 1, 2.3

S. Saigal, T. Y. Yang. *Free vibrations of a tire as a toroidal membrane.* Journal of Sound and Vibration, 107(1):71-82, 1986. 2

U. Sandberg G. Descornet. *Road surface influence in tire/road noise.* In *Proceedings of inter.noise 1980*, Miami, Florida, 1980. 1.2

U. Sandberg. *Will tire / road noise limit future vehicle noise reductions?* In *Proceedings of inter.noise 1982*, San Francisco, USA, 1982. (document)

U. Sandberg. *Noise emission of road vehicles - effects of regulation. Status report of an I-INCE party* In *Proceedings of inter.noise 93*, Leuven, Belgium, 1993. (document)

U. Sandberg. *Tyre / road noise – Myths and realities* In *Proceedings of Inter.Noise 2001*, The Hague, The Netherlands, 2001. (document)

U. Sandberg, J. A. Ejsmont. *Tyre / road noise reference book* Informex, Kisa, Sweden, 640p, 2002. 1.1

K. Schaaf D. Ronneberger. *Noise radiation from rolling tires - Sound amplification by the "horn effect".* In *Proceedings of inter.noise 1982*, San Francisco, USA, 1982. 1, 7, 4.3

M. R. Schroeder. *Integrated–impulse method measuring sound decay without using impulses.* Journal of the Acoustical Society of America, 66:497–500, 1979. 4

W. Soedel. *On the dynamic response of rolling tires according to thin shell approximations.* Journal of Sound and Vibration, 41:(2): 233-246, 1975. 2

L. Song, G.H. Koopmann, J.B. Fahnline. *A method for computing acoustic fields based on the principle of wave superposition.* Journal of the Acoustical Society of America, 89:(6): 2625–2633, 1991. Appendix I

S. A. Stansfeld. *The non–auditory health effects of noise exposure.* Acoustique et Techniques 28, CIDB publication, 2002. (document)

D. Stanners, P. Bourdeau. *Europe's environment.* Technical report European Environment Agency, 1995. (document)

S.-I. Thomasson. *Reflection from a point source by an impedance boundary.* Journal of the Acoustical Society of America, 146:: 303–322, 1976. 6

S.-I. Thomasson. *Sound propagation above a layer with large refraction index.* Journal of the Acoustical Society of America, 61:659–674, 1977. 1.3

P. J. Thorsson *Optimization of low-height noise barriers using the equivalent sources method.* Acustica - Acta Acustica, 86(5):811–821, 2000. 21

T.M. Tomilina. *The equivalent sources approach to acoustical design of forced vibrating systems.* In *Proceedings of inter.noise 1993*, Moscow, Russia, 1993. 21

G.-P. J. Too S. M. wang. *The application of Source Methods in estimation of an interior sound field.* Acustica - Acta Acustica, 63(3):295–310, 2001. 21

Z. Wang, S.F. Wu. *Helmholtz equation-least-squares method for reconstructing the acoustic pressure field.* Journal of the Acoustical Society of America, 102(4):2020–2032, 1997. 21

G. R. Watts, S. N. Chandler-Wilde, P. A. Morgan. *The combined effect of porous asphalt surfacing and barriers on traffic noise.* Applied Acoustics, 58:351–377, 1999. (document)

J. T. Weaver. *Image theory for an arbitrary quasi–static field in the presence of a conducting half space.* Radio Science, 6(6):647–653, 1971. 21

E. G. Williams. *Inverse Problems in Sound Radiation.* In *Proceedings of ICA 2001*, Rome, Italy, 2001. 21

T. ten Wolde. *On the validity and application of reciprocity in acoustical mechano–acoustical and other dynaminal systems.* Acustica - Acta Acustica, 28:23–32, 1973. 1

F. Wullens. *Towards an optimisation of tyre / road parameters for noise reduction.* Technical report F 02-01, Department of Applied Acoustics - Chalmers, 2002. 3

C. Zwikker, C. W. Kosten. *Sound absorbing materials.* Elsevier New-York, 175p, 1949. 1.3

M. Ögren, H. Jonasson. *Measurement of the acoustic impedance of the ground.* SP Report 1998:28, Swedish National Testing and Research Institute, Borås, Sweden, 1998. Appendix IV

M. Ögren, W. Kropp. *The equivalent sources method applied to a 2D city canyon.* In *Proceedings of Forum Acusticum 2002*, Sevilla, Spain, 2002. 21

Appended Papers

On the Sound Radiation from Tyres

W. Kropp, F.-X. Bécot, S. Barrelet.

In Acustica - Acta Acustica, vol 86(5) : 769–779, 2000.

An Efficient Application of Equivalent Sources to Noise Propagation Over Inhomogeneous Ground

F.-X. Bécot, P. J. Thorsson, W. Kropp.

In Acustica - Acta Acustica, vol 88(6) : 853–860, 2002.

Line Source Radiation Over Inhomogeneous Ground Using an Extended Rayleigh Integral Method

F.-X. Bécot, P. J. Thorsson, W. Kropp.

In Proceedings of I.C.A, Rome, Italy, 2001.

Modélisation du bruit de contact pneu / chaussée – Quels sont les facteurs clés d'une réduction des nuisances sonores?

F.-X. Bécot.

In 12^{emes} Rencontres Régionales de la Recherche.